Site NGHP-01-07

By T. Collett, M. Riedel, J. Cochran, R. Boswell, J. Presley, P. Kumar, A. Sathe,
A. Sethi, M. Lall, and the National Gas Hydrate Program Expedition 01 Scientists

Scientific Investigations Report 2012–5054

U.S. Department of the Interior
U.S. Geological Survey

Contents

Figures

Tables

Site NGHP-01-07

By T. Collett, M. Riedel, J. Cochran, R. Boswell, J. Presley, P. Kumar, A. Sathe, A. Sethi, M. Lall, and the National Gas Hydrate Program Expedition 01 Scientists

Background and Objectives

Site NGHP-01-07 (Prospectus Site KGGH06-A) is located at 16° 31.2785' N, 082° 40.8572' E in the Krishna-Godawari (KG) Basin (fig. 1). The water depth is ~1,285 m. Site NGHP-01-07 is situated within the Reliance Industry Ltd D6 block.

The objectives of the work carried out at this site follow the general objectives of the India NGHP Expedition 01:

- Study the occurrence of gas hydrate and establish the background geochemical, geological, geophysical and microbiological baselines for gas-hydrate proxy studies;
- Define the relationship between the sedimentology and structure of the sediments and the occurrence and concentration of gas hydrate;
- Calibrate remote sensing data such as seismic data by acquiring LWD/MWD and wire-line log data as well as VSP data for time-depth matching.

For Site NGHP-01-07, two main lines are used (inline 1539 and crossline 3900, extracted from a large-scale 3D cube) to describe the seismostratigraphic setting (figs. 2 and 3).

A distinct BSR, is imaged cross-cutting inclined beds on inline 1539 between traces 3830 and 4200. The BSR is less distinct between traces 3600 and 3800. The BSR is estimated at a depth of 188 mbsf (0.235 TWT) using a constant velocity of 1,600 m/s for the entire sediment column.

The seafloor generally deepens to the SE, but is interrupted by a ridge (near trace 3840 on inline 1539), which is elevated 45–50 m above the surrounding topography. This ridge is associated with an underlying fault that dips to the NW. The sediments between the seafloor and the BSR show only minor evidence of deformation or faulting, and form a distinct package that is unique from the surrounding sediments that tend to exhibit a more chaotic internal reflectivity. This unique package of more uniform stratigraphy extends on inline 1539 from traces 3810 to 4080 and on crossline 3900 between traces 1490 and 1590. From trace 1590 to 1700, the package gets buried underneath a more chaotic series of reflections.

Two distinct reflections can be identified within the sediment package overlying the BSR at Site NGHP-01-07. Below the proposed drilling site, a strong reflector at ~70 mbsf and a high-reflectivity band between 130 mbsf and 150 mbsf are seen. Both reflectors are most likely associated with the occurrence of gas hydrate as identified on precoring LWD data.

Operations

This operations summary covers the Leg 2 transit from Site NGHP-01-06 (KGGH04-A) to Site NGHP-01-07 (KGGH06-A), Leg 2 LWD/MWD operations at Site NGHP-01-07, the Leg 3B transit from Site NGHP-01-03 (GDGH05-A) to Site NGHP-01-07, and drilling/coring operations for Holes NGHP-01-07A through NGHP-01-07D (fig. 4). Schedule details and statistics for this site can be found as Appendixes:

- Appendix 1: NGHP Expedition 01 Operations Schedules
- Appendix 2: NGHP Expedition 01 Operations Statistics

Included in the Glossary is a list of standard or commonly used operations terms and acronyms.

Hole NGHP-01-07A

The first hole of Site NGHP-01-07 was drilled on Leg 2 of NGHP Expedition 01 as the seventh hole in a twelve-hole LWD/MWD transect. The 44.1 NMI transit from Site NGHP-01-06 (KGGH04-A) was completed in 4.6 hr at a speed of 9.6 knots. The vessel was switched from cruise mode to DP control, and a positioning beacon was deployed at the prospectus coordinates at 1025 hr on May 27, 2006. Prior to deploying the LWD/MWD tools, a data upload task was completed, a continuity test was conducted, the nuclear source was loaded, and the drill string was lowered to a depth of 113.6 mbrf. A second function test was performed at that depth before continuing the pipe trip to the sea floor. The drill string was spaced out for spudding and a tag of the sea floor indicated a mudline depth of 1,297.0 mbrf. After offsetting the vessel 2 meters north of the prospectus coordinates, the top drive was picked up, and Hole NGHP-01-07A was spudded at 1539 hr on May 27. LWD/MWD drilling continued at a controlled rate of 18.6 m/h (average net ROP including connection time) to a total depth of 260.0 mbsf. The hole was displaced with 79 barrels of weighted 10.5 ppg Sepiolite mud. After recovering the drill string, the BHA was racked back in the derrick, the LWD/MWD source was removed, data was downloaded, and the bit/float valve was inspected. The LWD/MWD tools were then laid out and secured on the pipe racker and riser hatch. The vessel was switched from DP to cruise control and got underway for Site NGHP-01-08 (MNGH01-1A) at 1145 hr on May 28, 2006.

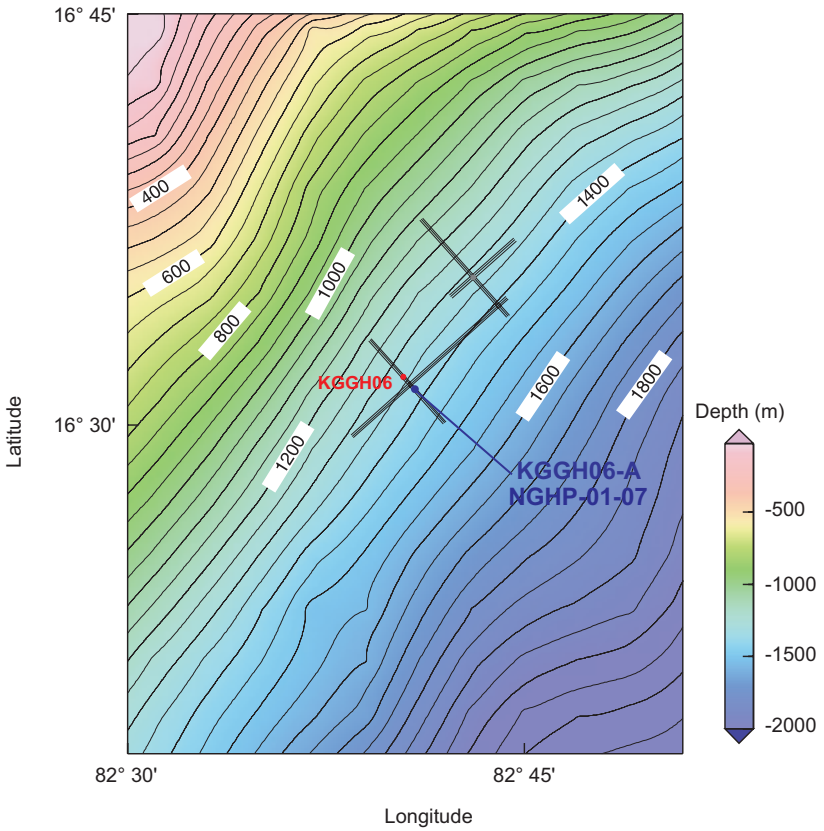

Figure 1. Location of Site NGHP-01-07 (Prospectus Site KGGH06-A) in the Krishna-Godavari Basin.

Hole NGHP-01-07B

Site NGHP-01-07 was occupied once again during Leg 3A after completing drilling/coring operations at Site NGHP-01-03 (GDGH05-A). The 58.0 NMI transit was made to Site NGHP-01-07 (KGGH06-A) in 5.0 hr at an average speed of 11.6 knots.

The sea voyage ended at 0145 hr and after lowering all thrusters/hydrophones the vessel was switched from cruise mode to DP control at 0200 hr on July 5, 2006. The first positioning beacon was deployed at 0230 hr; however, this beacon inexplicably switched to a one-half repetition rate and a second beacon was deployed at 0512 hr. The ice bath was installed in the moon pool and the same BHA as was used on the previous Site NGHP-01-03 was deployed from its racked position in the derrick.

Hole NGHP-01-07B was planned as a continuous APC/XCB cored hole to 260.0 mbsf with several pressure cores targeting the gas hydrate stability field. Temperature measurements were also to be taken using the APCT–3, APCT, and DVTP systems to define a thermal gradient from seafloor to TD. Hole NGHP-01-07B was designed to be an "all inclusive" core hole, eliminating the need for a "tools hole" by combining continuous conventional and pressure cores. The hole was to culminate with a complete suite of wire-line logs.

The vessel was offset 10 meters to the SE of Hole NGHP-01-07A while the drill string was tripped to bottom. The bit was positioned at a depth of 1,285.0 mbrf and the first attempt was made to spud Hole NGHP-01-07B. This core barrel recovered only water so the drill string was lowered an additional 4.0 m to 1,289.0 mbrf. Hole NGHP-01-07B was ultimately spudded at 0740 hr on July 5, establishing a seafloor depth of 1,295.8 mbrf. The PDR depth for this site, corrected to the rig floor DES, was 1,297.4 mbrf. APC Core NGHP-01-07B-01H was ondeck at 0750 hr and APC coring continued through Core NGHP-01-07B-09H to a depth of 78.7 mbsf.

Temperature measurements were taken using the APCT–3 shoe on Cores NGHP-01-07B-03H and NGHP-01-07B-05H (21.7 mbsf and 40.7 mbsf, respectively), and the APCT shoe on Core NGHP-01-07B-07H (59.7 mbsf). A new "micro logger", miniature temperature/pressure probe (PTP), was deployed with the APC in a shipboard built carrier mounted to a modified APC piston head. These microloggers were originally brought to the ship to be included with the pressure core shipments thus providing a temperature/pressure history during the shipping process. Early on it was recognized that these small recorders could provide useful scientific information on the temperature/pressure history of the gas-hydrate cores during retrieval and rig floor handling. Microloggers were deployed on Cores NGHP-01-07B-05H through NGHP-01-07B-09H.

A single short (5.5m) XCB Core NGHP-01-07B-10X was cut and the hole was swept with a 10 bbl Sepiolite mud sweep prior to cutting the first pressure core. PCS Core

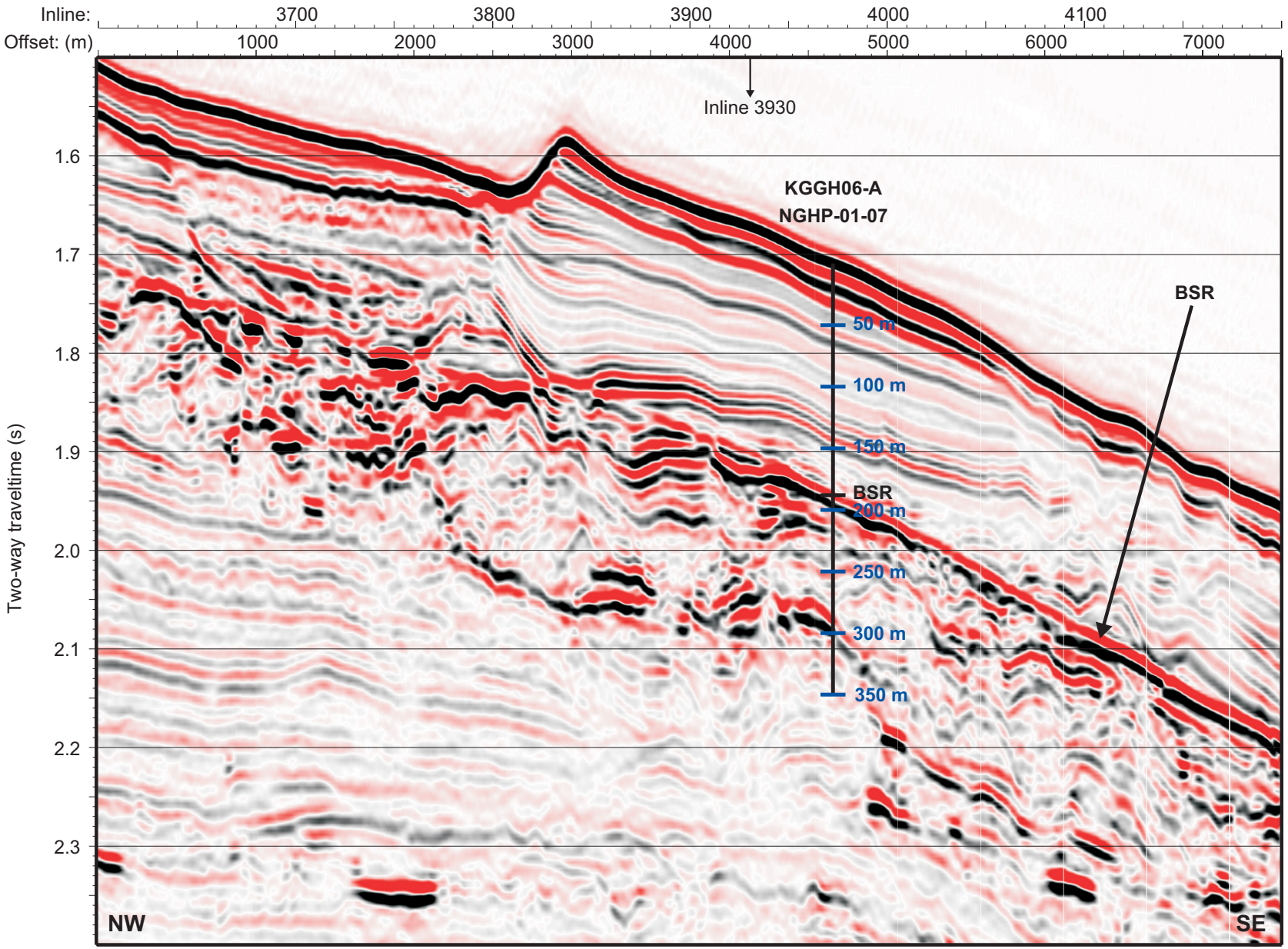

Figure 2. Seismic inline 1539 (oriented NW–SE) intersecting with Site NGHP-01-07 (Prospectus Site KGGH06-A). Formation and BSR depths were estimated using a constant velocity of 1,600 m/s for the entire sediment column. [BSR, bottom-simulating reflector]

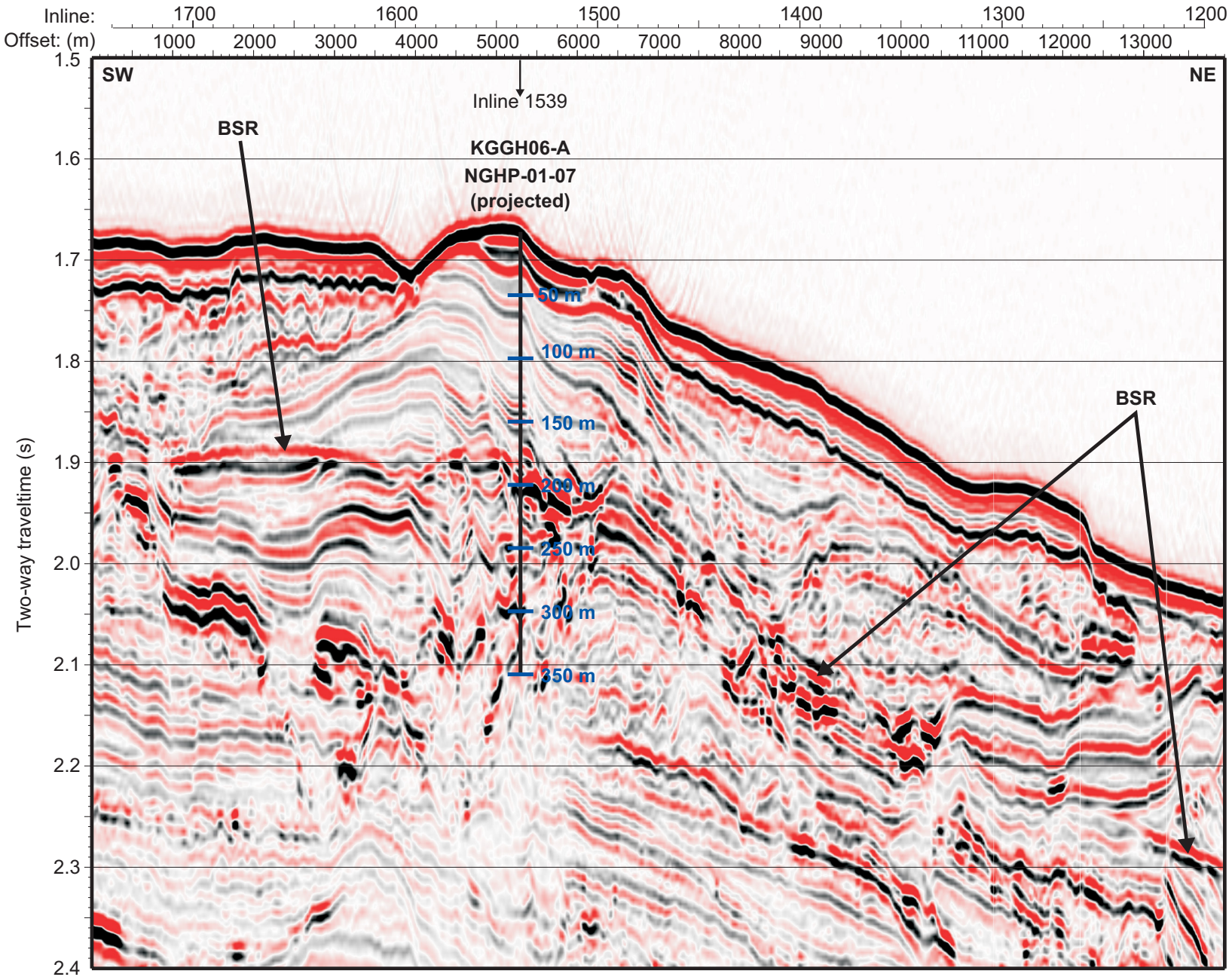

Figure 3. Section of seismic crossline 3900 near Site NGHP-01-07 (Prospectus Site KGGH06-A). Formation and BSR depths were estimated using a constant velocity of 1,600 m/s for the entire sediment column. [BSR, bottom-simulating-reflector]

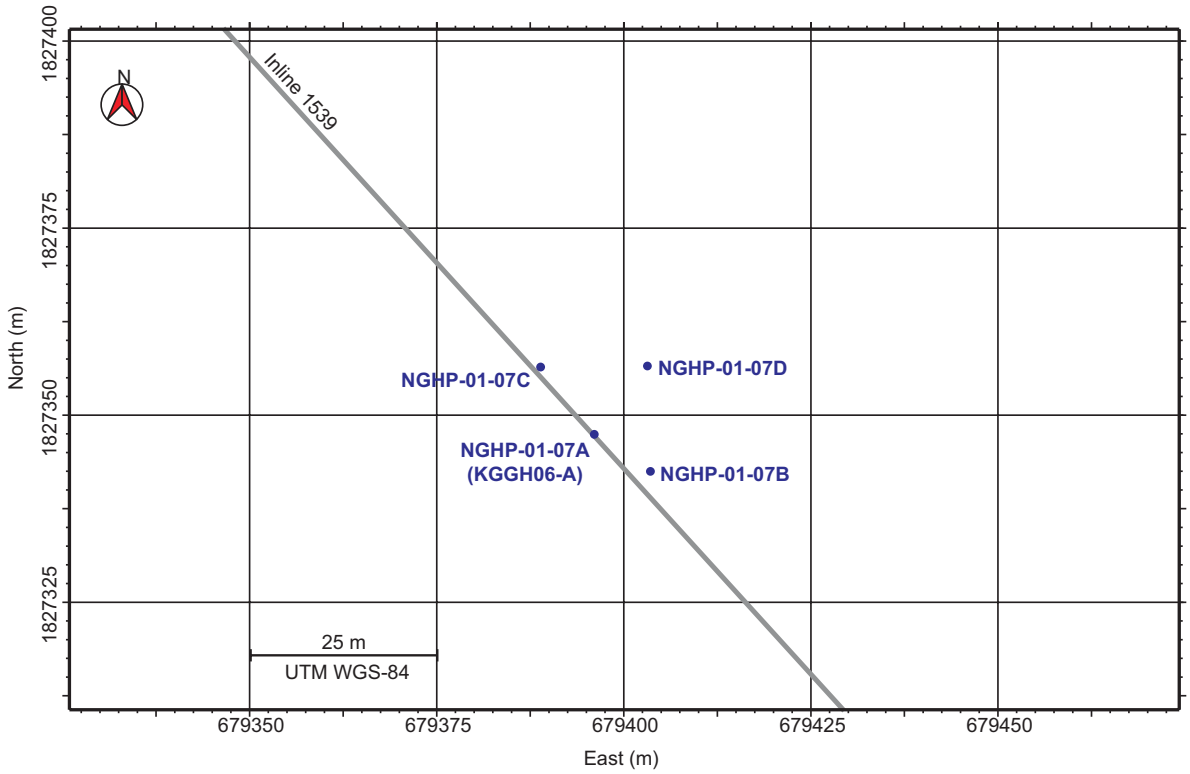

Figure 4. Map showing all holes occupied at Site NGHP-01-07 (KGGH06-A).

NGHP-01-07B-11P was recovered from 85.2 mbsf. This was followed by the first FPC Core NGHP-01-07B-12Y to 86.2 mbsf. XCB Cores NGHP-01-07B-13X through NGHP-01-07B-15X set up the second FPC Core NGHP-01-07B-16Y cored to 115.2 mbsf. The first DVTP temperature measurement was successfully taken at that depth. Four XCB Cores NGHP-01-07B-17X through NGHP-01-07B-20X to 148.2 mbsf were recovered and a second DVTP temperature measurement was successfully taken. A second PCS Core NGHP-01-07B-21P was then recovered from 149.2 mbsf followed by the first HRC Core NGHP-01-07B-22E to 150.2 mbsf. Three more XCB Cores NGHP-01-07B-23X through NGHP-01-07B-25X set up the last series of pressure cores. The third PCS Core NGHP-01-07B-28P was cored to a depth of 194.4 mbsf followed by the third FPC Core NGHP-01-07B-29Y cored to 195.4 mbsf.

After cutting XCB Core NGHP-01-07B-31X to a depth of 211.6 mbsf (TD), there was difficulty retrieving the core barrel. Several hours were spent attempting to jar the core barrel free; however, these attempts were unsuccessful. The barrel could be moved slightly up and down leading to the suspicion that the XCB cutting shoe may have overheated and mechanically swelled to a larger diameter than could pass through the bit throat. The XCB extension sub was in use to try and improve core recovery; however, this increased the overheating potential due to being further away from the XCB bit jets and an inability to fully retract flush with the bit face when a hard layer is encountered.

At 0315 hr on July 7, 2006, the hole was displaced with 75 barrels of 10.5 ppg mud, the top drive was set back, and the pipe was POOH to the surface. The bit cleared the sea floor at 0440 hr ending Hole NGHP-01-07B and beginning Hole NGHP-01-07C. Upon reaching the rig floor, suspicions were confirmed and a deformed/swollen XCB cutting shoe had to be cut off the barrel using a torch to allow recovery of XCB Core NGHP-01-07B-31X. Total depth for Hole NGHP-01-07B was 211.6 mbsf.

All three PCS deployments included successful recovery of data with the PCS Methane tool. Rates of penetration with the XCB were highly variable ranging from 6.0 m/h to 38.4 m/h. XCB recovery was also quite variable, ranging from 23 percent to 96 percent.

Whirlpaks (microbeads) commonly used for microbiological contamination control were not used for coring; however, accelerated core barrel handling protocols were still used for all core systems (APC, XCB, and PCS) deployed in this hole. All APC/XCB core barrels were laid down immediately upon arrival at the rig floor before making another drill pipe connection or deploying the next core barrel.

For all HYACINTH pressure coring systems (FPC and HRC), a 15–20 minute wait period was employed at the mudline on the way in the hole and again during retrieval. This was to cool the core barrels down thus aiding in keeping any entrained gas hydrate within the stability field. At the rig floor, all pressure-core barrels (PCS, FPC, and HRC) showing signs of proper actuation were placed in the moon pool ice bath prior to processing.

Hole NGHP-01-07C

Hole NGHP-01-07C was intended to drill to the total depth of Hole NGHP-01-07B in order to resume XCB coring at that depth and complete the program outlined for Hole NGHP-01-07B.

After completing the drill string trip back to the rig floor and removing core barrel NGHP-01-07B-31X, the bit and LFV were inspected for damage. All was well and the drill string was tripped back to the seafloor. The vessel was offset 10 meters to the northwest of Hole NGHP-01-07A and using the same seafloor depth (1,295.8 mbrf) as Hole NGHP-01-07B, Hole NGHP-01-07C was spudded at 1140 hr on July 7, 2006.

The hole was drilled down to a depth of 184.2 mbsf at a rate of 35.1 m/h (average net ROP including connection time) when the driller reported ~350 PSI drop in pump pressure. The pressure fluctuated from normal when WOB was applied (~10K pounds) to 350 psi low when the drill bit was picked up off bottom. It was not felt to be related to hole instability or a cuttings loaded annulus since the hole appeared to be free of debris and top drive torque was minimal. This indicated that there may be a crack or washout somewhere around the top of the first stand of drill collars. Since this pressure fluctuation had not been observed on any other hole, particularly Hole NGHP-01-07B drilled just 20 m away, it was decided that the drill string should be recovered and inspected rather than risk drilling ahead. A factor in the decision was the fact that only two seal bore drill collars (required for APC/XCB coring) were aboard ship and one of those two was installed in the current BHA. A loss could have left the expedition with only one remaining seal bore drill collar with nearly 40 days of operations remaining.

After drilling terminated at a depth of 184.2 mbsf, the hole was displaced with 50 barrels of 10.5 ppg mud, and the bit was pulled clear of the mudline at 2005 hr on July 7 ending Hole NGHP-01-07C and beginning Hole NGHP-01-07D.

Hole NGHP-01-07D

Prior to tripping the remaining string back to the ship, the subsea TV camera was deployed on the VIT sleeve to visually inspect the drill string. An XCB center bit was installed and the top drive was used to circulate drilling mud at 70 SPM or ~700 psi pressure. No leaks were readily identified in the drill pipe or BHA, so the camera and XCB center bit were recovered, the top drive was set back, and the pipe trip to the surface resumed at 2245 hr. Both stands (six joints of 5-1/2 in) of transition pipe were checked for proper make-up torque and all drill collar/BHA connections were NDT inspected upon recovery. No indications of cracks were found.

The vessel was offset 10 m to the northeast of Hole NGHP-01-07A and the drill string was once again tripped to the sea floor. Hole NGHP-01-07D was spudded at 0750 hr on July 8, 2006 using the same sea floor depth of 1295.8 mbrf. Drilling with the XCB center bit continued for 7.75 hr to a depth of 231.2 mbsf at a rate of 29.8 m/h (average net ROP including connection time).

The hole was swept clean with a Sepiolite mud pill and the XCB center bit was recovered prior to initiating XCB coring. XCB Cores NGHP-01-07D-01X through NGHP-01-07D-04X were cut to the target depth of 260.0 mbsf where a final DVTP temperature measurement was taken.

After pulling one stand of drill pipe and setting back the top drive, 1.50 hours were spent conducting a wiper trip to logging depth and back. Only 2 m of fill was found on bottom and this was readily circulated out. A go-devil was pumped to lock the LFV in the open position and the hole was displaced with 100 barrels of 10.5 ppg weighted mud. The drill string was then tripped setting the EOP at 57.7 mbsf.

At 0345 hr on July 9, 2006, rig-up for logging began. The first logging run was made with the Triple Combo tool suite. This suite of tools reached total depth and was out by 1015 hr. The VSP logging tools were deployed next so that the seismic gun firing could be conducted during daylight hours. This was to enable simultaneous mammal watch in accordance with IODP protocols. VSP operations were completed at 1800 hr (dusk) and the tools were out by 1900 hr. The third suite of tools consisted of the FMS-Sonic. These tools reached total depth as well; however problems were experienced getting the tools back inside the bit. After working and pumping, the tools were recovered and the logging sheaves were rigged down by 0115 hr on July 10, 2006. The drill string was pulled clear of the sea floor at 0125 hr and the pipe trip back to the surface was completed routinely. Both positioning beacons were recovered by 0530 hr and the vessel was placed in cruise mode. The transit to Site NGHP-01-14 (GDGH14-A) commenced at 0600 hr on July 10, 2006.

Lithostratigraphy

Site NGHP-01-07 is the northernmost site drilled in the Krishna-Godavari (KG) Basin located along the eastern continental margin of India. Four holes were drilled at Site NGHP-01-07: Hole NGHP-01-07A for LWD/MWD; Hole NGHP-01-07B for APC/XCB coring to 211.6 mbsf (short of the 260.0 mbsf objective); Hole NGHP-01-07C, a dedicated wire-line logging hole that reached a total depth of 184.2 mbsf; and Hole NGHP-01-07D for XCB coring between 231.2 mbsf and 260 mbsf followed by wire-line logging. Core recovery in Hole NGHP-01-07B was 85 percent, whereas in Hole NGHP-01-07D gas expansion led to 113 percent recovery (see “Operations”).

Similar to sites in the southern part of the KG Basin, there is no lithostratigraphic justification to divide the sedimentary sequence recovered at Site NGHP-01-07 into more than

one lithostratigraphic unit. Designation of Lithostratigraphic Unit I (fig. 5 and Site NGHP-01-07 Visual Core Descriptions in the supplemental data files; see "Physical Properties" and "Downhole Logging") was based on sedimentological criteria (for example, variations in sedimentary structure, grain size, and biogenic/terrigenous/authigenic lithologic components), physical properties (for example, magnetic susceptibility), and LWD/wire-line logging data (for example, gamma ray logs). We also integrated the core data with the available seismic data to help define and interpret the stratigraphic sequence (see "Background and Objectives").

The lithostratigraphy recovered at Site NGHP-01-07 is in many ways similar to the lithostratigraphy of sites previously drilled in the southern part of the KG Basin. The sedimentary sequence at Site NGHP-01-07 is composed of nannofossil-bearing to rich clay, to foraminifera bearing clay. Major components include nonbiogenic grains (quartz, feldspar, mica, clay, pyrite, authigenic carbonates, and heavy minerals) and biogenic elements (calcareous nannofossils, foraminifera, and mollusk shell fragments). Terrestrial organic matter is also typically high at Site NGHP-01-07 as in the southern KG Basin sites. However, compared to other KG Basin sites, sand/silt laminae and beds occur more frequently at Site NGHP-01-07 and sands (fig. 5) are more common and in places coarser grained (gravel is also encountered in one instance; figs. 5 and 6).

As observed at the other KG Basin sites, the physical and chemical properties measured on cores or in the hole by logging are likely affected by the degree, type, and location of diagenesis within the sedimentary column (that is, authigenic carbonates, iron monosulfide and pyrite precipitation, and the degree of lithification, as well as overprinting of certain physical and chemical properties by gas hydrate and free gas). This, together with the more dynamic depositional history at this site (as interpreted by the presence of thicker and more frequent sand and silt beds) precludes direct correlation between Site NGHP-01-07 and other KG Basin sites.

Lithostratigraphic Unit

Lithostratigraphic Unit I

Intervals: Hole NGHP-01-07B, Sections NGHP-01-07B-01H-1 to NGHP-01-07B-31X-CC; Hole NGHP-01-07D, Sections NGHP-01-07D-01X-1 to NGHP-01-07D-04X-CC

Depths: Hole NGHP-01-07B, 0–184.2 mbsf; Hole NGHP-01-07D, 0–260 mbsf

Age: Quaternary

Core recovery was good in Hole NGHP-01-07B for the upper ~90 mbsf (APC and pressure cores and the first two XCB cores); in Hole NGHP-01-07D recovery was also good, although it is probably overestimated due to gas expansion (fig. 5). There is no clear correlation between recovery and the location of the gas-hydrate stability zone or the BSR. Instead, low recovery appears to be related to the XCB coring technique, and most likely, lithologies that are difficult to recover (sand or silt rich zones).

Lithostratigraphic Unit I is composed primarily of clay and nannofossil-bearing to rich clay with a thin interval of foraminifera-bearing clay between ~74 and 78 mbsf and a ~10 m thick silty clay at the bottom of the drilled interval. Sediments appear semi-lithified in Hole NGHP-01-07D and authigenic carbonate-rich bands are preferentially transformed into limestone. Sediment color varies from dark olive gray (5Y 3/ 2) at the top of the core to very dark gray (2.5Y 3/1, 5Y 3/1, N 3/1) or very dark greenish gray (5GY 3/ 1, 10Y 3/1) to black (5Y 2.5/1) and greenish black (10Y 2.5/1). Terrestrial organic matter is common (trace to 5 percent) in smear slides taken throughout Lithostratigraphic Unit I (tables 1 and 2) and in the coarse fraction up to 20 percent, (but examined in Hole NGHP-01-07D only; table 3). Except for the upper ~17 mbsf where they occur sporadically, thin silt/sand laminae and beds (submillimeter to several centimeters) are abundant throughout Lithostratigraphic Unit I (fig. 6; tables 4 and 5); in one case (in Section NGHP-01-07B-08H-4) granules and gravel (bigger then 2 mm in diameter up to 2 cm) were recovered (fig. 7). Similar to all the sites drilled in the KG Basin, the lack of *Discoaster* spp. suggests that the entire Lithostratigraphic Unit I at Site NGHP-01-07 was deposited in the Quaternary; however, additional biostratigraphy may help constrain this initial estimate.

Shell fragments, visible foraminifera tests, and, more rarely, mollusk shells and woody debris, occur sporadically throughout the Unit (fig. 5 and Site NGHP-01-07 Visual Core Descriptions in the supplemental data files). Authigenic carbonates occur primarily as nodules, preferentially larger than 1 cm (fig. 8), in the upper ~155 mbsf of the sequence at Site NGHP-01-07, whereas carbonate bands are dominant below that depth (fig. 9). Within the carbonate bands, stratification is apparent indicating carbonate precipitation occurred as cement within horizontally bedded sediments. Authigenic carbonate precipitation apparently bears no relationship to the current SMI (sulfate-methane interface), occurring both below and above it (fig. 5 and Site NGHP-01-07 Visual Core Descriptions). Furthermore, authigenic carbonates are absent or very rare in the upper part of the gas hydrate stability zone between ~95 and 140 mbsf.

Intact silt/sand laminae and beds throughout Unit I (fig. 6) indicate that bioturbation is rare at Site NGHP-01-07, suggesting a high sedimentation rate typical of an unstable, dynamic environment that was inhospitable to abundant benthic infaunal organisms (fig. 5 and Site NGHP-01-07 Visual Core Descriptions in the supplemental data files).

Lithostratigraphic Unit I, as determined from smear slides, is primarily composed of clay-sized grains (75–100 percent) with minor amounts of silt-sized grains (up to 20 percent) and some sand (tables 1 and 2). Several silty clay beds (silt-sized grains >20 percent of total sediment) were also encountered. Minor lithologies described in smear slide included silt/sand beds, authigenic carbonates, and iron sulfide rich zones. Non-biogenic components of Lithostratigraphic Unit I are clay minerals, quartz, feldspar, mica, volcanic glass, and heavy minerals. Opaque grains, sulfides, or heavy minerals, are common in all grain sizes, and typically comprise trace amounts of the total sediment in the clays, but higher percentages in the silt layers (tables 1 and 2). Authigenic carbonate precipitates were also observed in smear slides (trace to 7 percent) in Hole NGHP-01-07B and are much more common in Hole NGHP-01-07D (2 to 32 percent; tables 1 and 2). The dominant biogenic components in the sediment are calcareous nannofossils, which comprise trace to 25 percent of the total (biogenic and non-biogenic) sediment grains (tables 1 and 2). Terrestrial organic matter was commonly observed in smear slide (trace to 5 percent) throughout Lithostratigraphic Unit I (tables 1 and 2). Foraminifera fragments were less common in the smear slides than at other KG Basin sites, except for the sporadic increases at the bottom of Hole NGHP-01-07B and in Hole NGHP-01-07D (that is, below ~170 mbsf). Description of the coarse fraction (>63 mm) components in the sediments in Hole NGHP-01-07D (table 3) shows that quartz, mica, heavy minerals, and wood/plant debris are dominant, whereas foraminifera are almost absent.

Gas Hydrate Occurrence

Although IW chemistry data (see "Inorganic Geochemistry") did not indicate significant gas-hydrate occurrences throughout the hole, small IR anomalies were observed in Core NGHP-01-07B-25X. Gas hydrate was also inferred from/recovered by pressure cores (Core NGHP-01-07B-21P; see "Pressure Coring"), and from the downhole logging data at 75–93 mbsf and 138–152 mbsf. No moussey or soupy sediments were observed in the recovered cores described on the sedimentology table.

Inorganic Geochemistry

The main objectives of the inorganic geochemistry program at Site NGHP-01-07 (Holes NGHP-01-07B and NGHP-01-7D) were to (1) identify and quantify the fluid and gas source(s), subsurface hydrology (transport mechanisms, and migration pathways), and biogeochemical reactions associated with subsurface gas hydrate; and (2) determine the quantity and distribution of gas hydrate based on dissolved chloride concentrations. Interstitial water (IW) chemical composition data are tabulated in table 6, and illustrated in figure 10.

A total of 63 IW samples were collected from Holes NGHP-01-07B and NGHP-01-07D, 58 and 5 respectively. There were 25 IW samples from APC cores from 1.4 to 71.9 mbsf, 28 from XCB cores between 83 and 200.1 mbsf and 5 from pressure cores at Hole NGHP-01-07B. Samples were collected at a higher sample spatial frequency, 3–5 per core, in the upper ~21 m of Hole NGHP-01-07B to characterize the SMI for future geochemical modeling studies. Five IW samples were collected from XCB cores taken below the BSR at Hole NGHP-01-07D, one per core between 235 and 260 mbsf to constrain background Cl^- concentrations for interpretation of Cl^- anomalies within the gas hydrate stability field. Whole-round lengths ranged from 10 to 40 cm, with longer sections subsampled from cores recovered deeper within the holes.

Interstitial Water Chloride—Gas-Hydrate Distribution

Chloride at this site was analyzed by ion chromatography rather than by titration, thus only general trends are being described. Between 1.4 and ~ 20 mbsf chloride concentrations are similar to that of seawater (fig. 10A). Between 30 and 160 mbsf, concentrations scatter to higher values. Below 230 mbsf, values are again similar to that of seawater.

Sulfate Concentrations and the SMI

Sulfate concentrations are depleted by up to 13 mM from that of seawater between 1.4 and ~29 mbsf (fig. 10B). Between 29 and 36 mbsf sulfate becomes depleted to concentrations near the detection limit. The sulfate methane interface (SMI) is in this interval. The sharp change in concentration gradient may reflect a sharp change in diffusivity or be the result of rapid sedimentation. A significant change in diffusivity is supported by large increases in resistivity between 31 and 40 mbsf where there is FeS mineralization (see "Lithostratigraphy" and "Physical Properties").

Figure 5 (following page). Lithostratigraphic summary of NGHP-01-07B and NGHP-01-07D. Note: Colored intervals exceed symbol size when there is a range in the occurrence. Center point of each symbol represents true depth of occurrence, therefore colored bars may slightly exceed core recovery; see Site NGHP-01-07 Visual Core Descriptions in the supplemental data files for the expanded scale, detailed core descriptions; see Site NGHP-01-07 Oversized Figure for the enlarged version of this summary.

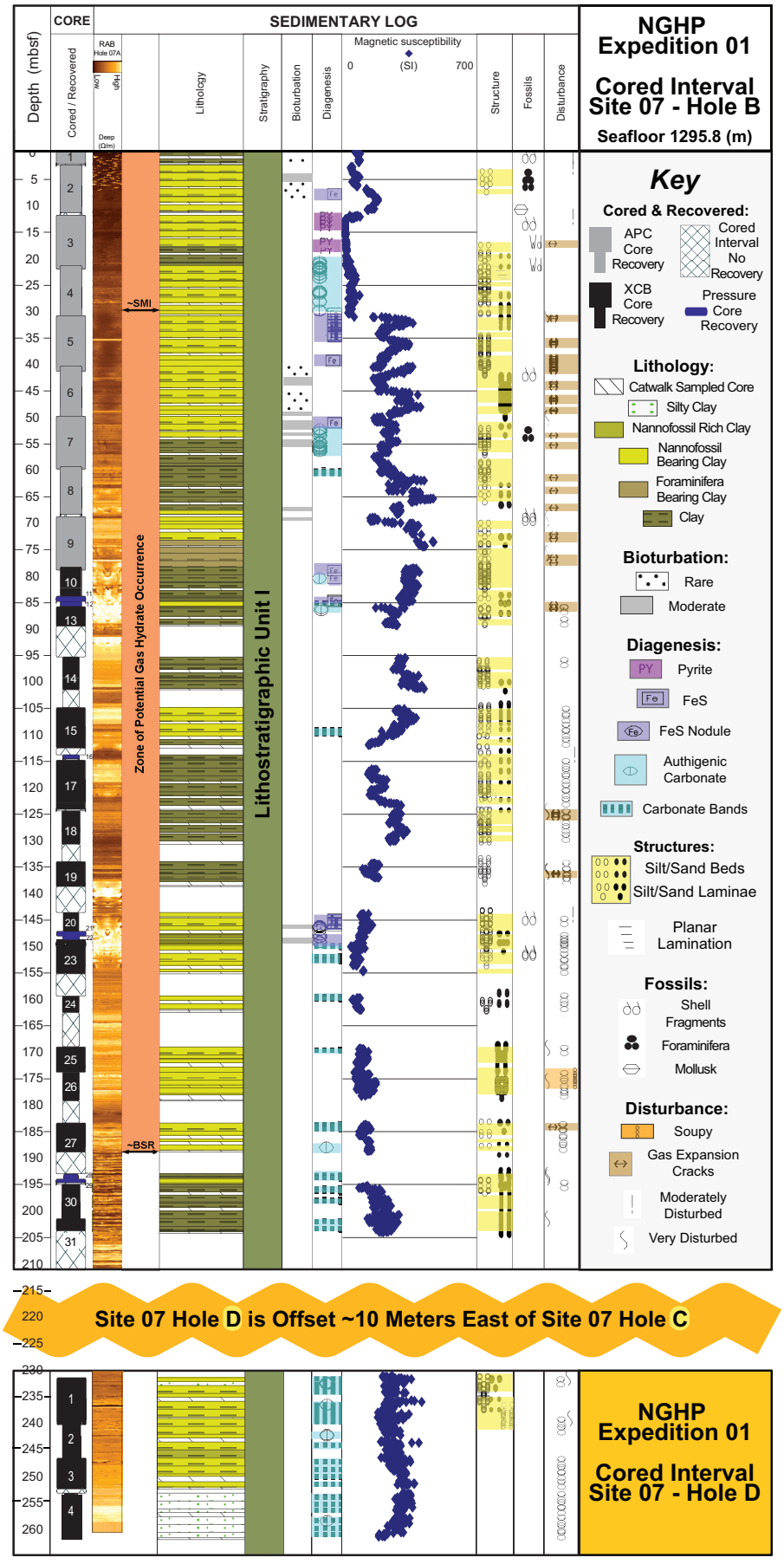
NGHP Expedition 01
Cored Interval
Site 07 - Hole B
Seafloor 1295.8 (m)
Depth (mbsf)
CORE
SEDIMENTARY LOG
Cored / Recovered
RAB Hole 07A
Lithology
Stratigraphy
Bioturbation
Diagenesis
Magnetic susceptibility
0 (SI) 700
Structure
Fossils
Disturbance
~SMI
~BSR
Zone of Potential Gas Hydrate Occurrence
Lithostratigraphic Unit I
Key
Cored & Recovered:
APC Core Recovery
Cored Interval No Recovery
XCB Core Recovery
Pressure Core Recovery
Lithology:
Catwalk Sampled Core
Silty Clay
Nannofossil Rich Clay
Nannofossil Bearing Clay
Foraminifera Bearing Clay
Clay
Bioturbation:
Rare
Moderate
Diagenesis:
Pyrite
FeS
FeS Nodule
Authigenic Carbonate
Carbonate Bands
Structures:
Silt/Sand Beds
Silt/Sand Laminae
Planar Lamination
Fossils:
Shell Fragments
Foraminifera
Mollusk
Disturbance:
Soupy
Gas Expansion Cracks
Moderately Disturbed
Very Disturbed
Site 07 Hole D is Offset ~10 Meters East of Site 07 Hole C
NGHP Expedition 01
Cored Interval
Site 07 - Hole D

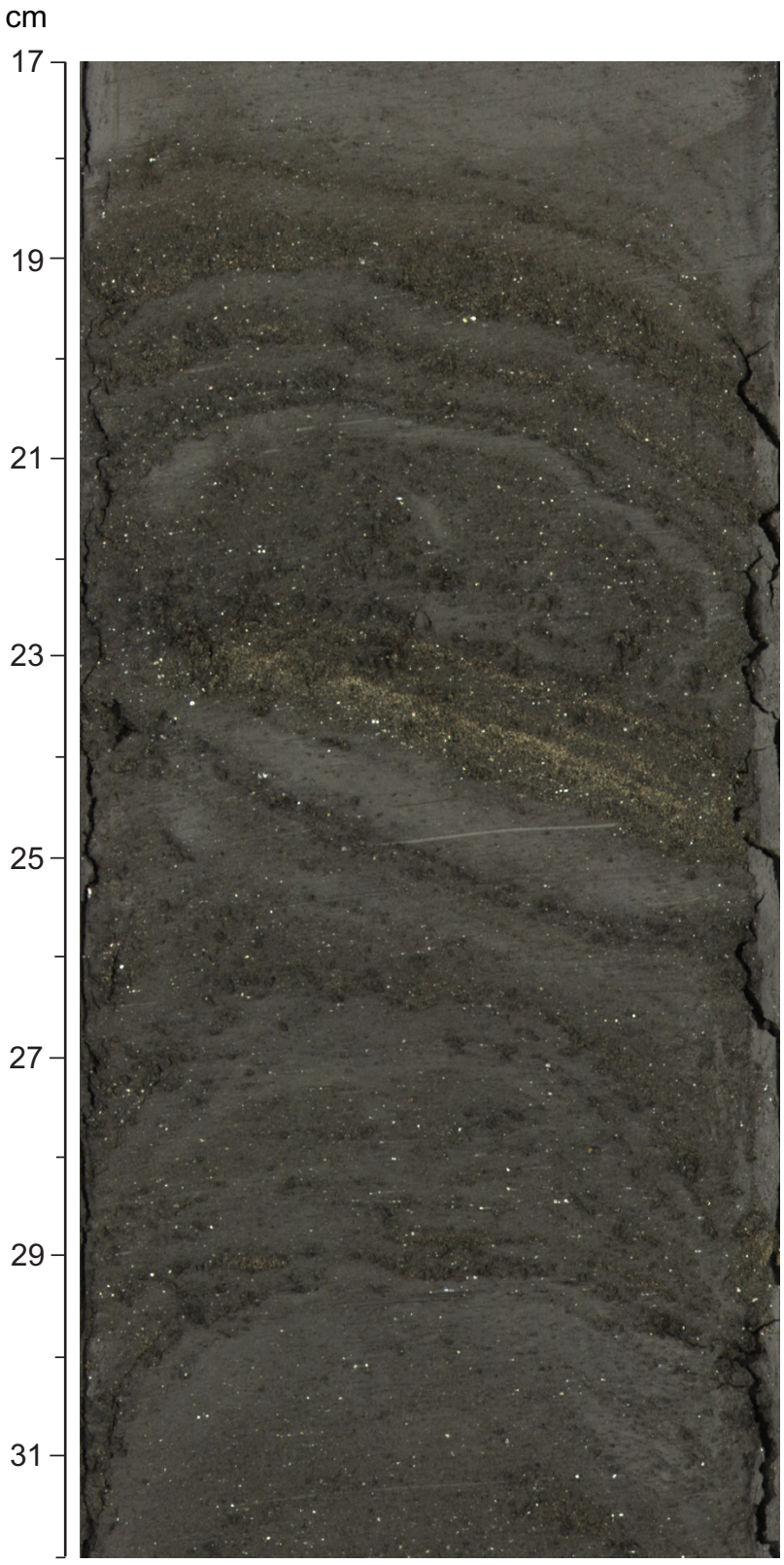

Figure 6. Silt/sand beds and laminae in Section NGHP-01-07B-08H-5, 17–32 cm typical of those recovered in Lithostratigraphic Unit I. Note the rigidity of the thickest sand bed that did not deform during APC coring. [APC, Advanced (Hydraulic) Piston Corer]

Alkalinity

Alkalinity shows a sharp increase from approximately 8 to 20 mM between 29 and 39 coincident with the SMI as expected from sulfate reduction (fig. 10C). The increase in alkalinity is only about half of that expected based on sulfate loss; the remainder most likely reflects carbonate precipitation as evidenced by the presence of authigenic carbonate between 20 and 30 mbsf. Between 120 and 137 mbsf there is a local minimum in concentration which may reflect either alkalinity consumption or the burial of lower alkalinity fluids.

At approximately 180 mbsf, there is a maximum of nearly 45 mM most likely due to carbonate dissolution driven by methanogenesis.

Bromide

The Br^-/Cl^- ratio is instead of Br^- concentration which is affected by gas hydrate dissolution during core recovery and for water loss due to gas hydrate formation (fig. 10D). Between 1.4 mbsf and 20 mbsf Br^- concentrations and Br^-/Cl^- ratios are relatively constant, similar to that of seawater. There is a sharp increase below the SMI indicating the decomposition of marine organic matter and then a more gradual increase through the rest of the section recovered consistent with the continued decomposition of marine organic matter. While Br^- is correlated to alkalinity near the SMI at greater depths they are not strongly correlated, possibly indicating that the alkalinity production in the deeper part of the section is dominated by the fermentation of non-marine organic matter.

Organic Geochemistry

Organic geochemical studies at Site NGHP-01-07 (KGGH-06A) included analysis of the composition of volatile hydrocarbons including methane, ethane, and propane (C_1–C_3) and fixed natural gases (that is, O_2, CO_2, and N_2+Ar) from headspace, void gas, and pressure-core sampler (PCS) degassing experiments. In general, these analyses indicate that methane and carbon dioxide are the predominant gases found in the cores at Site NGHP-01-07. However, ethane was present at low level concentrations in void gas and pressure core samples at depths greater than 50 mbsf. The headspace samples of core overlying the sulfate-methane interface (SMI) were dominated by air and depleted in carbon dioxide. Methane was enriched below the SMI and above the seismically-inferred bottom simulating reflector (BSR). Specific details of the shipboard gas chemistry results for Site NGHP-01-07, Holes B and D are provided in the following discussion.

Headspace gas analyses were performed on 57 samples from Hole NGHP-01-07B and five samples from Hole NGHP-01-07D ranging in depth from 0.95 to 260.4 meters below seafloor (mbsf). The concentrations given here represent minimum proxy measurements of the actual concentrations due to limitations of the gas headspace method (Kvenvolden and Lorenson, 2000). The sediment pore water contained methane at concentrations ranging from non-detectable near the surface to 7.86 mM at ~35 mbsf (table 7). Theoretical methane saturation in pore water under site-specific physical conditions, calculated using the Duan and others (1992) and Xu (2002, 2004) methodologies, ranges from 53.8 mM at the seafloor to 137.6 mM at 200 mbsf, then declines to 132.8 mM near the borehole completion depth of 260 mbsf. C_2 and C_3 hydrocarbon gases were not detected in headspace samples, suggesting a biogenic source of methane. Methane concentrations increase step-wise from nondetectable to 7.9 mM at ~35 mbsf likely denoting the sulfate-methane interface (SMI) (fig. 11). Deeper in the section at ~135 mbsf the methane concentration is anomalous and may be associated with the presence of free gas or gas hydrate. Pressure cores taken from 148 to 149 mbsf were both saturated with methane, indicating that gas hydrate was present. Other proxy measurements indicated that gas hydrate may be present in this interval (see "Downhole Logging"). Methane concentration gradually decreases to less than 1 mM below the bottom simulating reflector (BSR). The methane concentrations were generally an order of magnitude below saturation throughout the length of the borehole (fig. 11). The only pressure core taken below the BSR at 188 mbsf was undersaturated in methane (see "Pressure Coring").

Carbon dioxide (CO_2) concentrations ranged from 0.3 to 17.6 mM in pore water contained within the sediment. An equivalent concentration expression of gas volume to sediment volume ranges from ~3,050 to nearly 157,000 microliters CO_2/liter wet sediment (table 7). CO_2 concentrations appear to show a consistent, increase with depth below the SMI until ~200 mbsf, with the exception of two measurements near 105 mbsf (fig. 12). The results can be roughly divided into three zones based on gas concentration. The lowest concentrations are found near the SMI at a depth ranging from 0 to 35 mbsf (fig. 12). This interval of depleted CO_2 corresponds well with the presence of large authigenic carbonate nodules (see "Lithostratigraphy"). Intermediate CO_2 concentrations were found in the entire interval below the SMI associated with an increase in alkalinity (see "Inorganic geochemistry"). The scatter of the data in this zone may be due to XCB coring that can highly disrupt sediment. Below the BSR, CO_2 concentrations sharply decline to less than 1 mM (similar to surficial levels). No apparent change in lithology could be inferred at or near this interval. The headspace-derived methane to carbon dioxide ratio does not reflect enrichment of methane where downhole logging inferred up to 30 percent gas hydrate in the intervals of 75–95 and 138–152 mbsf (fig. 13). The air gases (N_2+Ar) and O_2 were the balance gases, however the (N_2+Ar)/O_2 ratios were typically greater than air indicating that some air was trapped in the headspace samples and some oxygen has likely dissolved preferentially compared to N_2. Air gases are present in all samples as the core plugs were degassed in an air headspace.

Table 1. Smear slide data for Hole NGHP-01-07B.

Sample reference		Texture			Mineral								
Core, section, depth (cm, in section)	Lithology	Sand	Silt	Clay	Quartz	Feldspar	Mica	Heavy minerals	Clay minerals	Volcanic glass	Glauconite	Iron sulfides	Authigenic carbonates
NGHP-01-07B													
1H-1,68	D		2	98	2				95			1	
1H-2,37	D		3	97	2		trace		94			trace	
2H-2,84	D		3	97	1				92			1	
2H-4,80	D		3	97	2				90			1	
3H-2,90	M		100						10			90	
3H-2,111	D		1	99	2				91				
3H-5,34	D		2	97	3				92			1	
3H-6,129	M		90	10	80	5	3	1				10	
4H-4,11.5	D			100	2				93				
4H-5,89	M	10	90		70	trace	trace	5				25	
4H-6,31	D		5	95	5				86			2	
5H-2,68	D		10	90	7	3	2	2	77	1			1
5H-4,77	M		90	10	50	20	10	10	4	2			
5H-5,33	D		7	93	5	2	1	2	77	1		1	
6H-3,70	D		5	95	2	1	1		80			trace	2
6H-6,51	M	99		1	90	2	5	trace	1			trace	
6H-7,50	D		5	95	3	1	1	trace	88			trace	1
7H-2,60	D	trace	15	85	7	2	3	trace	79			2	2
7H-4,46	M	2	10	88	5	2	2	trace	83			trace	5
7H-7,43	D		13	87	6	4	2	trace	79			trace	5
8H-1,80	D		20	80	7	5	5	1	76			2	1
8H-5,23	M	80	15	5	60	5	15	3	5			6	1
8H-7,30	D	trace	10	90	5	3	2	trace	81			1	2
9H-5,17	M	15	5	80	6	3	6	1	70	trace	1	5	
9H-4,60	D	5	20	75	15	2	2	1	71			1	1
10X-3,65	D	2	15	83	7	4	3	1	81			3	trace
10X-3,57	M	20	10	70	10	3	5	4	68			8	2
11P-1,60	D		3	97	10	1			76			5	
12Y-1,68	D			100	1				90				
13X-2,92	D		5	95	2				92				
13X-4,44	D		1	99	1				97				
14X-4,39	D		20	80	10	2			84			2	
14X-5,104	D		5	95	5	1	trace		85			5	
14X-5,88.5	M	80	20		89	5	2					2	
15X-1,97	D		1	99	1				94			trace	
15X-4,45	M	25	75		8	1	2	2	81			5	
15X-5,35	D	2	10	88	2				93			1	
16Y-1,41	D		5	95	3				87			5	
17X-1,76	D		5	95	10	trace	trace	1	83			1	
17X-3,22.5	M	10	90		93	trace	1	3				3	
17X-4,32	D		2	98	5	trace	trace	5	88			1	
18X-1,58	D		7	93	3	1	1	2	86	1			2
18X-2,83	D		9	91	3	1	1	2	82	1		1	2
19X-1,115	D		7	93	4	trace	trace	2	87	trace			2
19X-1,99	M		70	30	28	10	10	15	26	1		2	3
19X-3,57	D		5	95	2	1	1	2	87			1	
20X-1,49	M	5	30	65	20	7	5	2	34			3	3
20X-2,81	D		20	80	10	4	5	1	63			2	3
20X-5,142	D		10	90	5	1	3	1	80			trace	2
23X-2,90	D	trace	10	90	3	2	2	1	77			2	
24X-2,50	D	trace	3	97	2	1	trace	trace	86			1	
24X-1,36	M	85	trace	15	39	25	10	6	13			3	trace
25X-1,90	D	trace	7	93	3	2	2	trace	82			1	
25X-1,91	M	60	5	35	34	15	10	3	30			1	2
25X-6,100	D		2	98	1	trace	trace		88			1	trace
26X-3,50	D	7	15	78	8	7	5	2	70	trace		1	
26X-3,52	M	90	2	8	67	3	5	3	8			7	
26X-2,56	D		5	95	2	1	1	trace	79	trace		2	7
28P-1,69	D		10	90	3	trace	trace		90			5	
29Y-1,9	M	90	2	7	35	15	30	7				5	3
29Y-1,33	D		1	99	trace	trace	trace		88				5
30X-2,34	M	100			85			5				5	
30X-3,62	D		10	90	5			1	87			2	
30X-6,59	D		10	90	5			2	85			4	
31X-1,46	D		5	95	5	trace			90				trace
31X-114,114	M			100					95			5	

Table 1. Smear slide data for Hole NGHP-01-07B.—Continued

Sample reference		Biogenic							Comments
Core, section, depth (cm, in section)	Lithology	Foraminifera	Nanno fossils	Carbonate shell fragments	Diatoms	Radiolarians	Sponge spicules	Plant debris	
NGHP-01-07B—Continued									
1H-1,68	D	trace	1					1	
1H-2,37	D		3					1	
2H-2,84	D		5					1	
2H-4,80	D	1	5					1	
3H-2,90	M								Bipyramidal pyrite crystals
3H-2,111	D	1	5					1	
3H-5,34	D	1	2					1	
3H-6,129	M	1							From silt layer
4H-4,11.5	D		5					trace	
4H-5,89	M								From silt layer
4H-6,31	D	2	5					trace	
5H-2,68	D		5					2	
5H-4,77	M		3					1	From silt layer
5H-5,33	D	2	7					2	Nice euhedral crystal
6H-3,70	D	1	13					trace	
6H-6,51	M	2						trace	From sand layer
6H-7,50	D	1	5					trace	
7H-2,60	D	trace	5					trace	
7H-4,46	M	1	2					trace	From silt layer
7H-7,43	D	1	3						
8H-1,80	D	1	2						
8H-5,23	M		5						From sand layer
8H-7,30	D	1	5						
9H-5,17	M	5	3					trace	From sand layer
9H-4,60	D	2	5					trace	
10X-3,65	D	trace	1				trace		
10X-3,57	M	trace							From sand layer
11P-1,60	D	1	2					5	
12Y-1,68	D	2	5					2	
13X-2,92	D	1	2					3	
13X-4,44	D		2					trace	
14X-4,39	D		1					1	
14X-5,104	D		1					3	Large organic debris
14X-5,88.5	M	2							From sand layer
15X-1,97	D		5						
15X-4,45	M	1							From silt layer
15X-5,35	D	trace	3					1	
16Y-1,41	D	1	2					2	
17X-1,76	D	trace	trace					5	Large organic debris
17X-3,22.5	M	trace							From silt layer
17X-4,32	D	trace						1	Large organic debris
18X-1,58	D		3					1	
18X-2,83	D	1	4					2	
19X-1,115	D		3					2	Possible apatite
19X-1,99	M		2					3	Possible apatite, amphibole
19X-3,57	D		4					2	
20X-1,49	M	1	25						From silt layer
20X-2,81	D	2	10						
20X-5,142	D	trace	8					trace	
23X-2,90	D	2	10					1	
24X-2,50	D		10					trace	
24X-1,36	M	1	3						From sand layer
25X-1,90	D	2	8						
25X-1,91	M	2	3						From sand layer
25X-6,100	D	trace	10						
26X-3,50	D	trace	7						
26X-3,52	M	7	trace						From sand layer
26X-2,56	D	1	7						
28P-1,69	D							2	
29Y-1,9	M		5						
29Y-1,33	D		7						
30X-2,34	M	5							From sand layer
30X-3,62	D	2						3	
30X-6,59	D	3						1	
31X-1,46	D		2					3	
31X-114,114	M								From carbonate band, small carbonate present

Note: M = minor lithology, D = dominant lithology.

Table 2. Smear slide data for Hole NGHP-01-07D.

Sample reference		Texture			Mineral								
Core, section, depth (cm, in section)	Lithology	Sand	Silt	Clay	Quartz	Feldspar	Mica	Heavy minerals	Clay minerals	Volcanic glass	Glauconite	Iron sulfides	Authigenic carbonates
NGHP-01-07D													
1X-1,116	M	70	10	20	30	18	10	6	15			8	
1X-1,103	M	20	trace	80	8	5	5	trace	10	trace		48	24
1X-2,65	D	7	10	83	7	3	3	1	67		3	3	8
1X-6,105	D	15	25	60	15	7	10	2	55			1	2
2X-2,99	D	trace	3	97	2	trace	1	trace	86		trace	2	2
2X-5,71	D		15	85	10	2	2	trace	68	trace		2	5
2X-5,70	M	2	5	93	4	1	2	trace	60	trace		2	5
3X-2,65	D	trace	10	90	7	trace	2		65			1	14
3X-2,66	M		10	90	5	3	3	trace	40			5	22
4X-1,62	D	trace	30	70	15	10	7		50	trace		5	13
4X-3,19	M	trace	7	93	5	trace	2	trace	45			4	32

Sample reference		Biogenic							Comments
Core, section, depth (cm, in section)	Lithology	Foraminifera	Nannofossils	Carbonate shell fragments	Diatoms	Radiolarians	Sponge spicules	Plant debris	
NGHP-01-07D									
1X-1,116	M	8	5					trace	Highly angular to sub-angular grains
1X-1,103	M		trace						From sand/carbonate layer
1X-2,65	D	3	2						
1X-6,105	D	1	7					trace	
2X-2,99	D		7					trace	Auth. carb. seem to surround opaques
2X-5,71	D		11						
2X-5,70	M		26					trace	From carbonate layer
3X-2,65	D		11						
3X-2,66	M		22						From carbonate layer
4X-1,62	D	trace						trace	
4X-3,19	M		12						From carbonate layer

Note: M = minor lithology, D = dominant lithology

Table 3. Coarse fraction (>63 µm) sieve data for Hole NGHP-01-07D.

Sample reference		Mineral										
Core, section, depth (cm, in section)	MBSF	Quartz	Feldspar	Mica	Heavy minerals	Volcanic glass	Pyrite	Iron sulfides	Framboidal pyrite	Rock fragments	Other minerals	Authigenic carbonates
NGHP-01-07D	232.47	70		20	5		3					
1X-1,103	232.23	80		2	10						3	
1X-2,65	233.35	40		30	2			2			3	
1X-6,105	239.75	80		10	5		2					
2X-2,99	241.49	80		10	3						2	
2X-5,71	245.71	70	13	7	10							
3X-2,65	248.75	75		15	5						2	

Sample reference		Biogenic								Comments
Core, section, depth (cm, in section)	Foraminifera	Carbonate shell fragments	Diatoms	Radiolarians	Silicoflagellates	Siliceous shell fragments	Sponge spicules	Other biogenic	Plant debris	
NGHP-01-07D									2	
1X-1,103									5	
1X-2,65								3	20	
1X-6,105									3	
2X-2,99									5	
2X-5,71									trace	
3X-2,65	1								2	

Table 4. Sand/silt laminae and beds, and silty clay occurrences at Hole NGHP-01-07B. (To view complete table, please refer to the ASCII files.)

Core, section	Position start	Position end	Depth top (mbsf)	Depth base (mbsf)	Type
			NGHP-01-07B		
2H-1	70	140	3.4	4.1	Silty clay
2H-2	10	140	4.3	5.6	Silty clay
2H-3	0	110	5.7	6.8	Silty clay
2H-4	0	27	7.2	7.47	Silty clay
3H-5	65	65	18.85		Silt bed
3H-6	41	41	20.11	20.11	Silt laminae
3H-6	66	67	20.36	20.37	Silt bed
3H-6	67	114	20.37	20.84	Multiple silt laminae
3H-6	120	120	20.9	20.9	v.f. sand bed
3H-6	128	129.5	20.98	20.995	Sand bed
3H-7	6	8	21.26	21.28	Silt laminae
4H-1	115	119	22.85	22.89	Multiple silt laminae
4H-1	142	142	23.12	23.12	Silt laminae
4H-2	35	72	23.55	23.92	Multiple silt laminae
4H-2	88	105	24.08	24.25	Multiple silt laminae
4H-3	11	14	24.81	24.84	Silt laminae
4H-3	50	72	25.2	25.42	Multiple silt laminae
4H-3	80	85	25.5	25.55	Multiple silt laminae
4H-3	90	90	25.6	25.6	Silt laminae
4H-3	96	98	25.66	25.68	Silt laminae
4H-3	104	105	25.74	25.75	Silt laminae
4H-4	22	54	26.42	26.74	Multiple silt laminae
4H-4	82	108	27.02	27.28	Multiple silt laminae
4H-4	113	116	27.33	27.36	Silt laminae
4H-4	123	123	27.43	27.43	Silt laminae
4H-4	132	133	27.52	27.53	Silt laminae
4H-4	140	140	27.6	27.6	Silt laminae
4H-4	145	145	27.65	27.65	Silt laminae
4H-4	148	149	27.68	27.69	Silt laminae
4H-5	0	20	27.7	27.9	Multiple silt laminae
4H-5	39	39	28.09	28.09	Silt laminae
4H-5	56	62	28.26	28.32	Silt laminae
4H-5	87	100	28.57	28.7	Multiple silt laminae
4H-6	44	44	29.64	29.64	Silt bed
4H-6	57	57	29.77	29.77	Silt bed
4H-6	75	75	29.95	29.95	Silt bed
4H-7	16	16	30.36	30.36	Silt bed
4H-7	23	29	30.43	30.49	Multiple silt beds
4H-7	39	39	30.59	30.59	Silt bed
4H-7	50	50	30.7	30.7	Silt bed
4H-7	55	55	30.75	30.75	Silt bed
4H-7	60	60	30.8	30.8	Silt bed
4H-7	63	63	30.83	30.83	Silt bed
5H-1	0	150	31.2	32.7	Silty clay
5H-1	18	18	31.38	31.38	Silt bed
5H-1	37	37	31.57	31.57	Silt bed
5H-1	47	47	31.67	31.67	Silt laminae
5H-1	123	125	32.43	32.45	Silt bed
5H-1	138	141	32.58	32.61	Multiple silt beds
5H-2	0	150	32.7	34.2	Silty clay
5H-2	23	25	32.93	32.95	Silt bed
5H-2	27	27	32.97	32.97	Silt laminae
5H-2	35	35	33.05	33.05	Silt laminae
5H-2	38	38	33.08	33.08	Silt laminae
5H-2	93	93	33.63	33.63	Silt laminae
5H-2	132	139	34.02	34.09	Silt laminae
5H-3	0	110	34.2	35.3	Silty clay
5H-4	0	150	35.7	37.2	Silty clay
5H-4	32	34	36.02	36.04	Silt bed
5H-4	54	54	36.24	36.24	Silt bed
5H-4	58	61	36.28	36.31	Silt bed
5H-4	64	64	36.34	36.34	Silt bed

Table 4. Sand/silt laminae and beds, and silty clay occurrences at Hole NGHP-01-07B. (To view complete table, please refer to the ASCII files.)—Continued

Core, section	Position start	Position end	Depth top (mbsf)	Depth base (mbsf)	Type
NGHP-01-07B—Continued					
5H-4	77	77	36.47	36.47	Silt bed
5H-4	84	86	36.54	36.56	Silt bed
5H-4	93	93	36.63	36.63	Silt bed
5H-4	114	115	36.84	36.85	Silt bed
5H-4	130	130	37	37	Silt bed
5H-5	5	5	37.25	37.25	Silt laminae
5H-5	10	10	37.3	37.3	Silt laminae
5H-5	20	20	37.4	37.4	Silt laminae
5H-5	24	28	37.44	37.48	Multiple silt laminae
5H-5	40	41	37.6	37.61	Silt laminae
5H-5	44	49	37.64	37.69	Multiple silt laminae
5H-6	46	50	39.16	39.2	Multiple silt laminae
5H-6	63	63	39.33	39.33	Silt bed
5H-6	74	75	39.44	39.45	Silt bed
5H-6	92	92	39.62	39.62	Silt laminae
5H-6	119	120	39.89	39.9	Silt laminae
6H-1	18	18	40.88	40.88	Silt laminae
6H-1	30	30	41	41	Silt laminae
6H-1	35	35	41.05	41.05	Silt laminae
6H-1	39	39	41.09	41.09	Silt laminae
6H-1	42	42	41.12	41.12	Silt laminae
6H-1	44	44	41.14	41.14	Silt laminae
6H-1	47	47	41.17	41.17	Silt laminae
6H-1	53	53	41.23	41.23	Silt laminae
6H-1	77	77	41.47	41.47	Silt laminae
6H-1	91	91	41.61	41.61	Silt laminae
6H-1	114	114	41.84	41.84	Silt laminae
6H-1	116	116	41.86	41.86	Silt laminae
6H-1	127	127	41.97	41.97	Silt laminae
6H-2	114	114	43.34	43.34	Silt laminae
6H-2	140	140	43.6	43.6	Sand laminae
6H-3	19	19	43.89	43.89	Sand laminae
6H-3	46	46	44.16	44.16	Sand laminae
6H-3	50	50	44.2	44.2	Sand laminae
6H-3	66	66	44.36	44.36	Sand laminae
6H-3	82	82	44.52	44.52	Sand laminae
6H-4	37	37	45.57	45.57	Sand laminae
6H-4	44	44	45.64	45.64	Sand filled burrow
6H-4	52	52	45.72	45.72	Sand filled burrow
6H-4	53	53	45.73	45.73	Sand filled burrow
6H-4	88	88	46.08	46.08	Silt laminae
6H-4	89	89	46.09	46.09	Silt laminae
6H-4	90	90	46.1	46.1	Silt laminae
6H-4	123	123	46.43	46.43	Sand laminae
6H-4	138	138	46.58	46.58	Silt laminae
6H-4	143	143	46.63	46.63	Silt laminae
6H-5	14	14	46.84	46.84	Silt laminae
6H-5	45	45	47.15	47.15	Silt laminae
6H-5	78	78	47.48	47.48	Sand filled burrow
6H-5	80	80	47.5	47.5	Silt laminae
6H-5	85	85	47.55	47.55	Silt laminae
6H-5	87	87	47.57	47.57	Silt laminae
6H-6	4	4	48.24	48.24	Silt laminae
6H-6	10	13	48.3	48.33	Multiple silt laminae
6H-6	19	19	48.39	48.39	Silt laminae
6H-6	23	23	48.43	48.43	Silt laminae
6H-6	28	28	48.48	48.48	Silt laminae
6H-6	51	52	48.71	48.72	Silt laminae
6H-6	58	58	48.78	48.78	Silt bed
6H-6	71	71	48.91	48.91	Silt bed
6H-7	19	19	49.16	49.16	Sand laminae

Table 4. Sand/silt laminae and beds, and silty clay occurrences at Hole NGHP-01-07B. (To view complete table, please refer to the ASCII files.)—Continued

Core, section	Position start	Position end	Depth top (mbsf)	Depth base (mbsf)	Type
NGHP-01-07B—Continued					
6H-7	31	31	49.28	49.28	Sand laminae
6H-7	33	33	49.3	49.3	Sand laminae
6H-7	37	37	49.34	49.34	Sand laminae
6H-7	39	39	49.36	49.36	Sand laminae
6H-7	41	41	49.38	49.38	Sand laminae
6H-7	43	43	49.4	49.4	Sand laminae
6H-7	63	63	49.6	49.6	Sand laminae
6H-7	75	75	49.72	49.72	Sand laminae
7H-2	117	117	52.87	52.87	Sand laminae
7H-3	29	29	53.41	53.41	Silt laminae
7H-3	36	36	53.48	53.48	Silt laminae
7H-3	73	73	53.85	53.85	Silt laminae
7H-4	2	3	54.64	54.65	Silt laminae
7H-4	10	10	54.72	54.72	Silt laminae
7H-4	26	26	54.88	54.88	Silt laminae
7H-4	45	46	55.07	55.08	Silt laminae
7H-4	48	48	55.1	55.1	Silt laminae
7H-4	52	52	55.14	55.14	Silt laminae
7H-4	86	86	55.48	55.48	Silt laminae
7H-4	96	96	55.58	55.58	Silt laminae
7H-4	102	102	55.64	55.64	Silt laminae
7H-4	134	134	55.96	55.96	Silt laminae
7H-5	24	24	56.36	56.36	Silt laminae
7H-5	42	42	56.54	56.54	Silt laminae
7H-5	45	45	56.57	56.57	Silt laminae
7H-5	84	84	56.96	56.96	Silt laminae
8H-1	14	14	59.84	59.84	Silt laminae
8H-1	27	27	59.97	59.97	Silt laminae
8H-1	32	32	60.02	60.02	Silt laminae
8H-1	57	57	60.27	60.27	Silt laminae
8H-2	8	8	61.15	61.15	Silt laminae
8H-2	18	18	61.25	61.25	Silt laminae
8H-2	19	19	61.26	61.26	Silt laminae
8H-2	23	23	61.3	61.3	Silt laminae
8H-2	48	48	61.55	61.55	Silt laminae
8H-2	51	51	61.58	61.58	Silt laminae
8H-2	57	57	61.64	61.64	Silt laminae
8H-2	57	57	61.64	61.64	Silt laminae
8H-2	58	58	61.65	61.65	Silt laminae
8H-2	60	60	61.67	61.67	Silt laminae
8H-2	64	64	61.71	61.71	Silt laminae
8H-2	65	65	61.72	61.72	Silt laminae
8H-2	69	69	61.76	61.76	Silt laminae
8H-2	108	150	62.15	62.57	Multiple silt laminae
8H-3	0	92	62.56	63.48	Multiple silt laminae
8H-4	0	150	63.98	65.48	Multiple silt laminae
8H-4	19	24	64.17	64.22	Sand bed w/pebble
8H-5	0	90	65.48	66.38	Multiple silt laminae
8H-5	23	23	65.71	65.71	Sand bed
8H-6	0	72	66.98	67.7	Multiple silt laminae
8H-6	72	100	67.7	67.98	Multiple sand laminae
9H-1	50	50	69.7	69.7	Silt filled burrow
9H-2	13	15	70.14	70.16	Silt filled burrow
9H-4	0	72	72.13	72.85	Multiple silt laminae
9H-3	70	70	72.43	72.43	Silt laminae
9H-6	15	15	75.18	75.18	Silt laminae
9H-6	16	16	75.19	75.19	Silt laminae
9H-6	23	23	75.26	75.26	Silt laminae
9H-6	38	38	75.41	75.41	Silt laminae
9H-5	14	17	75.45	75.45	Multiple silt laminae
9H-6	48	48	75.51	75.51	Silt filled burrow

Table 4. Sand/silt laminae and beds, and silty clay occurrences at Hole NGHP-01-07B. (To view complete table, please refer to the ASCII files.)—Continued

Core, section	Position start	Position end	Depth top (mbsf)	Depth base (mbsf)	Type
NGHP-01-07B—Continued					
9H-6	72	72	75.75	75.75	Silt laminae
8H-7	0	150	76.05	77.55	Multiple silt laminae
10X-1	27	27	78.97	80.97	Silt laminae
10X-1	40	40	79.1	79.1	Silt laminae
10X-1	44	44	79.14	79.14	Silt laminae
10X-1	56	57	79.26	79.27	Silt laminae
10X-1	60	63	79.3	79.33	Multiple silt laminae
10X-1	73	73	79.43	79.43	Silt laminae
10X-1	84	84	79.54	79.54	Silt laminae
10X-1	92	93	79.62	79.63	Silt laminae
10X-1	99	102	79.69	79.72	Multiple silt laminae
10X-1	135	137	80.05	80.07	Silt laminae
10X-2	20	21	80.4	80.41	Silt laminae
10X-2	35	37	80.55	80.57	Silt laminae
10X-2	44.5	44.5	80.645	80.645	Silt laminae
10X-2	58	60	80.78	80.8	Silt laminae
10X-2	75	78	80.95	80.98	Multiple silt laminae
10X-2	88	89	81.08	81.09	Silt laminae
10X-2	105	105	81.25	81.25	Silt laminae
10X-2	112	112	81.32	81.32	Silt laminae
10X-2	113	113	81.33	81.33	Silt laminae
10X-2	115	115	81.35	81.35	Silt laminae
10X-2	124	128	81.44	81.48	Multiple silt laminae
10X-3	13	13	81.83	81.83	Silt laminae
10X-3	18	19	81.88	81.89	Silt laminae
10X-3	46	46	82.16	82.16	Silt laminae
10X-3	57	57	82.27	82.27	Silt laminae
10X-3	59	59	82.29	82.29	Silt laminae
10X-3	61	61	82.31	82.31	Silt laminae
10X-3	68	70	82.38	82.4	Silt laminae
10X-3	76	77	82.46	82.47	Silt laminae
10X-4	3	3	83.23	83.23	Silt laminae
10X-4	15	17	83.35	83.37	Silt laminae
11P-1	0	20	84.2	84.4	Silty clay
11P-1	50	90	84.7	85.1	Silty clay
10X-5	12	12	84.82	84.82	Silt laminae
10X-5	13	13	84.83	84.83	Silt laminae
12Y-1	0	89	85.2	86.09	Multiple silt laminae
13X-2	90	90	87.4	87.4	Silt laminae
13X-2	99	99	87.49	87.49	Silt laminae
13X-2	113	113	87.63	87.63	Silt laminae
13X-2	129	131	87.79	87.81	Silt laminae
10X-6	10	10	88.42	88.42	Silt laminae
10X-6	18	18	88.42	88.42	Silt laminae
10X-6	24	24	88.42	88.42	Silt laminae
10X-6	41	41	88.42	88.42	Silt laminae
13X-4	12	42	88.72	89.02	Silty clay
13X-4	48	48	89.08	89.08	Silty clay
13X-4	53	53	89.13	89.13	Silty clay
14X-1	3	3	95.73	95.73	Silt bed
14X-1	10	13	95.8	95.83	Silt bed
14X-1	29	31	95.99	96.01	Silt bed
14X-1	33	41	96.03	96.11	Multiple silt laminae
14X-1	57	69	96.27	96.39	Multiple silt laminae
14X-1	72	74	96.42	96.44	Silt laminae
14X-1	84	90	96.54	96.6	Multiple silt beds
14X-2	12	12	97.32	97.32	Silt laminae
14X-2	32	34	97.52	97.54	Silt laminae
14X-2	68	70	97.88	97.9	Silt laminae
14X-3	0	6	98.7	98.76	Multiple silt laminae
14X-3	21	22	98.91	98.92	Silt bed

Table 4. Sand/silt laminae and beds, and silty clay occurrences at Hole NGHP-01-07B. (To view complete table, please refer to the ASCII files.)—Continued

Core, section	Position start	Position end	Depth top (mbsf)	Depth base (mbsf)	Type
NGHP-01-07B—Continued					
14X-3	30	36	99	99.06	Multiple silt laminae
14X-3	40	42	99.1	99.12	Silt bed
14X-3	52	56	99.22	99.26	Multiple silt laminae
14X-3	63	63	99.33	99.33	Silt bed
14X-3	65	74	99.35	99.44	Multiple silt beds
14X-4	8	9	99.78	99.79	Silt/sand bed
14X-4	14	16	99.84	99.86	Silt/sand bed
14X-4	21	21	99.91	99.91	Silt/sand bed
14X-4	27	30	99.97	100	Silt/sand bed
14X-4	46	50	100.16	100.2	Multiple silt/sand beds
14X-5	3	9	100.43	100.49	Multiple silt beds
14X-5	16	16	100.56	100.56	Silt bed
14X-5	20	20	100.6	100.6	Silt bed
14X-5	27	27	100.67	100.67	Silt bed
14X-5	29	40	100.69	100.8	Multiple silt beds
14X-5	48	49	100.88	100.89	Silt bed
14X-5	56	59	100.96	100.99	Multiple silt beds
14X-5	83	83	101.23	101.23	Sand bed
14X-5	86.5	89	101.265	101.29	Multiple sand beds
14X-5	91	91	101.31	101.31	Sand bed
14X-5	100	100	101.4	101.4	Sand bed
14X-5	112	112	101.52	101.52	Sand bed
15X-1	10	10	105.4	105.4	Sand bed
15X-1	22	22	105.52	105.52	Sand bed
15X-1	34	34	105.64	105.64	Sand bed
15X-1	37	38	105.67	105.68	Sand bed
15X-1	46	46	105.76	105.76	Sand bed
15X-1	51	56	105.81	105.86	Multiple silt laminae
15X-1	62	65	105.92	105.95	Multiple silt laminae
15X-1	82	82	106.12	106.12	Sand bed
15X-1	86	90	106.16	106.2	Multiple silt laminae
15X-1	101	102	106.31	106.32	Silt laminae
15X-1	115	117	106.45	106.47	Silt laminae
15X-1	133	133	106.63	106.63	Silt laminae
15X-2	0	3	106.76	106.79	Silty sand bed
15X-2	17	22	106.93	106.98	Silty sand bed
15X-2	28	28	107.04	107.04	Sand bed
15X-2	48	50	107.24	107.26	Sand bed
15X-2	56	56	107.32	107.32	Sand bed
15X-2	63	67	107.39	107.43	Multiple silt beds
15X-2	72	74	107.48	107.5	Multiple silt beds
15X-2	77	78	107.53	107.54	Silt bed
15X-2	81	82	107.57	107.58	Silt bed
15X-2	87	87	107.63	107.63	Silt bed
15X-3	12	12	108.38	108.38	Sand bed
15X-3	33	42	108.59	108.68	Multiple silt beds
15X-3	46	46	108.72	108.72	Silt bed
15X-3	49	51	108.75	108.77	Multiple silt beds
15X-3	61	63	108.87	108.89	Multiple silt beds
15X-3	65	65	108.91	108.91	Silt bed
15X-4	8	14	109.84	109.9	Silt laminae
15X-4	20	20	109.96	109.96	Silt laminae
15X-4	24	27	110	110.03	Multiple silt laminae
15X-4	32	32	110.08	110.08	Silt laminae
15X-4	45	45	110.21	110.21	Silt laminae
15X-4	67	68	110.43	110.44	Sand bed
15X-5	28.5	28.5	111.545	111.545	Silt bed
15X-5	31	31	111.57	111.57	Silt bed
15X-5	47	52	111.73	111.78	Silt bed
17X-1	0	150	114.2	115.7	Silty clay
16Y-1	10	18	114.3	114.38	Silty clay

Table 4. Sand/silt laminae and beds, and silty clay occurrences at Hole NGHP-01-07B. (To view complete table, please refer to the ASCII files.)—Continued

Core, section	Position start	Position end	Depth top (mbsf)	Depth base (mbsf)	Type
NGHP-01-07B—Continued					
16Y-1	19	19	114.39	114.39	Sand bed
16Y-1	25	25	114.45	114.45	Sand bed
16Y-1	41	48	114.61	114.68	Multiple silt laminae
16Y-1	67	76	114.87	114.96	Multiple silt laminae
16Y-1	80	80	115	115	Silt laminae
17X-1	92	93	115.12	115.13	Sand bed
17X-1	105	106	115.25	115.26	Silt bed
17X-2	12	12	116.82	116.82	Silt bed
17X-2	33	33	117.03	117.03	Silt bed
17X-2	55	55	117.25	117.25	Silt bed
17X-3	23	23	118.43	118.43	Sand bed
17X-3	37	41	118.57	118.61	Silty clay
17X-4	2	2	119.68	119.68	Silt bed
17X-4	39	40	120.05	120.06	Silt bed
17X-4	57	57	120.23	120.23	Silt bed
17X-4	81	85	120.47	120.51	Multiple silt laminae
17X-4	110	110	120.76	120.76	Silt bed
17X-5	2	2	121.18	121.18	Silt bed
17X-5	8	11	121.24	121.27	Multiple silt laminae
17X-5	20	26	121.36	121.42	Multiple silt laminae
17X-5	32	34	121.48	121.5	Silt laminae
17X-5	51	56	121.67	121.72	Multiple silt laminae
17X-5	63	65	121.79	121.81	Silt laminae
17X-6	57	86	123.07	123.36	Silty clay
17X-6	86	86	123.36	123.36	Sand bed
17X-6	101	101	123.51	123.51	Silt bed
17X-6	111	111	123.61	123.61	Sand bed
17X-6	118	120	123.68	123.7	Sand bed
18X-1	19	19	124.99	124.99	Silt laminae
18X-1	24	24	125.04	125.04	Silt laminae
18X-1	31	31	125.11	125.11	Silt laminae
18X-1	47	54	125.27	125.34	Multiple silt laminae
18X-1	63	63	125.43	125.43	Silt laminae
18X-1	66	66	125.46	125.46	Silt laminae
18X-1	73	73	125.53	125.53	Silt laminae
18X-1	87	88	125.67	125.68	Silt bed
18X-1	100	104	125.8	125.84	Multiple silt laminae
18X-1	114	121	125.94	126.01	Multiple silt laminae
18X-2	47	50	126.57	126.6	Multiple silt beds
18X-2	62	62	126.72	126.72	Silt laminae
18X-2	65	65	126.75	126.75	Silt laminae
18X-2	74	74	126.84	126.84	Silt laminae
18X-2	77	79	126.87	126.89	Multiple silt laminae
18X-2	97	97	127.07	127.07	Silt laminae
18X-3	12	14	127.72	127.74	Multiple silt laminae
18X-3	18	18	127.78	127.78	Silt bed
18X-3	29	29	127.89	127.89	Silt laminae
18X-3	42	44	128.02	128.04	Multiple silt laminae
18X-3	47	47	128.07	128.07	Silt laminae
18X-3	55	58	128.15	128.18	Silt bed
18X-3	67	67	128.27	128.27	Silt laminae
18X-3	69	69	128.29	128.29	Silt laminae
18X-3	73	73	128.33	128.33	Silt laminae
18X-3	77	77	128.37	128.37	Silt bed
18X-3	84	84	128.44	128.44	Silt bed
18X-3	96	96	128.56	128.56	Silt laminae
18X-3	106	108	128.66	128.68	Multiple silt laminae
18X-4	6	6	129.16	129.16	Silt bed
18X-4	9	9	129.19	129.19	Silt laminae
18X-4	14.5	14.5	129.245	129.245	Silt laminae
18X-4	17.5	17.5	129.275	129.275	Silt bed

Table 4. Sand/silt laminae and beds, and silty clay occurrences at Hole NGHP-01-07B. (To view complete table, please refer to the ASCII files.)—Continued

Core, section	Position start	Position end	Depth top (mbsf)	Depth base (mbsf)	Type
NGHP-01-07B—Continued					
18X-4	19	19	129.29	129.29	Silt laminae
18X-4	25	35	129.35	129.45	Multiple silt laminae
18X-4	39	39	129.49	129.49	Silt laminae
18X-4	44	66	129.54	129.76	Multiple silt laminae
18X-4	74	74	129.84	129.84	Silt bed
18X-4	76	76	129.86	129.86	Silt laminae
18X-4	84	84	129.94	129.94	Silt bed
18X-4	86	89	129.96	129.99	Multiple silt laminae
18X-4	95	97	130.05	130.07	Multiple silt laminae
18X-4	107	107	130.17	130.17	Silt laminae
18X-4	113	113	130.23	130.23	Silt laminae
18X-4	117	117	130.27	130.27	Silt laminae
18X-4	130	133	130.4	130.43	Multiple silt laminae
18X-4	136	137	130.46	130.47	Silt laminae
19X-1	26	27	134.66	134.67	Silt bed
19X-1	86	86	135.26	135.26	Silt bed
19X-1	137	137	135.77	135.77	Silt bed
19X-3	3	5	136.73	136.75	Multiple silt laminae
19X-3	42	43	137.12	137.13	Silt laminae
19X-3	63	64	137.33	137.34	Silt laminae
20X-1	47	47	144.47	144.47	Silt laminae
20X-1	57	57	144.57	144.57	Silt laminae
20X-1	69	69	144.69	144.69	Silt laminae
20X-1	70	70	144.7	144.7	Silt laminae
20X-2	50	50	145.51	145.51	Silt laminae
20X-2	70	70	145.71	145.71	Silt laminae
20X-2	117	117	146.18	146.18	Silt laminae
20X-2	121	121	146.22	146.22	Silt laminae
20X-2	123	123	146.24	146.24	Silt laminae
20X-3	43	43	146.94	146.94	Silt laminae
20X-3	46	47	146.97	146.98	Silt laminae
20X-3	59	61	147.1	147.12	Multiple silt laminae
20X-3	70	70	147.21	147.21	Silt laminae
20X-3	73	73	147.24	147.24	Silt laminae
20X-4	15	15	148.16	148.16	Silt laminae
20X-4	32	32	148.33	148.33	Silt laminae
20X-4	68	70	148.69	148.71	Multiple silt laminae
20X-4	84	84	148.85	148.85	Silt laminae
20X-5	12	12	149.63	149.63	Silt laminae
20X-5	13	13	149.64	149.64	Silt laminae
20X-5	23	23	149.74	149.74	Silt laminae
20X-5	29	29	149.8	149.8	Silt laminae
20X-5	38	38	149.89	149.89	Silt laminae
20X-5	65	67	150.16	150.18	Multiple silt laminae
23X-1	2	2	150.22	150.22	Silt laminae
23X-1	3	3	150.23	150.23	Silt laminae
20X-5	75	83	150.26	150.34	Multiple silt laminae
23X-1	21	21	150.41	150.41	Silt laminae
23X-1	30	30	150.5	150.5	Silt laminae
20X-5	101	101	150.52	150.52	Sand laminae
23X-1	48	48	150.68	150.68	Silt laminae
23X-2	60	68	152.3	152.38	Multiple silt laminae
23X-2	127	130	152.97	153	Multiple silt laminae
23X-3	40	40	153.6	153.6	Silt laminae
24X-1	8	8	159.88	159.88	Sand bed
24X-1	36	37	160.16	160.17	Sand bed
24X-1	50	53	160.3	160.33	Multiple sand beds
24X-1	67	75	160.47	160.55	Multiple sand beds
24X-2	17	17	161.47	161.47	Silt laminae
24X-2	26	26	161.56	161.56	Silt laminae
24X-2	32	32	161.62	161.62	Silt laminae

Table 4. Sand/silt laminae and beds, and silty clay occurrences at Hole NGHP-01-07B. (To view complete table, please refer to the ASCII files.)—Continued

Core, section	Position start	Position end	Depth top (mbsf)	Depth base (mbsf)	Type
NGHP-01-07B—Continued					
24X-2	67	67	161.97	161.97	Silt laminae
24X-2	72	72	162.02	162.02	Silt laminae
24X-2	88	88	162.18	162.18	Silt laminae
25X-1	41	41	169.81	169.81	Sand laminae
25X-1	46	46	169.86	169.86	Sand laminae
25X-1	66	66	170.06	170.06	Sand laminae
25X-1	70	71	170.1	170.11	Sand laminae
25X-1	77	77	170.17	170.17	Sand laminae
25X-1	82	82	170.22	170.22	Sand laminae
25X-1	90	90	170.3	170.3	Sand laminae
25X-1	95	95	170.35	170.35	Sand laminae
25X-1	100	100	170.4	170.4	Sand laminae
25X-1	104	104	170.44	170.44	Sand laminae
25X-1	117	118	170.57	170.58	Sand laminae
25X-1	124	125	170.64	170.65	Sand laminae
25X-1	132	133	170.72	170.73	Sand laminae
25X-1	141	141	170.81	170.81	Sand laminae
25X-1	144	144	170.84	170.84	Sand laminae
25X-2	0	13	170.9	171.03	Multiple sand laminae
25X-2	18	18	171.08	171.08	Sand laminae
25X-2	20	21	171.1	171.11	Sand laminae
25X-2	29	30	171.19	171.2	Sand laminae
25X-2	39	39	171.29	171.29	Sand laminae
25X-2	55	56	171.45	171.46	Sand laminae
25X-2	59	59	171.49	171.49	Sand laminae
25X-2	63	63	171.53	171.53	Sand laminae
25X-3	0	7	171.68	171.75	Multiple sand beds
25X-3	12	25	171.8	171.93	Multiple sand beds
25X-3	34	34	172.02	172.02	Sand bed
25X-3	50	55	172.18	172.23	Multiple sand beds
25X-3	61	62	172.29	172.3	Sand bed
25X-3	79	83	172.47	172.51	Multiple sand beds
26X-1	45	50	174.65	174.7	Multiple sand laminae
25X-6	85	85	176.47	176.47	Sand bed
25X-6	29	29	176.91	176.91	Sand bed
26X-2	73	73	176.43	176.43	Sand laminae
25X-6	39	39	176.56	176.56	Sand laminae
25X-6	38	38	176.41	176.42	Sand laminae
25X-6	23	24	176.93	176.97	Sand laminae
25X-6	75	79	176.89	176.89	Multiple sand laminae
25X-6	71	71	176.79	176.79	Sand laminae
25X-6	61	61	176.62	176.62	Sand laminae
25X-6	44	44	176.83	176.83	Sand bed
25X-6	65	65	176.71	176.73	Sand bed
25X-6	53	55	177.23	177.25	Sand bed
25X-6	105	107	176.28	176.28	Multiple sand laminae
25X-6	10	10	176.68	176.68	Sand bed
25X-6	50	50	176.51	176.51	Sand laminae
25X-6	33	33	176.8	176.8	Sand laminae
25X-6	62	62	176.7	176.73	Sand laminae
25X-5	52	55	179.31	179.31	Multiple sand beds
25X-5	16	17	179.31	179.31	Sand bed
25X-5	63	64	179.31	179.31	Sand bed
25X-5	5	5	179.31	179.31	Sand bed
25X-5	9	9	179.31	179.31	Sand bed
25X-5	33	33	179.31	179.31	Sand bed
25X-5	71	71	179.31	179.31	Sand bed
27X-1	0	150	183.8	185.3	Multiple sand laminae
27X-3	27	30	185.57	185.6	Multiple silt/sand laminae
27X-4	0	35	187.9	188.25	Multiple silt/sand laminae
27X-4	90	104	188.8	188.94	Multiple silt/sand laminae (2 cm thick)

Table 4. Sand/silt laminae and beds, and silty clay occurrences at Hole NGHP-01-07B. (To view complete table, please refer to the ASCII files.)—Continued

Core, section	Position start	Position end	Depth top (mbsf)	Depth base (mbsf)	Type
NGHP-01-07B—Continued					
28P-1	21	21	193.61	193.61	Sand bed
28P-1	28	28	193.68	193.68	Sand bed
28P-1	35	36	193.75	193.76	Sand bed
28P-1	83	84	194.23	194.24	Sand bed
29Y-1	0	3	194.4	194.43	Multiple sand beds
29Y-1	7	12	194.47	194.52	Multiple sand beds
29Y-1	13	20	194.53	194.6	Multiple sand beds
29Y-1	15	15	194.55	194.55	Sand bed
29Y-1	22	22	194.62	194.62	Sand bed
29Y-1	23	23	194.63	194.63	Sand bed
29Y-1	26	27	194.66	194.67	Sand bed
29Y-1	28	28	194.68	194.68	Sand bed
29Y-1	29	29	194.69	194.69	Sand bed
29Y-1	31	31	194.71	194.71	Sand bed
29Y-1	32	32	194.72	194.72	Sand bed
29Y-1	44	44	194.84	194.84	Sand bed
29Y-1	49	49	194.89	194.89	Sand bed
29Y-1	63	63	195.03	195.03	Sand bed
29Y-1	67	67	195.07	195.07	Sand bed
29Y-1	70	70	195.1	195.1	Sand bed
30X-1	5	5	195.45	195.45	Silt bed
30X-1	10	13	195.5	195.53	Multiple silt beds
30X-1	18	20	195.58	195.6	Multiple silt beds
30X-1	31	31	195.71	195.71	Silt bed
30X-1	32	32	195.72	195.72	Silt bed
30X-1	48	49	195.88	195.89	Silt bed
30X-2	5	5	195.98	195.98	Sand bed
30X-2	17	21	196.1	196.14	Multiple sand beds
30X-2	34	34	196.27	196.27	Sand bed
30X-2	51	51	196.44	196.44	Sand bed
30X-2	52	53	196.45	196.46	Sand bed
30X-2	64	65	196.57	196.58	Sand bed
30X-2	69	73	196.62	196.66	Multiple silt beds
30X-3	2	3	197.45	197.46	Sand bed
30X-3	6	7	197.49	197.5	Sand bed
30X-3	20	21	197.63	197.64	Sand bed
30X-3	21	21	197.64	197.64	Sand bed
30X-3	25	25	197.68	197.68	Sand bed
30X-3	30	31	197.73	197.74	Sand bed
30X-3	40	40	197.83	197.83	Sand bed
30X-3	47	47	197.9	197.9	Sand bed
30X-3	53	53	197.96	197.96	Sand bed
30X-3	65	65	198.08	198.08	Sand bed
30X-3	67	67	198.1	198.1	Sand bed
30X-3	70	72	198.13	198.15	Sand bed
30X-3	82	83	198.25	198.26	Sand bed
30X-3	86	87	198.29	198.3	Sand bed
30X-3	106	108	198.49	198.51	Sand bed
30X-3	125	125	198.68	198.68	Sand bed
30X-4	5	5	198.98	198.98	Sand bed
30X-4	12	13	199.05	199.06	Sand bed
30X-4	21	22	199.14	199.15	Sand bed
30X-4	29	29	199.22	199.22	Sand bed
30X-4	35	43	199.28	199.36	Multiple sand beds
30X-4	48	48	199.41	199.41	Sand bed
30X-4	55	55	199.48	199.48	Sand bed
30X-4	62	65	199.55	199.58	Multiple sand beds
30X-5	3	6	200.46	200.49	Multiple sand beds
30X-5	17	17	200.6	200.6	Sand bed
30X-5	44	44	200.87	200.87	Sand bed
30X-5	48	48	200.91	200.91	Sand bed

Table 4. Sand/silt laminae and beds, and silty clay occurrences at Hole NGHP-01-07B. (To view complete table, please refer to the ASCII files.)—Continued

Core, section	Position start	Position end	Depth top (mbsf)	Depth base (mbsf)	Type
NGHP-01-07B—Continued					
30X-5	62	62	201.05	201.05	Sand bed
30X-5	75	75	201.18	201.18	Sand bed
30X-5	78	78	201.21	201.21	Sand bed
30X-5	80	80	201.23	201.23	Sand bed
30X-5	83	83	201.26	201.26	Sand bed
30X-5	92	92	201.35	201.35	Sand bed
30X-5	100	100	201.43	201.43	Sand bed
30X-5	113	113	201.56	201.56	Sand bed
30X-5	139	139	201.82	201.82	Sand bed
31X-1	9	10	201.99	202	Sand bed
30X-6	15	15	202.08	202.08	Silt bed
30X-6	25	28	202.18	202.21	Multiple silt beds
31X-1	36	36	202.26	202.26	Sand bed
30X-6	38	41	202.31	202.34	Multiple sand beds
31X-1	49	49	202.39	202.39	Sand bed
30X-6	47	47	202.4	202.4	Sand bed
30X-6	51	52	202.44	202.45	Sand bed
30X-6	54	54	202.47	202.47	Sand bed
31X-1	58	60	202.48	202.5	Sand bed
31X-1	63	63	202.53	202.53	Sand bed
31X-1	67	68	202.57	202.58	Sand bed
31X-1	70	70	202.6	202.6	Sand bed
30X-6	75	75	202.68	202.68	Sand bed
30X-6	77	77	202.7	202.7	Sand bed
31X-1	81	81	202.71	202.71	Sand bed
31X-1	86	87	202.76	202.77	Sand bed
30X-6	83	83	202.76	202.76	Sand bed
31X-1	90	91	202.8	202.81	Sand bed
30X-6	91	91	202.84	202.84	Sand bed
31X-1	98	100	202.88	202.9	Sand bed
30X-6	97	97	202.9	202.9	Sand bed
31X-1	105	105	202.95	202.95	Sand bed
31X-1	107	107	202.97	202.97	Sand bed
31X-1	112	112	203.02	203.02	Sand bed
31X-1	115	115	203.05	203.05	Sand bed
31X-1	118	118	203.08	203.08	Sand bed
30X-6	116	117	203.09	203.1	Sand bed
31X-1	120	120	203.1	203.1	Sand bed
31X-1	127	127	203.17	203.17	Sand bed
30X-6	138	139	203.31	203.32	Sand bed
31X-2	4	5	203.44	203.45	Sand bed
30X-7	18	18	203.61	203.61	Sand bed
31X-2	22	22	203.62	203.62	Sand bed
31X-2	27	27	203.67	203.67	Sand bed
31X-2	29	29	203.69	203.69	Sand bed
30X-7	33	33	203.76	203.76	Sand bed
30X-7	41	41	203.84	203.84	Sand bed
31X-2	54	55	203.94	203.95	Sand bed
30X-7	54	54	203.97	203.97	Sand bed
30X-7	56	56	203.99	203.99	Sand bed
30X-7	59	59	204.02	204.02	Sand bed
30X-7	60	60	204.03	204.03	Sand bed
30X-7	69	69	204.12	204.12	Sand bed
30X-7	70	73	204.13	204.16	Multiple sand beds
30X-7	75	75	204.18	204.18	Sand bed
30X-7	83	83	204.26	204.26	Sand bed

Table 5. Sand/silt laminae and beds and silty clay occurrences at Hole NGHP-01-07D.

Core, section	Position start	Position end	Depth top (mbsf)	Depth base (mbsf)	Type
			NGHP-01-07D		
1X-1	65	70	231.85	231.9	Silt/sand laminae
1X-1	70	70	231.9	231.9	Silt/sand laminae
1X-1	84	92	232.04	232.12	Silt/sand laminae
1X-1	103	104	232.23	232.24	Silt/sand laminae
1X-1	115	117	232.35	232.37	Silt/sand laminae
1X-1	141	141	232.61	232.61	Silt/sand laminae
1X-2	0	20	232.7	232.9	Multiple silt/sand laminae
1X-2	42	42	233.12	233.12	Silt/sand laminae
1X-2	89	89	233.59	233.59	Silt/sand laminae
1X-2	95	95	233.65	233.65	Silt/sand laminae
1X-2	109	109	233.79	233.79	Silt/sand laminae
1X-2	110	110	233.8	233.8	Silt/sand laminae
1X-2	114	114	233.84	233.84	Silt/sand laminae
1X-2	116	116	233.86	233.86	Silt/sand laminae
1X-2	120	120	233.9	233.9	Silt/sand laminae
1X-2	122	122	233.92	233.92	Silt/sand laminae
1X-2	125	125	233.95	233.95	Silt/sand laminae
1X-2	129	129	233.99	233.99	Silt/sand laminae
1X-2	146	146	234.16	234.16	Silt/sand laminae
1X-3	38	39	234.58	234.59	Silt/sand laminae
1X-4	33	66	236.03	236.36	Silt/sand laminae
1X-4	77	79	236.47	236.49	Silt/sand laminae
1X-4	84	84	236.54	236.54	Silt/sand laminae
1X-4	102	102	236.72	236.72	Silt/sand laminae
1X-4	106	106	236.76	236.76	Silt/sand laminae
1X-4	112	112	236.82	236.82	Silt/sand laminae
1X-4	118	118	236.88	236.88	Silt/sand laminae
1X-5	8	8	237.28	237.28	Silt/sand laminae
1X-5	127	127	238.47	238.47	Silt/sand laminae
1X-5	136	136	238.56	238.56	Silt/sand laminae
1X-5	140	140	238.6	238.6	Silt/sand laminae
1X-6	18	18	238.88	238.88	Silt/sand laminae
1X-6	27	27	238.97	238.97	Silt/sand laminae
1X-6	29	29	238.99	238.99	Silt/sand laminae
1X-6	52	52	239.22	239.22	Silt/sand laminae
1X-6	62	62	239.32	239.32	Silt/sand laminae
1X-6	73	80	239.43	239.5	Multiple silt/sand laminae
1X-6	96	96	239.66	239.66	Silt/sand laminae
4X-2	0	150	254.8	256.3	Thin silt laminae rare throughout
4X-3	0	70	256.3	257	Thin silt laminae rare throughout
4X-4	0	150	257.8	259.3	Thin silt laminae rare throughout

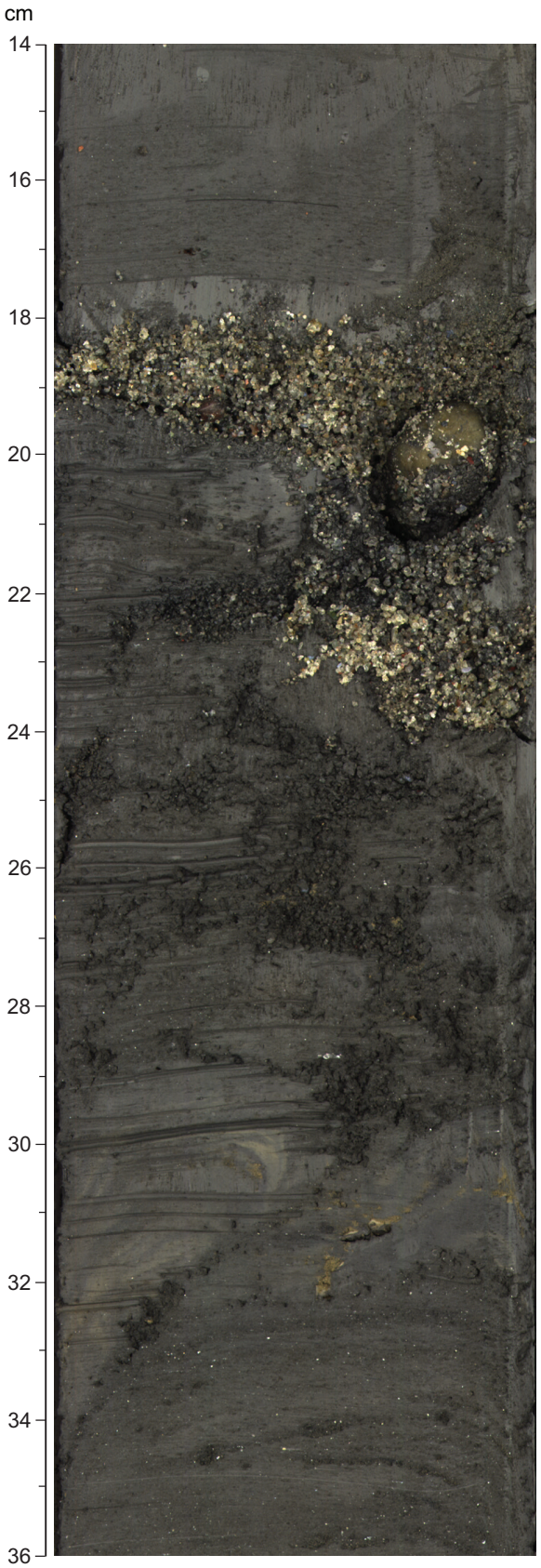

Figure 7. Sand, granule, and gravel bed recovered in Section NGHP-01-07B-08H-4.

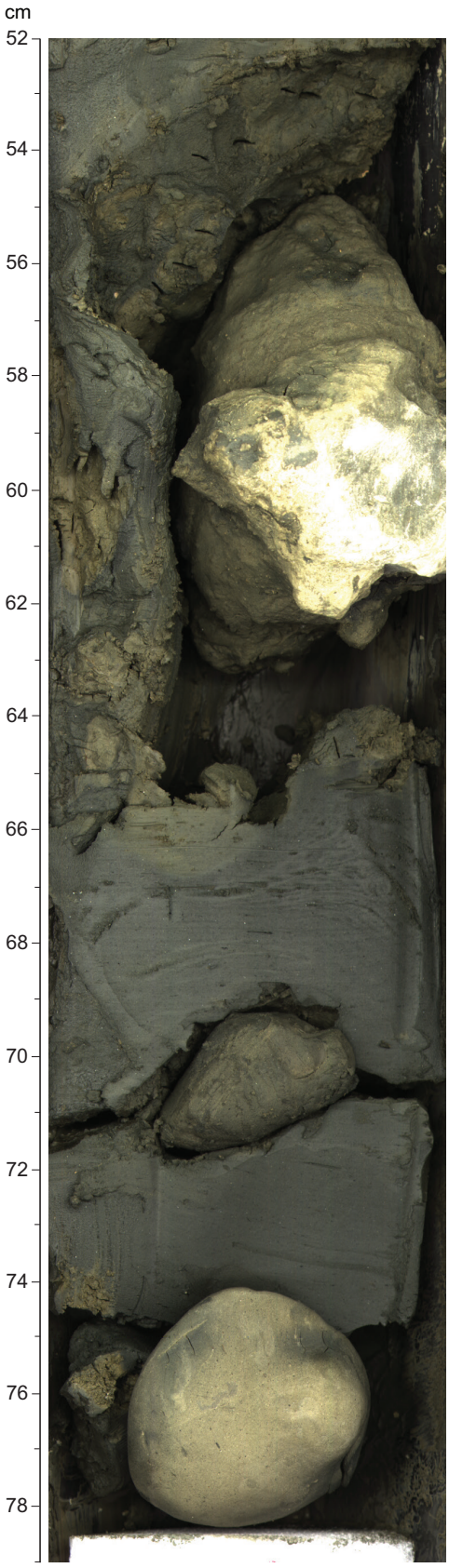

Figure 8. Large authigenic carbonate nodules typical of Hole NGHP-01-07A (in Section NGHP-01-07A-04H-1).

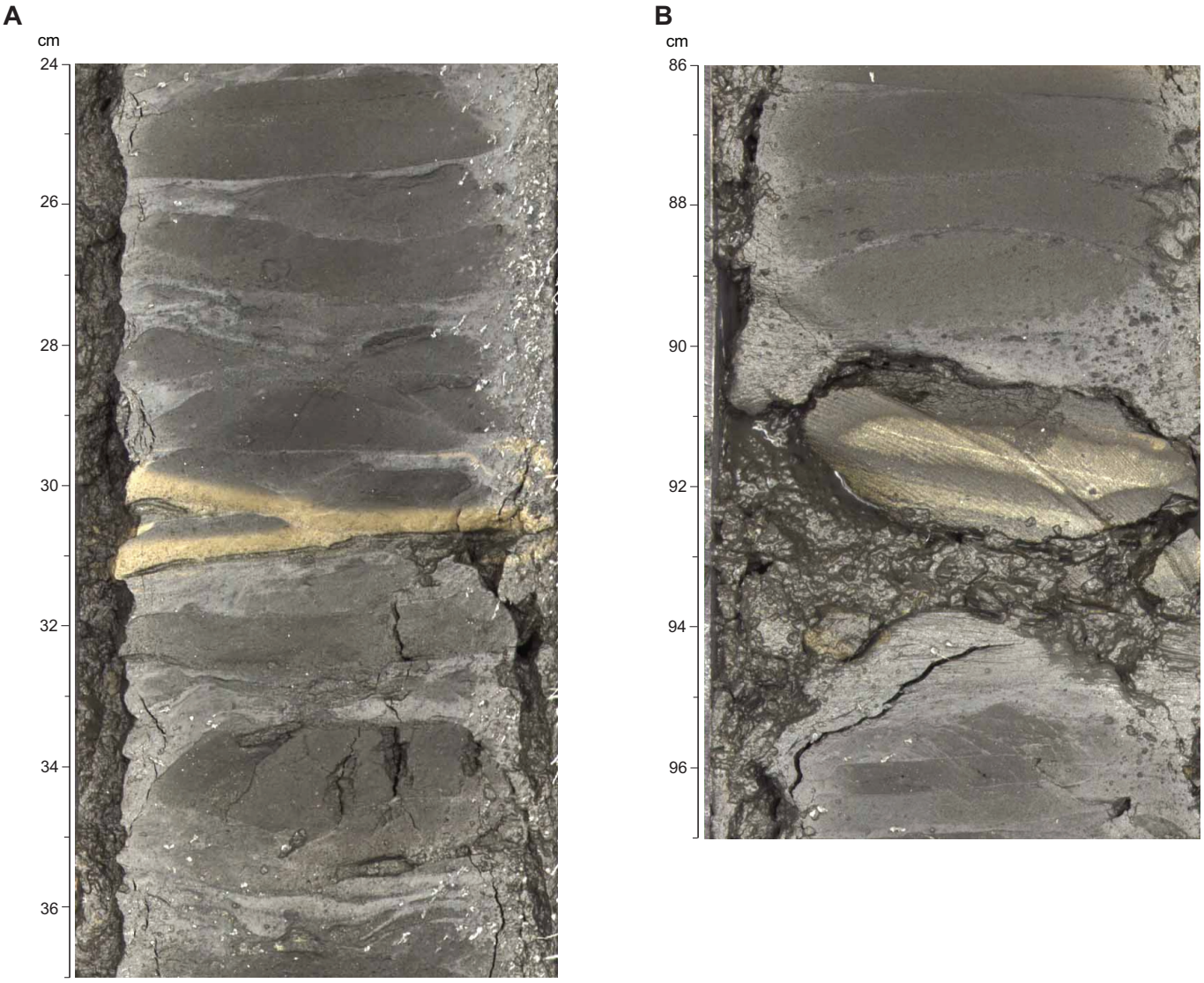

Figure 9. Limestone bands in Core NGHP-01-07D-04X. A, branched, thin limestone band of a relatively pure carbonate in Section B, stratified, dirty limestone with variable content of terrigenous components in Section NGHP-01-07D-04X-1.

Table 6. Interstitial water data for Holes NGHP-01-07B and NGHP-01-07D. Note that a dash indicates the value was not determined.

Core, section	Top	Bottom	Depth (mbsf)	Volume (mL)	pH	Alkalinity (mM)	Salinity	Cl– by IC (mM)	Br– (mM)	SO_4^{2-} (mM)
NGHP-01-07B										
1H-1	140	150	1.4	35.5	8.2	6.09	35	555	0.83	24.0
1H-2	76	86	2.3	32	7.8	8.92	35.0	572	0.86	21.5
2H-1	140	150	4.1	33	7.8	8.96	-	559	0.85	20.3
2H-2	140	150	5.6	31	7.9	8.37	35.0	560	0.85	20.3
2H-3	140	150	7.1	31	7.9	8.26	-	556	0.85	20.2
2H-4	140	150	8.6	31	7.9	8.56	35.0	545	0.78	23.8
2H-5	140	150	10.1	34	8.0	8.83	-	548	0.83	20.4
2H-6	116	126	11.4	29	7.9	9.00	34.5	564	0.88	20.0
3H-1	140	150	13.6	28	8.0	9.57	34.5	546	0.83	18.5
3H-2	140	150	15.1	29	8.1	9.88	-	545	0.81	18.3
3H-3	140	150	16.6	30	8.1	10.02	35.0	589	0.92	17.8
3H-4	140	150	18.1	30	8.1	9.91	34.5	554	0.82	17.7
3H-5	140	150	19.6	30	8.1	10.37	34.5	571	-	20.0
3H-6	140	150	21.1	28	8.0	10.24	34.5	571	-	19.9
4H-3	140	150	26.1	24	8.1	9.78	34.0	579	0.96	15.9
4H-5	140	150	29.1	30	8.2	8.62	35.0	624	1.03	20.8
5H-3	140	150	35.6	30	-	-	33.7	563	0.93	BDL
5H-5	140	150	38.6	25	7.9	19.71	-	547	0.88	BDL
6H-3	140	150	45.1	30	7.9	21.24	34.5	575	1.04	0.7
6H-5	135	150	48.1	31	7.9	21.12	34.5	615	1.18	BDL
7H-3	140	150	54.5	29	7.8	22.90	34.0	553	0.97	BDL
7H-5	140	150	57.5	30	7.7	22.91	34.0	-	-	BDL
8H-3	122	142	63.8	30	7.9	18.75	34.0	647	1.39	BDL
8H-5	130	150	66.8	30	7.9	19.52	34.5	-	-	-
9H-3	130	150	71.9	30	8.1	17.97	34.0	-	-	0.4
10X-3	130	150	83.0	30	7.9	17.34	33.5	593	1.24	0.4
10X-5	130	150	86.0	30	8.0	-	33.5	569	1.18	BDL
11P-1	40	50	84.6	11	-	-	33.5	587	1.20	0.2
13X-3	40	60	88.4	30	8.0	16.63	-	573	1.19	BDL
14X-1	130	150	97.0	30	8.0	14.66	34.0	592	1.28	BDL
14X-2	130	150	98.5	20	8.1	14.09	32.5	594	1.28	BDL
14X-4	50	70	100.2	30	8.1	12.55	32.0	561	1.20	0.2
15X-2	130	150	108.1	15.5	8.0	11.24	33.0	581	1.27	0.2
15X-4	130	150	111.1	20	7.9	10.64	33.0	610	1.35	BDL
17X-3	126	146	119.5	19.5	8.0	8.09	32.0	-	-	-
17X-5	114	134	122.3	19	8.0	8.28	32.0	613	1.36	BDL
18X-2	130	150	127.4	16	8.2	9.36	31.5	597	1.37	BDL
18X-3	130	150	128.9	15.5	8.2	8.84	31.0	595	1.37	BDL
19X-3	69	99	137.4	19	7.8	9.74	31.8	586	1.36	BDL
19X-4	94	124	138.6	17	8.2	9.57	33.5	591	1.36	BDL
20X-1	81	101	144.8	18.5	7.7	13.67	34.5	583	1.36	0.2
20X-3	120	150	147.7	16	7.7	16.99	32.3	598	1.36	0.2
21P-1	18	38	148.4	23	7.6	12.66	33.0	580	1.14	8.6
22E-1	50	60	149.7	11	-	-	33.5	598	1.36	0.3
23X-1	115	150	151.4	22	7.8	-	34.0	603	1.37	0.8
23X-3	115	150	154.4	22	7.8	23.20	34.0	602	1.37	BDL
24X-1	115	150	161.0	21	7.8	34.53	34.0	587	1.36	BDL
25X-2	68	78	171.6	23	7.9	32.25	30.5	521	1.17	2.1
25X-3	115	150	172.8	16	7.7	40.28	-	560	1.32	BDL
25X-5	115	150	175.8	25	7.6	42.63	34.0	560	1.30	0.2
26X-2	115	150	176.9	22	7.6	41.79	31.5	518	1.19	0.9
26X-4	74	109	178.9	25	7.4	44.84	34.5	534	1.25	0.3
27X-2	115	150	186.5	22	7.6	42.30	35.0	537	1.27	0.4
27X-3	75	110	187.6	26	7.6	40.90	34.0	557	1.32	BDL
28P-1	47	63	193.9	15	7.6	38.24	32.5	542	1.27	BDL
29Y-1	52	60	194.9	16.5	7.8	36.81	33.0	574	1.38	BDL
30X-2	115	150	197.1	33	7.8	35.86	34.5	538	1.21	2.8
30X-4	115	150	200.1	16	7.7	38.60	34.3	547	1.30	0.2
NGHP-01-07D										
1X-3	110	150	235.3	25	8.0	-	34	549	1.31	BDL
2X-3	110	150	243.1	15	7.9	30.29	33.0	567	1.37	0.3
3X-3	110	150	250.7	21	8.0	28.00	33.0	549	1.34	BDL
4X-3	110	150	257.4	26	8.0	25.64	32.0	537	1.31	0.2
4X-5	110	150	260.4	12	-	-	32.0	543	1.32	BDL

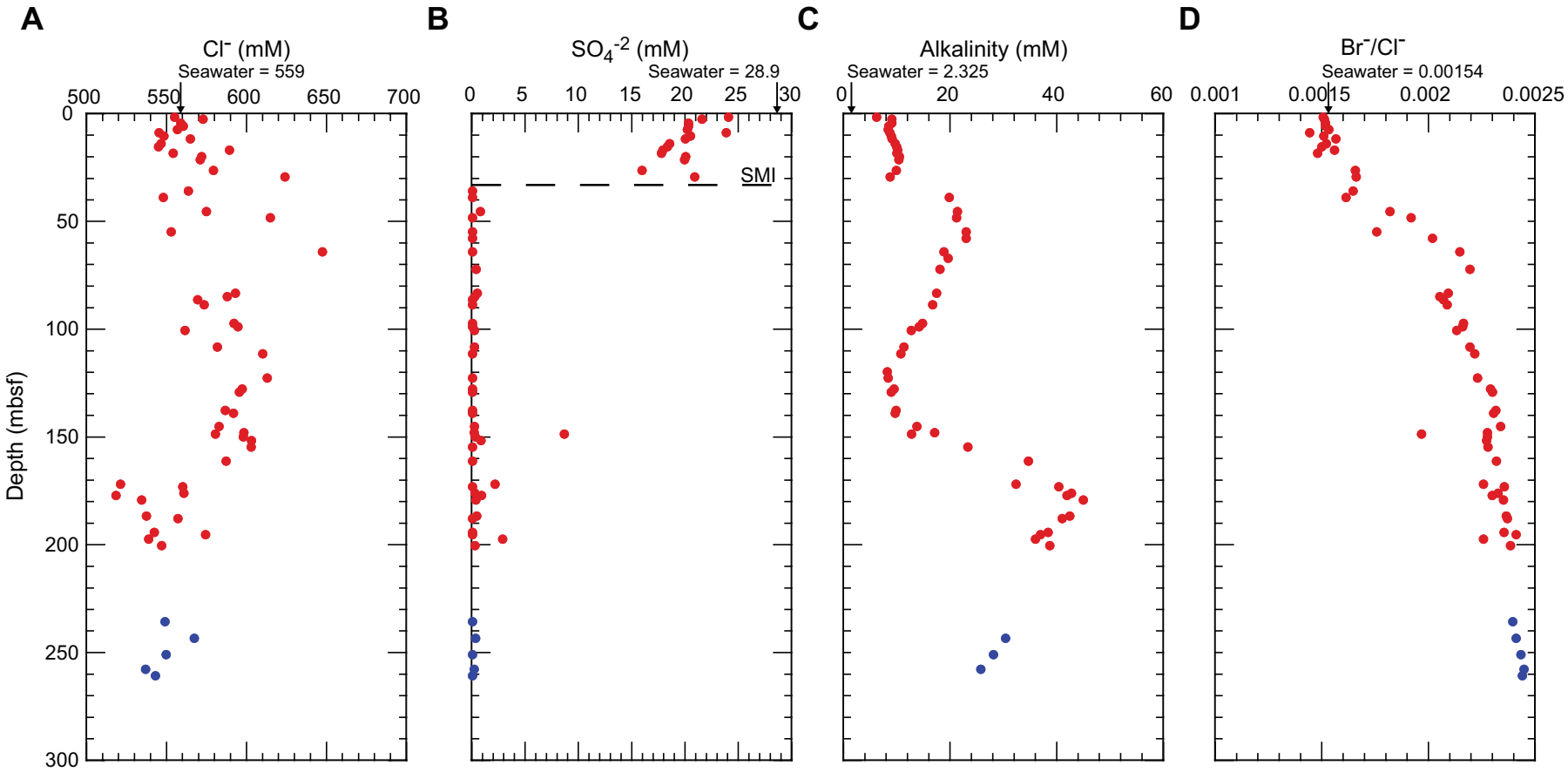

Figure 10. Concentration depth profiles of A, chloride; B, sulfate; C, alkalinity; and D, bromide/chloride ratio at Holes NGHP-01-07A and NGHP-01-07B. Symbol key; red circles, Hole NGHP-01-07B; blue circles, Hole NGHP-01-07D.

Table 7. Headspace gas composition for Site NGHP-01-07.

Sample	Site	Hole	Core	Section	Interval (cm)	Sed wt. (g)	Sample depth (mbsf)	CO_2	C_1	C_2
									(ppmv)	
7B-1H1-95-100	7	B	1	1	95–100	8.6	0.95	4,500	nd	nd
7B-1H2-71-76	7	B	1	2	71–76	8.4	2.21	4,700	nd	nd
7B-2H1-135-140	7	B	2	1	135–140	8.2	4.05	2,500	nd	nd
7B-2H2-135-140	7	B	2	2	135–140	8.1	5.55	2,400	nd	nd
7B-2H3-105-110	7	B	2	3	105–110	8.0	6.75	2,900	nd	nd
7B-2H4-135-140	7	B	2	4	135–140	9.2	8.55	3,800	nd	nd
7B-2H5-95-100	7	B	2	5	95–100	8.1	9.65	4,100	nd	nd
7B-2H6-111-116	7	B	2	6	111–116	8.2	11.31	2,600	nd	nd
7B-3H1-135-140	7	B	3	1	135–140	8.2	13.55	4,900	nd	nd
7B-3H2-135-140	7	B	3	2	135–140	8.6	15.05	4,100	nd	nd
7B-3H3-105-110	7	B	3	3	105–110	8.8	16.25	5,000	nd	nd
7B-3H4-135-140	7	B	3	4	135–140	9.7	18.05	5,000	nd	nd
7B-3H5-95-100	7	B	3	5	95–100	9.0	19.15	4,800	nd	nd
7B-3H6-135-140	7	B	3	6	135–140	9.6	21.05	3,300	nd	nd
7B-4H3-105-110	7	B	4	3	105–110	8.6	25.75	4,500	nd	nd
7B-4H5-95-100	7	B	4	5	95–100	9.1	28.65	4,500	nd	nd
7B-5H3-105-110	7	B	5	3	105–110	8.2	35.25	16,100	33,400	nd
7B-5H5-95-100	7	B	5	5	95–100	9.0	38.15	22,200	33,400	nd
7B-6H3-105-110	7	B	6	3	105–110	8.5	44.75	10,400	5,100	nd
7B-6H5-90-95	7	B	6	5	90–95	9.0	47.60	18,300	6,200	nd
7B-7H3-105-110	7	B	7	3	105–110	10.3	54.17	40,700	11,100	nd
7B-7H5-95-100	7	B	7	5	95–100	11.0	57.07	41,000	9,900	nd
7B-8H3-87-92	7	B	8	3	87–92	12.2	63.43	23,000	5,900	nd
7B-8H5-85-90	7	B	8	5	85–90	11.2	66.33	22,000	3,100	nd
7b-9H3-85-90	7	B	9	3	85–90	12.7	71.48	12,500	7,300	nd
7B-10X3-95-100	7	B	10	3	95–100	10.8	82.65	7,000	2,100	nd
7B-10X5-85-90	7	B	10	5	85–90	12.8	85.55	9,900	2,500	nd
7B-11P-50-55	7	B	11	P	50–55	11.1	84.70	17,300	3,300	nd
7B-13X2-145-150	7	B	13	2	145–150	11.7	87.95	20,000	5,000	nd
7B-14X1-125-130	7	B	14	1	125–130	14.2	96.95	11,300	12,400	nd
7B-14X2-85-90	7	B	14	2	85–90	11.6	98.05	18,700	9,200	nd
7B-14X4-45-50	7	B	14	4	45–50	13.1	100.15	15,700	14,100	nd
7B-15X2-95-100	7	B	15	2	95–100	12.2	107.71	1,900	2,200	nd
7B-15X4-85-90	7	B	15	5	85–90	11.1	110.61	3,200	3,400	nd
7B-17X3-95-100	7	B	17	3	95–100	6.3	119.11	10,200	5,700	nd
7B-17X5-85-90	7	B	17	5	85–90	8.5	121.85	10,800	7,100	nd
7B-18X2-95-100	7	B	18	2	95–100	9.7	127.05	9,800	8,100	nd
7B-18X3-110-115	7	B	18	3	110–115	10.9	128.70	10,700	8,900	nd
7B-19X3-64-69	7	B	19	3	64–69	7.3	137.35	5,500	21,600	nd
7B-19X4-39-44	7	B	19	4	39–44	9.2	138.09	6,000	9,200	nd
7B-20X1-76-81	7	B	20	1	76–81	9.4	144.76	27,000	10,300	nd
7B-20X3-85-90	7	B	20	3	85–90	9.6	147.36	21,800	7,100	nd
7B-20X4-85-90	7	B	20	4	85–90	8.2	148.70	24,700	8,000	nd
7B-21P-50-55	7	B	21	P	50–55	13.1	148.86	16,800	4,900	nd
7B-23X1-80-85	7	B	23	1	80–85	9.9	151.00	12,200	3,400	nd
7B-23X3-70-75	7	B	23	3	70–75	11.1	153.90	58,900	1,000	nd
7B-24X1-70-75	7	B	24	1	70–75	11.9	160.50	53,800	11,800	nd
7B-25X2-63-68	7	B	25	2	63–68	11.1	171.53	55,900	11,900	nd
7B-25X3-80-85	7	B	25	3	80–85	9.0	172.48	6,900	1,500	nd
7B-25X5-70-75	7	B	25	5	70–75	8.9	175.38	36,800	9,100	nd
7B-26X2-80-85	7	B	26	2	80–85	9.9	176.50	43,800	5,900	nd
7B-26X4-29-34	7	B	26	4	29–34	11.3	178.49	22,800	3,300	nd
7B-27X2-70-75	7	B	27	2	70–75	11.3	186.00	45,600	7,800	nd
7B-27X3-40-45	7	B	27	3	40–45	8.3	187.20	24,500	3,000	nd
7B-28P-63-68	7	B	28	P	80–85	9.4	194.20	66,800	9,400	nd
7B-30X2-80-85	7	B	30	2	80–85	13.4	196.73	20,300	10,600	nd
7B-30X4-70-75	7	B	30	4	70–75	9.4	199.63	38,400	5,900	nd
7D-1X3-65-70	7	D	1	3	65–70	11.8	234.85	46,900	5,800	nd
7D-2X3-65-70	7	D	2	3	65–70	12.9	242.65	68,000	5,300	nd
7D-3X3-65-70	7	D	3	3	65–70	11.4	250.25	28,000	5,300	nd
7D-4X3-65-70	7	D	4	3	65–70	9.9	256.95	5,600	3,300	nd
7D-4X5-105-110	7	D	4	5	105–110	9.6	260.35	3,500	1,900	nd

Table 7. Headspace gas composition for Site NGHP-01-07.—Continued

Sample	C_3	O_2	N_2+Ar	H_2S	C_1	C_1	CO_2	CO_2	C_1/CO_2
	(ppmv)				(mL/L WS)	(mM PW)	(mL/L WS)	(mM PW)	
7B-1H1-95-100	nd	189,000	750,100	nd	nd	nd	11,900	0.5	-
7B-1H2-71-76	nd	189,400	755,700	nd	nd	nd	12,800	0.7	-
7B-2H1-135-140	nd	190,600	751,900	nd	nd	nd	7,100	0.4	-
7B-2H2-135-140	nd	190,300	746,400	nd	nd	nd	6,800	0.4	-
7B-2H3-105-110	nd	192,600	755,500	nd	nd	nd	8,400	0.5	-
7B-2H4-135-140	nd	192,400	757,400	nd	nd	nd	9,100	0.6	-
7B-2H5-95-100	nd	189,900	748,300	nd	nd	nd	12,000	0.8	-
7B-2H6-111-116	nd	187,400	751,700	nd	nd	nd	7,400	0.5	-
7B-3H1-135-140	nd	188,700	749,100	nd	nd	nd	13,800	1.0	-
7B-3H2-135-140	nd	187,900	752,600	nd	nd	nd	10,900	0.8	-
7B-3H3-105-110	nd	189,200	754,000	nd	nd	nd	12,900	0.9	-
7B-3H4-135-140	nd	190,700	755,900	nd	nd	nd	11,300	0.8	-
7B-3H5-95-100	nd	189,000	757,900	nd	nd	nd	12,000	0.9	-
7B-3H6-135-140	nd	189,100	754,200	nd	nd	nd	7,400	0.6	-
7B-4H3-105-110	nd	191,300	747,800	nd	nd	nd	11,900	0.9	-
7B-4H5-95-100	nd	186,600	728,300	nd	nd	nd	11,100	0.9	-
7B-5H3-105-110	nd	174,400	733,800	nd	94,900	7.9	45,800	3.8	2.1
7B-5H5-95-100	nd	159,500	748,700	nd	83,600	7.1	55,400	4.7	1.5
7B-6H3-105-110	nd	178,300	731,000	nd	13,700	1.2	28,200	2.4	0.5
7B-6H5-90-95	nd	171,500	752,000	nd	15,400	1.3	45,800	4.0	0.3
7B-7H3-105-110	nd	163,700	731,400	nd	22,800	2.1	83,800	7.6	0.3
7B-7H5-95-100	nd	169,800	736,400	nd	18,500	1.7	76,300	7.0	0.2
7B-8H3-87-92	nd	174,200	740,800	nd	9,300	0.9	36,300	3.5	0.3
7B-8H5-85-90	nd	168,000	748,200	nd	5,600	0.5	39,800	3.8	0.1
7b-9H3-85-90	nd	165,000	739,500	nd	10,900	1.1	18,500	1.8	0.6
7B-10X3-95-100	nd	184,900	741,900	nd	4,000	0.4	13,500	1.3	0.3
7B-10X5-85-90	nd	180,500	723,000	nd	3,700	0.4	14,400	1.5	0.3
7B-11P-50-55	nd	172,100	745,200	nd	6,100	0.6	31,800	3.1	0.2
7B-13X2-145-150	nd	163,600	801,600	nd	8,500	0.8	33,900	3.4	0.3
7B-14X1-125-130	nd	13,800	866,800	nd	15,100	1.6	13,700	1.4	1.1
7B-14X2-85-90	nd	147,300	864,700	nd	15,800	1.6	32,000	3.3	0.5
7B-14X4-45-50	nd	122,100	886,300	nd	19,800	2.1	22,000	2.3	0.9
7B-15X2-95-100	nd	190,500	752,400	nd	3,500	0.4	3,100	0.3	1.2
7B-15X4-85-90	nd	185,000	739,300	nd	6,200	0.6	5,800	0.6	1.1
7B-17X3-95-100	nd	181,500	752,500	nd	22,900	2.3	40,700	4.1	0.6
7B-17X5-85-90	nd	182,500	751,100	nd	19,200	2.0	29,300	3.0	0.7
7B-18X2-95-100	nd	177,200	769,400	nd	18,200	1.9	21,900	2.3	0.8
7B-18X3-110-115	nd	168,000	761,300	nd	16,800	1.8	20,200	2.1	0.8
7B-19X3-64-69	nd	172,900	761,100	nd	71,500	7.4	18,100	1.9	3.9
7B-19X4-39-44	nd	179,800	758,100	nd	22,300	2.4	14,600	1.5	1.5
7B-20X1-76-81	nd	147,200	770,700	nd	24,100	2.6	63,500	6.8	0.4
7B-20X3-85-90	nd	162,400	748,100	nd	16,300	1.7	49,800	5.3	0.3
7B-20X4-85-90	nd	159,400	756,600	nd	22,800	2.4	70,100	7.4	0.3
7B-21P-50-55	nd	172,200	758,100	nd	6,800	0.8	23,600	2.7	0.3
7B-23X1-80-85	nd	160,100	762,100	nd	7,500	0.8	26,600	2.9	0.3
7B-23X3-70-75	nd	95,400	811,500	nd	1,900	0.2	108,200	11.9	0.0
7B-24X1-70-75	nd	128,700	771,900	nd	19,400	2.2	88,600	9.9	0.2
7B-25X2-63-68	nd	134,900	754,700	nd	21,800	2.4	102,700	11.5	0.2
7B-25X3-80-85	nd	181,800	718,100	nd	3,700	0.4	17,400	1.9	0.2
7B-25X5-70-75	nd	153,000	738,500	nd	23,100	2.5	93,300	10.2	0.2
7B-26X2-80-85	nd	142,300	764,200	nd	12,900	1.4	95,600	10.6	0.1
7B-26X4-29-34	nd	156,300	756,000	nd	5,800	0.7	40,700	4.6	0.1
7B-27X2-70-75	nd	113,100	774,300	nd	14,000	1.6	81,400	9.3	0.2
7B-27X3-40-45	nd	184,300	750,200	nd	8,500	0.9	68,300	7.5	0.1
7B-28P-63-68	nd	113,900	787,300	nd	22,100	2.5	157,000	17.6	0.1
7B-30X2-80-85	nd	133,400	780,500	nd	14,400	1.7	27,400	3.3	0.5
7B-30X4-70-75	nd	154,000	752,500	nd	13,800	1.6	90,300	10.2	0.2
7D-1X3-65-70	nd	117,700	793,100	nd	9,600	1.2	78,300	9.4	0.1
7D-2X3-65-70	nd	20,400	831,400	nd	7,700	0.9	98,000	12.0	0.1
7D-3X3-65-70	nd	97,300	837,000	nd	9,300	1.1	49,300	5.9	0.2
7D-4X3-65-70	nd	164,600	761,100	nd	7,300	0.9	12,300	1.5	0.6
7D-4X5-105-110	nd	184,100	743,500	nd	4,400	0.5	8,100	1.0	0.5

Notes: nd = not detected. WS = Wet sediment. PW = porewater. Approximate detection limits are about 15 ppmv for methane, 30 ppmv for ethane, 50 ppmv for propane, and 20 ppmv for hydrogen sulfide.

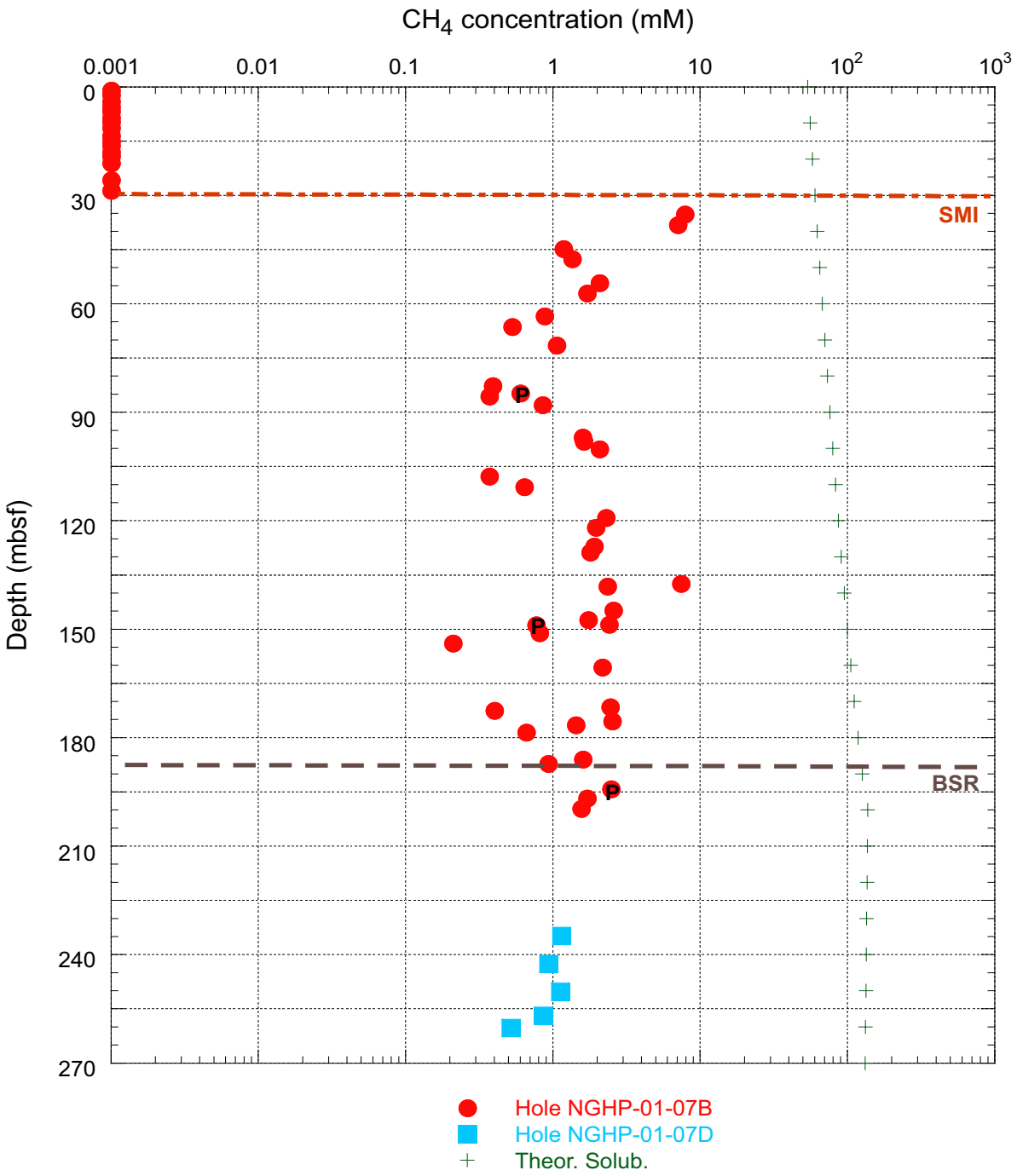

Figure 11. Plot of headspace methane gas concentration (mM) with depth for Site NGHP-01-07, Holes B and D. Note the methane gradient at ~35 mbsf denoting the SMI. Values less than 0.003 mM are below instrument detection limits, but plotted for reference. Text inside a symbol denotes special coring tool (E, HRC; P, PCS; Y, FPC). Theoretical solubility of methane calculated using the Duan and others (1992) and Xu (2002, 2004) methodologies. Hole NGHP-01-07D was not sampled continuously, thus resulting in the random data collection intervals at depth. [SMI, sulfate-methane interface]

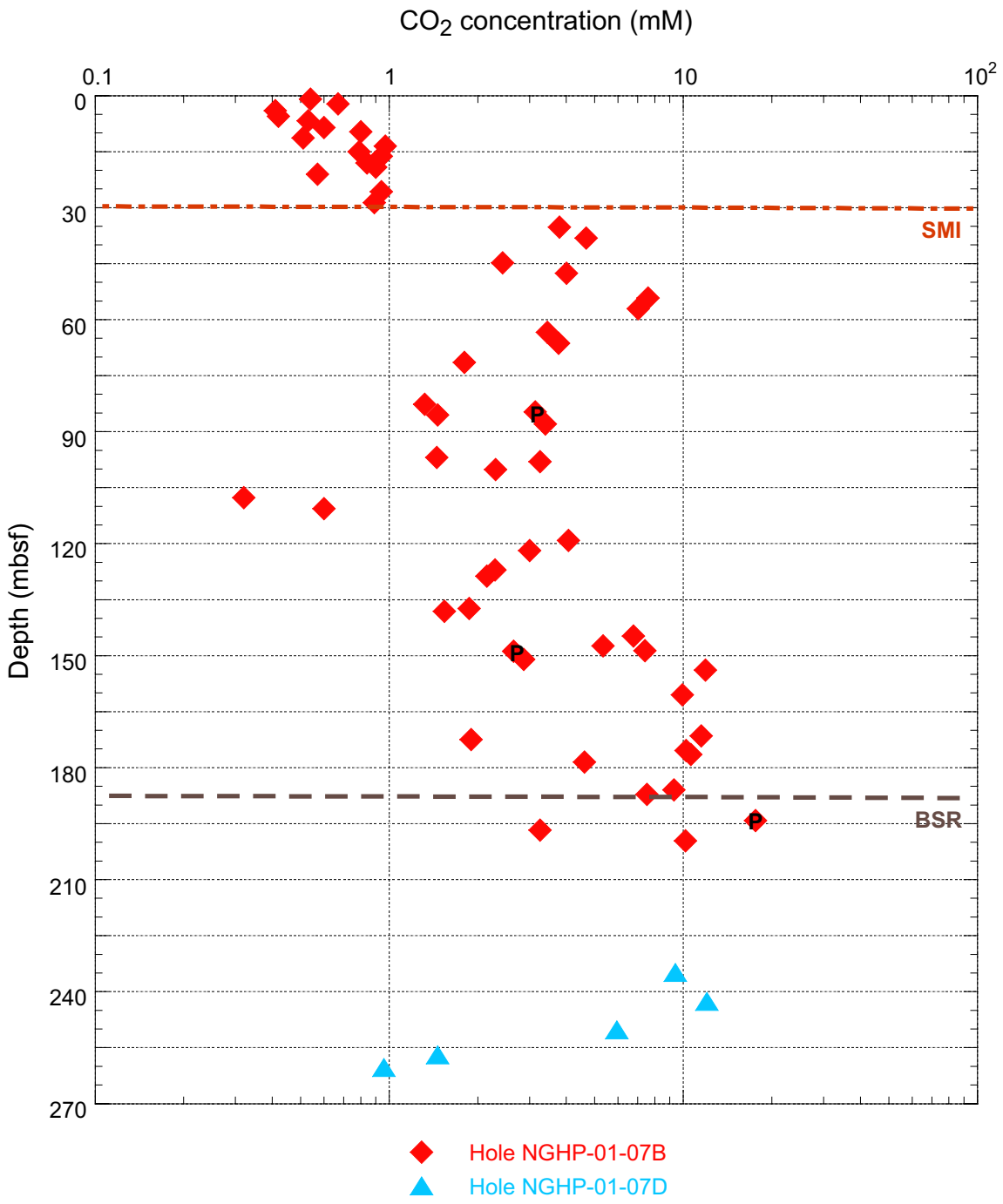

Figure 12. Plot of headspace carbon dioxide gas concentration (mM) with depth for Site NGHP-01-07, Holes B and D. Text inside a symbol denotes special coring tool (E, HRC; P, PCS; Y, FPC). Hole NGHP-01-07D was not sampled continuously, thus resulting in the random data collection intervals at depth, and as such could not confirm the elevated concentration at depth.

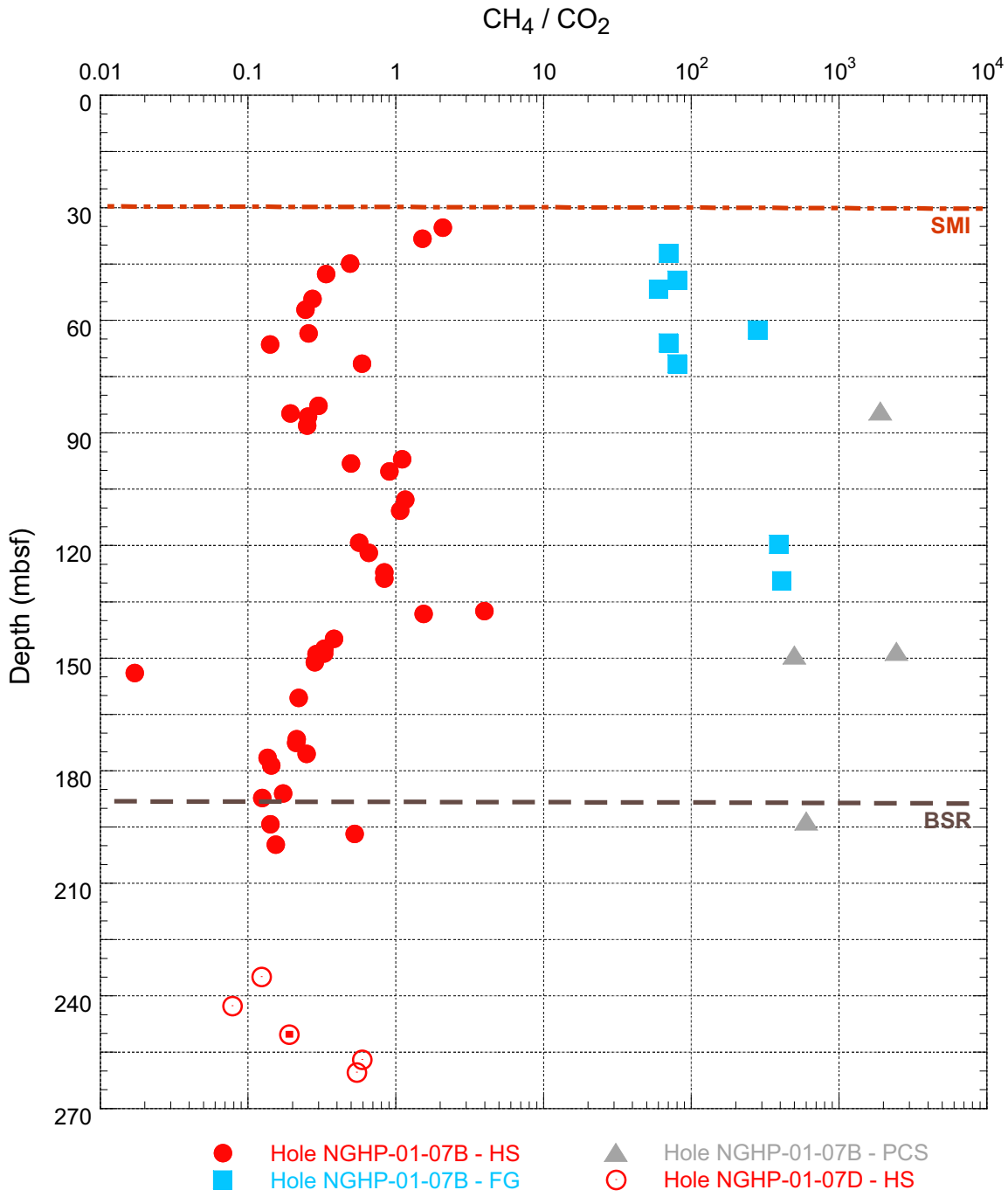

Figure 13. Plot of methane to carbon dioxide gas ratio with depth for headspace, free/void gas, and PCS gas for Site NGHP-01-07, Holes B and D. Note the spikes in methane concentration, perhaps indicating the presence of free gas or gas hydrate. Hole NGHP-01-07D was not sampled continuously and free gas samples are rarely obtained after XCB coring begins (~80 mbsf at this site), thus resulting in the random data collection intervals at depth. [PCS, pressure core sampler; XCB, extended core barrel]

Void gas samples were collected from nine different intervals ranging in depth from 21.2 to 129.4 mbsf. The void gas samples contained methane above 73 percent at all intervals except near the surface and ~ 49 mbsf, as noted in table 8. Methane concentrations within voids averaged nearly 721,000 ppm (±383,000 or 72.1 percent ± 38.3 percent); however higher molecular weight hydrocarbon gases were not detected. Carbon dioxide concentrations ranged from ~800 to 16,200 ppmv and are tabulated with other gas data in table 8. The methane to carbon dioxide ratios increase slightly with increasing depth between the SMI and the BSR, indicating that gas-hydrate formation may have concentrated the methane relative to carbon dioxide with depth (fig. 13). This trend does not occur in headspace gas samples, although the magnitude of the ratio near the SMI and at ~135 mbsf exhibit defined peaks. Headspace C_1/CO_2 is typically 2 orders of magnitude less due to the preferential loss of volatile methane by the headspace sample method. Void gases exhibited the presence of low level C_2 concentrations, ranging from non-detectable to ~29 ppmv. The air gases (N_2+Ar) and O_2 composed the balance gases, however the (N_2+Ar)/O_2 ratios showed a decreasing trend with depth in the core, indicating that there is less air contamination of the core with depth.

Gas was collected from four pressure cores (PCS), all in Hole NGHP-01-07B. The gas concentration results are very similar to the void gas results (tables 8 and 9), including CO_2 concentrations, as exhibited by C_1/CO_2 ratio (fig. 13). PCS core gases did indicate the presence of low level C_2 concentrations, ranging from nondetectable to ~10 ppmv. Ratio values for C_1 to C_2 gases ranged from ~69,100 to ~93,400 ppmv (average 79,870 ppmv), and showed no apparent trend with depth (fig. 14). The concentrations are focused in the center of the "normal" occurrence interval as depicted in the graph. These high methane concentrations versus low concentrations of ethane are strong evidence of a microbially dominated hydrocarbon gas source.

Microbiology

Hole NGHP-01-07B

Analysis of all microbiological samples will be shore-based. Twenty-three samples were collected for cell enumeration (CEL), and 23 for hydrogenase activity analysis (SPH) (table 10). Samples were collected as described in the "Methods." Additional microbiological samples were taken (Lab code JUD, 39 samples; Lab code JAN, 23 samples).

Hole NGHP-01-07D

Four samples were collected for cell enumeration (CEL), and four were for hydrogenase activity analysis (SPH) (table 10). Samples were collected as described in the "Methods." Additional microbiological samples were taken (Lab code JUD, 4 samples; Lab code JAN, 4 samples).

Table 8. Void gas composition for Site NGHP-01-07.

Sample	Site	Hole	Core	Section	Interval (cm)	Sample depth (mbsf)	CO_2	C_1	C_2	C_3	O_2	N_2+Ar	H_2S	C_1/CO_2	C_1/C_2
							(ppmv) normalized to nitrogen+argon								
7B-3H6-149	7	B	3	6	149	21.19	800	nd	nd	nd	135,300	863,900	nd	-	-
7B-6H1-145	7	B	6	1	145	42.15	13,500	930,600	nd	nd	11,100	44,700	nd	70	-
7B-6H7-30	7	B	6	7	30	49.27	5,000	379,000	nd	nd	131,200	484,800	nd	80	-
7B-7H1-150	7	B	7	1	150	51.7	16,200	969,300	10	nd	2,900	11,600	nd	60	96,900
7B-8H2-150	7	B	8	2	150	62.57	3,500	989,200	30	nd	1,900	5,300	nd	280	33,000
7B-8H5-57	7	B	8	5	57	66.05	11,300	822,500	10	nd	35,400	130,800	nd	70	82,300
7B-9H3-100	7	B	9	3	100	71.63	11,500	954,600	30	nd	9,800	24,100	nd	80	31,800
7B-17X3-145	7	B	17	3	145	119.65	1,900	739,000	10	nd	58,300	200,800	nd	390	73,900
7B-18X4-31	7	B	18	4	31	129.41	2,400	984,300	20	nd	3,400	9,900	nd	410	49,200

Notes: nd = not detected. nr = not recorded. Approximate detection limits are about 15 ppmv for methane, 30 ppmv for ethane, 50 ppmv for propane, and 20 ppmv for hydrogen sulfide.

Table 9. Pressure Core Sampler gas composition for Site NGHP-01-07.

Sample	Site	Hole	Core	Section	Sample depth (mbsf)	Time	Gas vol. (ml)	CO_2	C_1	C_2	C_3	O_2	N_2+Ar	H_2S	C_1/CO_2	C_1/C_2
								(ppmv) normalized to nitrogen+argon								
7B-11P-t1	7	B	11	P	84.2	1	-	500	971,100	nd	nd	6,900	21,600	nd	1,900	-
7B-21P-t1	7	B	21	P	148.2	1	-	200	771,400	10	nd	26,100	202,300	nd	3,900	77,100
7B-21P-t2	7	B	21	P	148.2	2	-	700	690,800	10	nd	36,100	272,400	nd	1,000	69,100
7B-22E-t1	7	B	22	E	149.2	1	-	900	422,300	nd	nd	126,200	450,600	nd	500	-
7B-28P-t1	7	B	28	P	193.4	1	-	1,600	933,700	10	nd	10,900	53,800	nd	600	93,400

Notes: nd= not detected. Approximate detection limits are about 15 ppmv for methane, 30 ppmv for ethane, 50 ppmv for propane, and 20 ppmv for hydrogen sulfide.

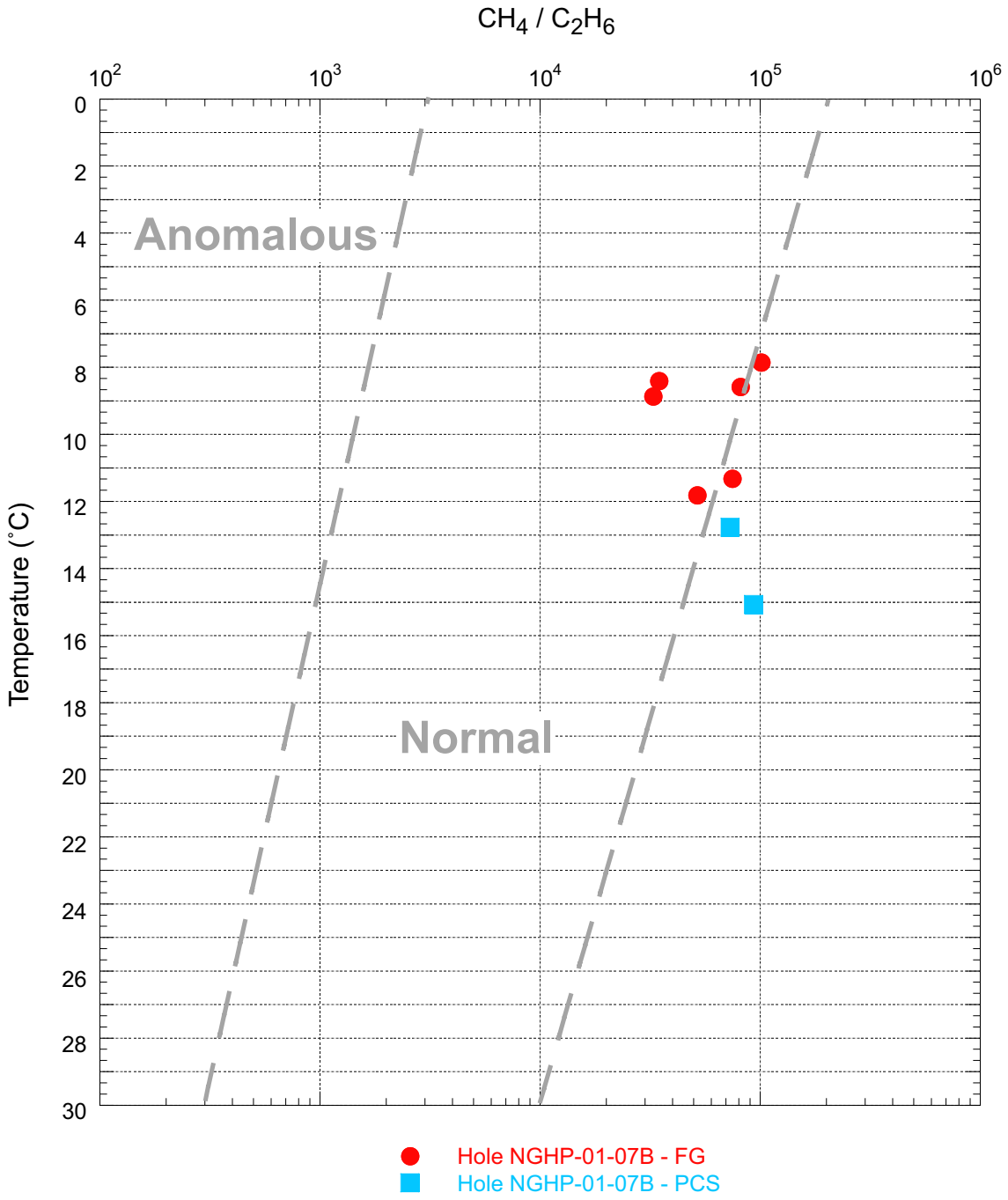

Figure 14. Plot of void gas and PCS methane to ethane gas ratio with depth for Site NGHP-01-07, Holes B and D. Ethane levels were below detection limits for all headspace samples (table 7). Note that the hydrocarbon gas occurrences fall into the typical range. [PCS, pressure coring sampler]

Table 10. List of microbiological samples taken for Site NGHP-01-07.

Sample reference						
Core, section	Sample code	Top (cm)	Bottom (cm)	Depth (mbsf)	Volume (cc)	Comments
NGHP-01-07B						
1H-1	CEL	95	100	0.95	5	
2H-5	CEL	95	100	9.65	5	
3H-5	CEL	95	100	19.15	5	
4H-5	CEL	95	100	28.65	5	
5H-5	CEL	95	100	38.15	5	
6H-5	CEL	90	95	47.6	5	
7H-5	CEL	95	100	57.07	5	
8H-5	CEL	85	90	66.33	5	
9H-3	CEL	85	90	71.48	5	
10X-5	CEL	85	90	85.55	5	
13X-2	CEL	145	150	87.95	5	
14X-2	CEL	85	90	98.05	5	
15X-4	CEL	85	90	110.61	5	
17X-5	CEL	69	74	121.85	5	
18X-3	CEL	110	115	128.7	5	
19X-4	CEL	39	44	138.09	5	
20X-3	CEL	85	90	147.36	5	
23X-3	CEL	70	75	153.9	5	
24X-1	CEL	70	75	160.5	5	
25X-5	CEL	70	75	175.38	5	
26X-4	CEL	29	34	178.49	5	
27X-2	CEL	70	75	186	5	
30X-4	CEL	70	75	199.63	5	
1H-1	JAN	105	110	1.05	187	
2H-5	JAN	105	110	9.75	187	
3H-5	JAN	105	110	19.25	187	
4H-5	JAN	105	110	28.75	187	
5H-5	JAN	105	110	38.25	187	
6H-5	JAN	100	105	47.7	187	
7H-5	JAN	105	110	57.17	187	
8H-5	JAN	95	100	66.43	187	
9H-3	JAN	95	100	71.58	187	
10X-5	JAN	95	100	85.65	187	
11P-1	JAN	20	30	84.4	374	
13X-3	JAN	5	10	88.05	187	
14X-2	JAN	95	100	98.15	187	
15X-4	JAN	95	100	110.71	187	
17X-5	JAN	79	84	121.95	187	
19X-4	JAN	49	54	138.19	187	
20X-4	JAN	95	100	148.96	187	
21P-1	JAN	38	46	148.58	299	
22E-1	JAN	14	24	149.34	187	
23X-3	JAN	80	85	154	187	
24X-1	JAN	80	85	160.6	187	
25X-5	JAN	80	85	175.48	187	
26X-4	JAN	39	44	178.59	187	
27X-2	JAN	80	85	186.1	187	
28P-1	JAN	39	44	193.79	187	
30X-4	JAN	80	85	199.73	187	
1H-1	JUD	120	130	1.2	374	
2H-3	JUD	120	130	6.9	374	
2H-5	JUD	120	130	9.9	374	
3H-3	JUD	120	130	16.4	374	
3H-5	JUD	120	130	19.4	374	
4H-3	JUD	120	130	25.9	374	
4H-5	JUD	120	130	28.9	374	
5H-3	JUD	120	130	35.4	374	
5H-5	JUD	120	130	38.4	374	
6H-3	JUD	120	130	44.9	374	
6H-5	JUD	115	125	47.85	374	
7H-3	JUD	120	130	54.32	374	
7H-5	JUD	120	130	57.32	374	
8H-3	JUD	102	112	63.58	374	
8H-5	JUD	110	120	66.58	374	
9H-3	JUD	110	120	71.73	374	
10X-3	JUD	110	120	82.8	374	
10X-5	JUD	110	120	85.8	374	
13X-3	JUD	20	30	88.2	374	
14X-2	JUD	110	120	98.3	374	
15X-2	JUD	110	120	107.86	374	
15X-4	JUD	110	120	110.86	374	
17X-3	JUD	106	116	119.26	374	
17X-5	JUD	94	104	122.1	374	
18X-2	JUD	110	120	127.2	374	
19X-4	JUD	64	74	138.34	374	
20X-3	JUD	100	110	147.51	374	
20X-4	JUD	110	120	149.11	374	
23X-1	JUD	95	105	151.15	374	
23X-3	JUD	95	105	154.15	374	
24X-1	JUD	95	105	160.75	374	
25X-3	JUD	95	105	172.63	374	
25X-5	JUD	95	105	175.63	374	
26X-2	JUD	95	105	176.65	374	
26X-4	JUD	54	64	178.74	374	
27X-2	JUD	95	105	186.25	374	
27X-3	JUD	55	65	187.35	374	
30X-2	JUD	95	105	196.88	374	
30X-4	JUD	95	105	199.88	374	
1H-1	SPH	100	105	1	187	
2H-5	SPH	100	105	9.7	187	
3H-5	SPH	100	105	19.2	187	
4H-5	SPH	100	105	28.7	187	
5H-5	SPH	100	105	38.2	187	
6H-5	SPH	95	100	47.65	187	
7H-5	SPH	100	105	57.12	187	
8H-5	SPH	90	95	66.38	187	
9H-3	SPH	90	95	71.53	187	
10X-5	SPH	90	95	85.6	187	
13X-3	SPH	0	5	88	187	
14X-2	SPH	90	95	98.1	187	
15X-4	SPH	90	95	110.66	187	
17X-5	SPH	74	79	121.9	187	
18X-3	SPH	115	120	128.75	187	
19X-4	SPH	44	49	138.14	187	
20X-4	SPH	90	95	148.91	187	
23X-3	SPH	75	80	153.95	187	
24X-1	SPH	75	80	160.55	187	
25X-5	SPH	75	80	175.43	187	
26X-4	SPH	34	39	178.54	187	
27X-2	SPH	75	80	186.05	187	
30X-4	SPH	75	80	199.68	187	
NGHP-01-07D						
1X-3	CEL	65	70	234.85	5	
2X-3	CEL	65	70	242.65	5	
3X-3	CEL	65	70	250.25	5	
4X-3	CEL	65	70	256.95	5	
1X-3	JAN	75	80	234.95	187	
2X-3	JAN	75	80	242.75	187	
3X-3	JAN	75	80	250.35	187	
4X-3	JAN	75	80	257.05	187	
1X-3	JUD	90	100	235.1	374	
2X-3	JUD	90	100	242.9	374	
3X-3	JUD	90	100	250.5	374	
4X-3	JUD	90	100	257.2	374	
1X-3	SPH	70	75	234.9	187	
2X-3	SPH	70	75	242.7	187	
3X-3	SPH	70	75	250.3	187	
4X-3	SPH	70	75	257	187	

Physical Properties

Whole-round cores at NGHP Expedition 01, Site 07 were imaged using an infrared (IR) camera on the catwalk to determine the location of temperature anomalies on the surface of core liners and enable sections containing potential gas hydrate to be quickly removed, preserved, and studied. After IR imaging was finished, nondestructive measurements were conducted on temperature-equilibrated whole-round core sections with the MSCL. Thermal conductivity measurements were also conducted on whole-round cores. Various tests were performed on split cores including: electrical resistivity by use of a Wenner array, P-wave velocity by inserted spades, and shear strength by mini-vane, Torvane, and Pocket Penetrometer. Core subsamples were placed in 10-mL beakers and dried at 105 °C to determine water content. Subsequently, the dried samples were analyzed for grain density using gas pycnometers, and other sediment relations were then calculated. See the "Physical Properties" section of the "Methods" chapter for more details.

The physical properties program at Site NGHP-01-07 focused primarily on Holes NGHP-01-07B and NGHP-01-07D that were located about 36 km off the east coast of India in ~ 1,285 m of water. Hole NGHP-01-07B was continuously cored to about 212 mbsf. Overall core recovery was 85 percent. Because of a drilling problem, Hole NGHP-01-07B was abandoned and Hole NGHP-01-07D was drilled to 231 mbsf and then four additional cores were obtained bringing the total penetration depth to 260 mbsf. Core recovery in Hole NGHP-01-07D was 113 percent due to gas expansion. No visible gas-hydrate samples were recovered at Site NGHP-01-07.

Infrared (IR) Imaging

Environmental Conditions

Catwalk environment was monitored during the entire drilling operation at Site NGHP-01-07 for temperature and humidity. Temperature on the catwalk averaged ~30 °C and ranged from 28.5 to 32.8 °C during the drilling operation that lasted over 90 hours, as shown in figure 15. Percent relative humidity of 81 ± 7.6 percent was typical (fig. 15), which is consistent with a marine environment setting in the Indian Ocean. A maximum temperature of 32.8 °C was recorded 55.5 hours into the operation, corresponding to the lowest relative humidity measurement (65 percent), illustrating the typical diurnal inverse relationship between temperature and humidity. No adverse environmental conditions such as thunderstorms, rough seas, lightning, or high winds persisted during drilling operations at this site. Also presented in figure 15 are the times at which each core was transferred onto the catwalk from the drill floor. The last core for Hole NGHP-01-07B (NGHP-01-07B-31X) arrived on the catwalk 49.4 hours after the first core (NGHP-01-07B-01H). Hole NGHP-01-07D produced the first core 87.4 hours into the drilling operation and concluded with the last core (NGHP-01-07D-04H) 6.5 hours later.

Infrared Images

All APC and XCB cores from Site NGHP-01-07 were systematically scanned upon arrival on the catwalk using the track-mounted IR camera described in the "Physical Properties" section of the "Methods" chapter. Infrared (IR) anomalies, commonly referred to as "cold spots," indicate gas-hydrate dissociation during core recovery, which subsequently provides guidance to catwalk sampling. Summary digital maps of the scans of all cores are available in the supplemental data file section (tables 11, 12, 13, and 14). Temperature arrays in text formatted files (comma separated value or CSV) were exported from the IR camera software and then concatenated for each core. The arrays were then further concatenated for all cores available in a given borehole and down core temperatures were averaged for each pixel row in the array, excluding pixels ~1 cm from the edge of the image and 2 cm along the midline of the image. Exclusion of these pixels minimizes the effects caused by major thermal artifacts in the images. This processing enables us to measure the average amplitude of the cold anomalies and separate warm anomalies due to voids from the background temperature field.

Infrared track imaging for Hole NGHP-01-07B consisted of 24 scans for a total scanned core length of 171 m. The complete set of IR images collected for Hole NGHP-01-07B is presented in figure 16 along with the corresponding down-core temperatures. The high median core temperature extracted from the IR images for Hole NGHP-01-07B ranged from a high of 31.1 °C and is related to voids in the core sediment due to gas expansion. The low median temperature of 21.6 °C was produced by Cores NGHP-01-07B-03H and NGHP-01-07B-26X. The lowest temperature (19.5 °C) measured by the IR imaging track on the 24 cores examined was in NGHP-01-07B-25X (169.4 mbsf). As shown in figure 16, the measured down-core temperature log generated from the IR imaging shows that sediment is initially cooler in the first two cores, but becomes progressively warmer down to 75 mbsf. Observations of the down-core temperature indicate thermal differences between the APC core technique and the XCB technique. The down-core temperature shows progressively elevated temperatures downhole, until the start of the XCB coring at 78.7 mbsf, where the first core temperature reading is 2 °C less than the prior APC core. The down-core temperature remains relatively constant for the remainder of the cores, with several cores (NGHP-01-07B-14H, -05X, and -26X) containing slightly cooler sections, an indication of gas-hydrate dissociation.

Infrared track imaging for Hole NGHP-01-07D consisted of four cores containing 31 m of scanned sediment. The complete set of IR images collected for Hole NGHP-01-07D

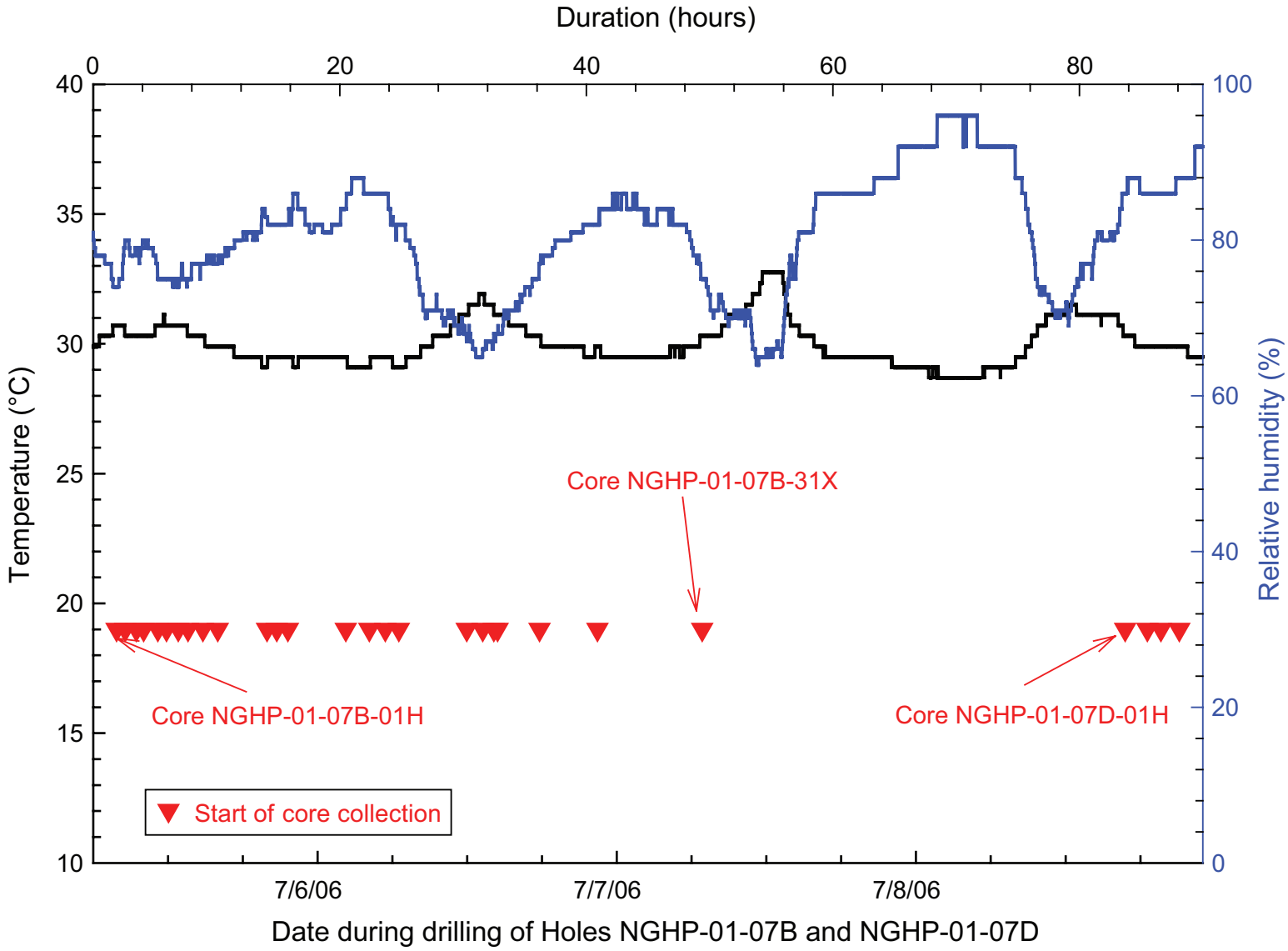

Figure 15. Catwalk temperature and humidity during drilling operations at Site NGHP-01-07.

Table 11. List of infrared image files collected on the catwalk from Hole NGHP-01-07B.

Core	Imaging length (cm)	First run	Date	Start time	Temperature (start/end) (˚C)	File ID	Screen image saved	Comments*
1H	240	x	7/5	7:55	29.5/29.5	NGHP-07-B-1	Yes	15–30 °C
2H	880	x	7/5	8:36	29.9/29.9	NGHP-07-B-2	Yes	15–30 °C
3H	970	x	7/5	9:30	29.9/29.9	NGHP-07-B-3	Yes	15–30 °C
4H	920	x	7/5	10:07	29.9/29.9	NGHP-07-B-4	Yes	15–30 °C
5H	970	x	7/5	11;15	29.9/29.9	NGHP-07-B-5	Yes	15–30 °C
6H	970	x	7/5	11:57	30.3/30.3	NGHP-07-B-6	Yes	15–30 °C
7H	970	x	7/5	12:55	30.3/30.3	NGHP-07-B-7	Yes	15–30 °C
8H	970	x	7/5	13:44	30.3/29.9	NGHP-07-B-8	Yes	15–30 °C
9H	500	x	7/5	14:52	29.5/29.5	NGHP-07-B-9	Yes	15–30 °C
10X	790	x	7/5	16:04	29.1/29.1	NGHP-07-B-10	Yes	15–30 °C
13X	860	x	7/5	20:04	28.7/28.7	NGHP-07-B-13	Yes	15–30 °C
14X	965	x	7/5	20:53	28.7/28.7	NGHP-07-B-14	Yes	15–30 °C
15X	890	x	7/5	21:51	28.7/28.7	NGHP-07-B-15	Yes	15–30 °C
17X	870	x	7/6	2:35	28.3/28.3	NGHP-07-B-17	Yes	15–30 °C
18X	630	x	7/6	4:26	28.3/28.3	NGHP-07-B-18	Yes	15–30 °C
19X	470	x	7/6	5:45	28.3/28.3	NGHP-07-B-19	Yes	15–30 °C
20X	700	x	7/6	6:45	28.3/28.3	NGHP-07-B-20	Yes	15–30 °C
23X	530	x	7/6	12:17	31.3/31.3	NGHP-07-B-23	Yes	15–30 °C
24X	260	x	7/6	13:38	31.5/31.5	NGHP-07-B-24	Yes	15–30 °C
25X	790	x	7/6	14:28	31.5/31.5	NGHP-07-B-25	Yes	15–30 °C
26X	510	x	7/6	14:49	30.7/30.7	NGHP-07-B-26	Yes	15–30 °C
27X	530	x	7/6	18:12	29.5/29.5	NGHP-07-B-27	Yes	15–30 °C
30X	970	x	7/6	22:52	28.7/28.7	NGHP-07-B-30	Yes	15–30 °C
31X	210	x	7/7	7:25	29.5/29.5	NGHP-07-B-31	Yes	15–30 °C

*Temperature range for images displayed during core collection.

is presented in figure 17 along with the corresponding downcore temperatures. Initially, the first three cores collected from Site NGHP-01-07 contained free gas causing the sediment to expand, which is evident from the thin yellow bands in the IR images (fig. 17). Less expansion was observed in the final core, Core NGHP-01-07D-04H, producing a more uniform color image. The median core temperature ranged between 23.8 and 25.1 °C, with the lowest temperature of 22.5 °C recorded in the last core collected (Core NGHP-01-07D-04H). Slight IR anomalies from this core were identified in three separate cores (Cores NGHP-01-07D-14X, -24X, and -25X).

IR images of the cut ends of core sections were acquired with a hand-held IR camera on the catwalk during sampling activities when possible. Twenty-seven core-end IR images were collected from Hole NGHP-01-07B and an additional four section end images were acquired from Hole NGHP-01-07D. Several IR images were acquired from the top of Sections NGHP-01-07B-05H-3, -06H-3, -07H-3, -13X-3, and -14X-2 and are presented in figure 18 with a temperature scale from 34 °C to 19 °C. The outside of the core end has a temperature of 26 °C and is evenly represented by the color red. The coldest portion of the core-end image is represented by the dark blue to black colors and can be seen as the dominant colors in the image. Notice that the inside temperature is approximately 20 °C for images with the darkest interiors (Sections NGHP-01-07B-05H-5, -13X-3, and -14X-2). These IR section end images are representative of the images typically collected from Site NGHP-01-07.

Core-End Temperature Readings

Core-end temperature readings were taken on all cores immediately following the IR track imaging. Typically four temperature probes were inserted approximately 8 cm into the end of each core and allowed to remain there until the core was completely processed and removed from the catwalk. A summary of the core-end temperature results (center position only) for Hole NGHP-01-07B is presented in figure 19. The shallowest core (Core NGHP-01-07B-01H) had the coldest (11 °C) end temperature in Hole NGHP-01-07B. Core NGHP-01-07B-13X, midway down the borehole at 86.2 mbsf also had a cold spot that measured 13 °C. The core-end temperatures vary between 15° and 20 °C for most of the cored interval, with no obvious trend. No temperatures below 11 °C were measured on cores collected from Hole NGHP-01-07B. Similar results were obtained from temperature measurements collected on Hole NGHP-01-07D.

Table 12. List of infrared image files collected on the catwalk from Hole NGHP-01-07D.

Core	Section	Top	Date	Time	Image #	Comments
2	4	x	7/5	8:50	G0705-01	IMG file
2	4	x	7/5	8:50	G0705-02	Core end, BMP
3	3	x	7/5	9:45	G0705-03	IMG file
3	3	x	7/5	9:45	G0705-04	Core end, BMP
4	4	x	7/5	10:20	G0705-05	IMG file
4	4	x	7/5	10:20	G0705-06	Core end, BMP
5	3	x	7/5	11:28	G0705-07	IMG file
5	3	x	7/5	11:28	G0705-08	Core end, BMP
6	3	x	7/5	12:18	G0705-09	IMG file
6	3	x	7/5	12:18	G0705-10	Core end, BMP
7	?	x	7/5	13:24	G0705-11	IMG file
7	?	x	7/5	13:24	G0705-12	Core end, BMP
8	3	x	7/5	2:02	G0705-13	IMG file
8	3	x	7/5	2:02	G0705-14	Core end, BMP
9	5		7/5	2:37	G0705-15	IMG file
9	5		7/5	2:37	G0705-16	secton, BMP
9	5		7/5	2:38	G0705-17	IMG file
9	5		7/5	2:38	G0705-18	secton, BMP
9	5		7/5	2:38	G0705-19	IMG file
9	5		7/5	2:38	G0705-20	secton, BMP
9	5		7/5	2:38	G0705-21	IMG file
9	5		7/5	2:38	G0705-22	secton, BMP
9	5		7/5	2:39	G0705-23	IMG file
9	5		7/5	2:39	G0705-24	secton, BMP
9	5		7/5	2:39	G0705-25	IMG file
9			7/5	2:39	G0705-26	secton, BMP
10	2	x	7/5	9:23	G0705-27	IMG file
10	2	x	7/5	9:23	G0705-28	Core end, BMP
13	3	x	7/5	9:57	G0705-29	IMG file
13	3	x	7/5	9:57	G0705-30	Core end, BMP
14	2	x	7/5	11:03	G0705-31	IMG file
14	2	x	7/5	11:03	G0705-32	Core end, BMP
15	3	x	7/5	12:02	G0705-33	IMG file
15	3	x	7/5	12:02	G0705-34	Core end, BMP
17	3	x	7/6	2:49	G0706-01	IMG file
17	3	x	7/6	2:49	G0706-02	Core end, BMP
18	3	x	7/6	4:36	G0706-03	IMG file
18	3	x	7/6	4:36	G0706-04	Core end, BMP
19	2	x	7/6	6:05	G0706-05	IMG file
19	2	x	7/6	6:05	G0706-06	Core end, BMP
20	5	x	7/6	7:00	G0706-07	IMG file
20	5	x	7/6	7:00	G0706-08	Core end, BMP
23	1	x	7/6	12:27	G0706-09	IMG file
23	1	x	7/6	12:27	G0706-10	Core end, BMP
24	3	x	7/6	13:50	G0706-11	IMG file
24	3	x	7/6	13:50	G0706-12	Core end, BMP
25	4	x	7/6	14:43	G0706-13	IMG file
25	4	x	7/6	14:43	G0706-14	Core end, BMP
26	3	x	7/6	17:11	G0706-15	IMG file
26	3	x	7/6	17:11	G0706-16	Core end, BMP
27	3	x	7/6	18:28	G0706-17	IMG file
27	3	x	7/6	18:28	G0706-18	Core end, BMP
30	4	x	7/6	23:11	G0706-19	IMG file
30	4	x	7/6	23:11	G0706-20	Core end, BMP

Table 13. List of infrared section-end image files collected from Hole NGHP-01-07B.

Core	Imaging length (cm)	First run	Date	Start time	Temperature (start/end) (°C)	File ID	Screen image saved	Comments
1H	860	x	7/8	17:44	29.9/29.9	NGHP-07-D-1	Yes	15–30 °C
2H	850	x	7/8	19:29	29.5/29.5	NGHP-07-D-2	Yes	15–30 °C
3H	530	x	7/8	20:38	29.5/29.5	NGHP-07-D-3	Yes	15–30 °C
4H	850	x	7/8	22:08	29.1/29.1	NGHP-07-D-4	Yes	15–30 °C

*Temperature range for images displayed during core collection.

Index Properties

Water content (related to solids) varies from a high of 128 percent to a low of 36 percent (table 15) and rapidly decreases to a subbottom depth of 22 mbsf. Porosity varies from 76 percent to 49 percent downhole. Water content and porosity decrease uniformly and linearly downhole in primarily nannofossil-bearing clay, foraminifera-bearing clay, and clay (see "Lithostratigraphy"). This overall trend is similar to the LWD data except for excursions immediately below the BSR at 188 mbsf. A Fugro Pressure Core (FPC) (NGHP-01-07B-29Y at 194.73 mbsf) had a substantially lower water content (13.7 percent) and porosity (26.7 percent) than adjacent recovered sediment. It is unlikely that such fine-grained sediment could dewater by FPC drilling, core recovery or core handling may alter water content and porosity in the time required for sampling, suggesting that this FPC may have coincidently sampled a drier layer *in situ*. However, this hypothesis is not supported by LWD measurements.

Except for an offset that decreases with subbottom depth, bulk density data from LWD are in close agreement with either MAD or MSCL values continuously downhole (fig. 20). Grain density varies from 2.51 to 2.79 g/cm^3 with an average value of 2.72 g/cm^3. Some of this variation is a result of performing mass measurements at sea on small sediment samples after the water has been removed by drying. This result is most pronounced in the upper sections of the hole where water contents are highest. Grain densities are lower in the upper part of the hole, possibly the result of increased marine organic content. The pycnometers often had difficulty measuring the volume of samples from the top of the hole.

Table 14. List of infrared section-end image files collected from Hole NGHP-01-07D.

Core	Section	Top	Date	Time	Image #	Comments
1	2	x	7/8	17:51	G0708-01	IMG file
1	2	x	7/8	17:51	G0708-02	Core end, BMP
2	4	x	7/8	19:35	G0708-03	IMG file
2	4	x	7/8	19:35	G0708-04	Core end, BMP
3	3	x	7/8	20:47	G0708-05	IMG file
3	3	x	7/8	20:47	G0708-06	Core end, BMP
4	3	x	7/8	22:22	G0708-07	IMG file
4	3	x	7/8	22:22	G0708-08	Core end, BMP

Strength

Shear strength increased linearly with depth to the boundary between APC and XCB cores (tables 16, 17, and 18; fig. 20). Below that depth, slightly more variation exists, illustrating the effect of disturbance caused by rotary coring on sediment. However, this effect is less at this site than previous drilled holes. Although testing was to be restricted to intact biscuits, it was occasionally difficult to differentiate between biscuits and adjacent disturbed sediment.

Pocket Penetrometer (PP) strengths in FPC NGHP-01-07B-29Y were appreciably higher than surrounding sediment reflecting a lower water content and higher density in that core. It is also possible that some pressure cores may be less disturbed than XCB cores. Below 239.5 mbsf Cores NGHP-01-07D-02X to NGHP-01-07D-04X were cut with a rock saw accompanied by substantial application of water. The core was also cleaned using a water hose. Interestingly, the water content does not appear to increase in those cores. However, sediment strength was degraded because a substantial number of PP results were invalidated due to various unacceptable failure mechanisms. The cores were split with a wire saw above this depth.

The measured shear strengths were normalized to the effective vertical stress, σ'_v (fig. 21) to provide qualitative information on the stress history of the sediment. The strength/effective vertical stress ranges from approximately 0.45 at the top of the hole (with one outlier at 0.79) to an average of about 0.075 near the bottom of the hole. These values are in overall agreement with a number of other normally consolidated clays (Holtz and Kovacs, 1981), although the values below 0.1 are probably an artifact of the more deeply recovered sediment from this hole compared to most engineering-type projects from which the published comparison samples were taken. Hunt (1984) states that the strength/effective vertical stress ratio typically is between 0.4 and 0.16. The wide scatter in the results at the top of the hole reflects the dependency of this ratio on the stress path as well as the test method (Bjerrum, 1972; Ladd, and others, 1977). Because almost all of the values are below 0.4, the implication is that these sediments are currently in a depositional environment and have not been overconsolidated by erosional or other geologic processes.

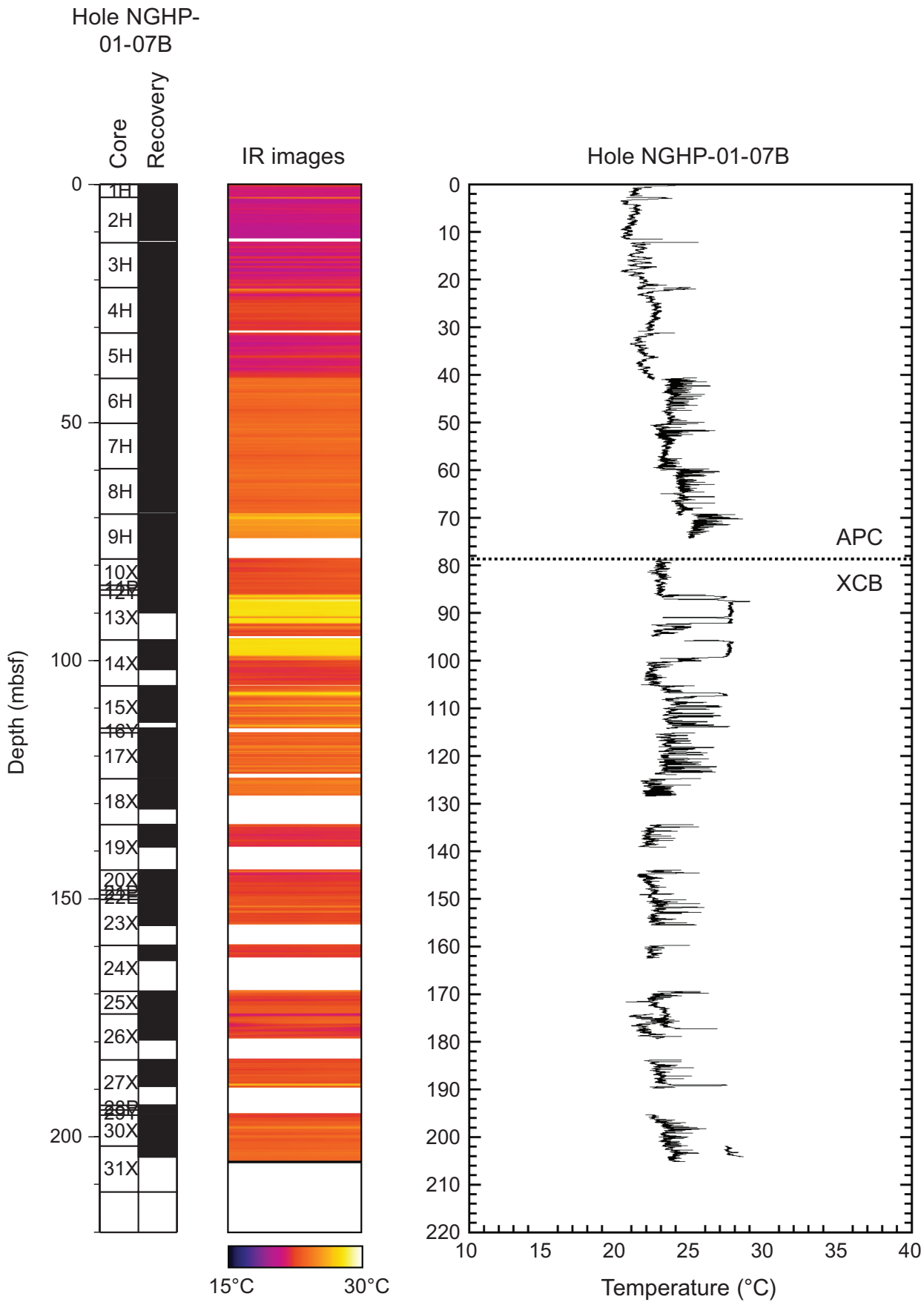

Figure 16. Infrared imaging and the derived downhole temperature profile for Hole NGHP-01-07B.

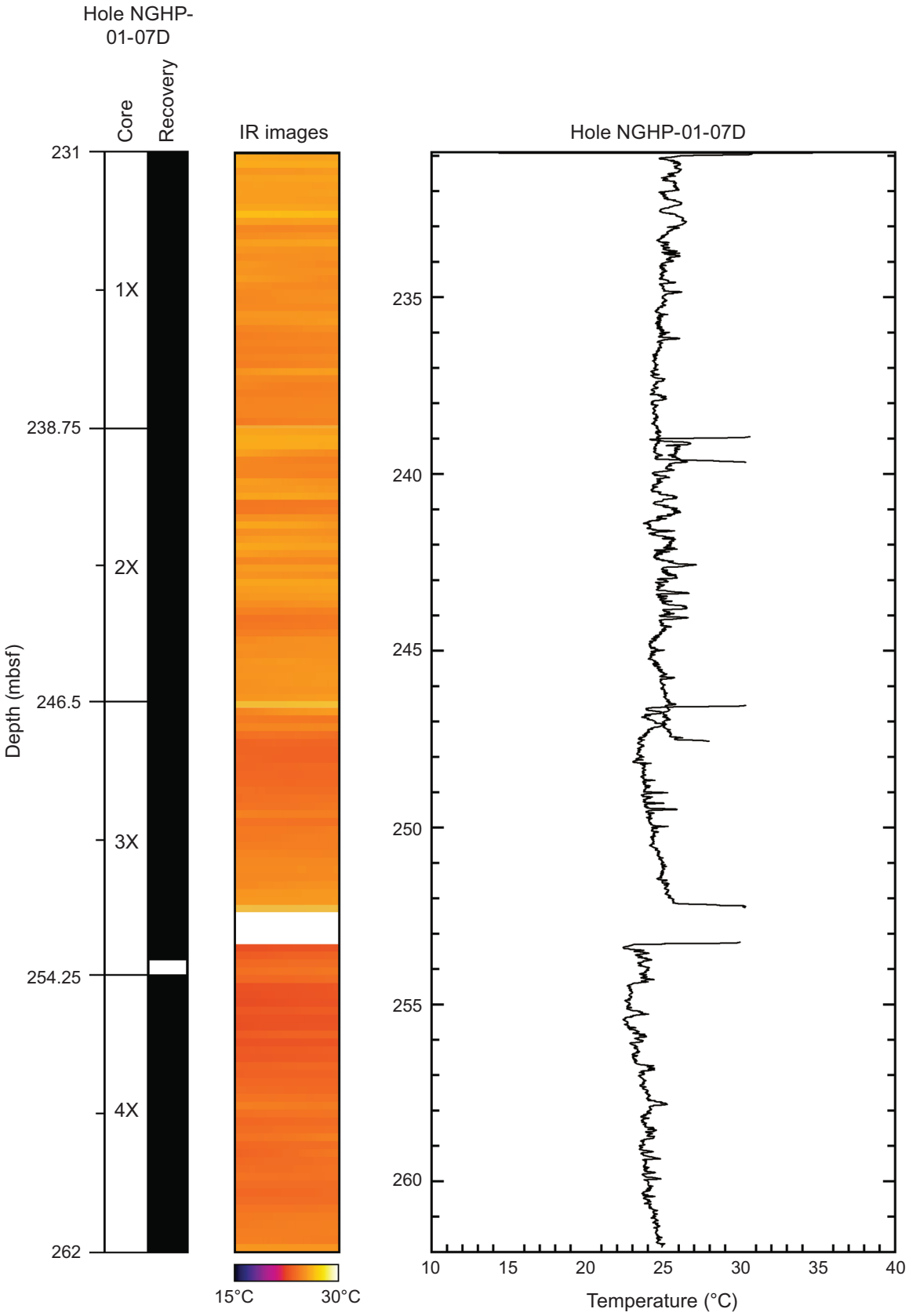

Figure 17. Infrared imaging and the derived downhole temperature profile for Hole NGHP-01-07D.

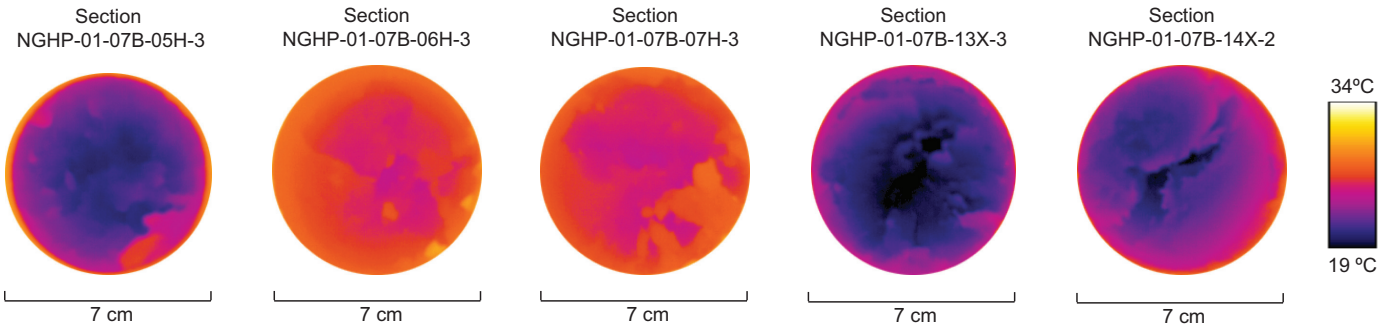

Figure 18. Core-end infrared image from Hole NGHP-01-07B, top, with the corresponding reference temperature scales.

Although a limited number of measurements were made, the peak (Sv) and remolded (Srem) vane shear strengths clearly increase with subbottom depth. The sensitivity (St), which equals Sv/Srem, decreased from 6 to 2 with depth (fig. 22). Sensitivity values represent the amount of strength loss after remolding and in extreme examples can reach values of 500 (Lambe and Whitman, 1969). This sediment has low to medium sensitivity (Holtz and Kovacs, 1981). High values of sensitivity are indicative of good quality core recovery because the sediment has not been highly disturbed.

Electrical Resistivity

With the exception of a few excursions, Logging-While-Drilling (LWD) conducted previously in Hole NGHP-01-07A indicates that resistivity values are fairly low and uniform downhole in overall agreement with the MSCL data. Unlike other holes, for example, Hole NGHP-01-10B, the resistivity-at-bit (RAB) image does not indicate that significant zones of high resistivity (and gas hydrate) are present in Hole NGHP-01-07A. The resistivity (except from 32 to 40 mbsf) determined using the Wenner array on split cores are also uniform (table 19); however, they are offset below both the MSCL and LWD values (fig. 23). This may in part be due to Wenner measurements being conducted on intact core material, rather than a wider portion of core that may contain voids or small expansion cracks. Lower MSCL values are more representative of undisturbed sediment as they are less impacted by the presence of such micro voids caused by gas expansion.

The apparent formation factor is the ratio of the resistivity of a saturated sediment to the resistivity of the pore fluid and provides an indication of the relationships between sediment structure, void space, tortuosity, and other factors, and the ability of fluid to flow through the formation. Because pore water salinity typically varies a small amount in the recovered sediment (see "Inorganic Geochemistry"), we have normalized the measured Wenner resistivity values by that of seawater (approximately 0.2 Ω-m) (table 19). Values range from about 2.0 at the top of the core to 4.0 at the bottom, with a spike between 33 and 40 mbsf (fig. 24). Other equations and methods exist for calculating formation factor; however, they require the use of empirical constants that have not yet been determined for these particular sediments.

P-Wave Velocity

P-wave velocity (V_P) measured with the MSCL increased slightly from 1.48 km/s in the top of the Hole (fig. 23) to 1.59 km/s at a subbottom depth of 30 m, which represents the depth where gas and voids present in the sediment prevented further valid measurements from being logged. The contact V_P values of 1.47 to 1.53 km/s (table 20) are in agreement with the MSCL values at the top of the hole. Valid contact V_P measurements could not be determined below 23.5 mbsf which is higher than an SMI located at about 29 mbsf (see "Inorganic Geochemistry"). Methane, which is typically produced below the SMI, may come out of solution if present in a high enough concentration and attenuate acoustic signals.

Magnetic Susceptibility

Wide excursions exist in the magnetic susceptibility data indicating that primary and secondary magnetic minerals are present in alternating non-uniform high and low frequency layers (fig. 23; see "Lithostratigraphy"). A low-level layer is present between about 12 and 21 mbsf and may be the result of diagenetic reduction of magnetic signatures.

Thermal Conductivity

Thermal conductivities vary between 0.817 and 1.119 W/(m×K) and increase slightly with subbottom depth (table 21; fig. 23). Such values are well within the range of marine sediments (for example, Novosel, and others, 2007), although they are all lower than values determined by Davis and others (1990) for sediment from Cascadia and the Nankai Trough.

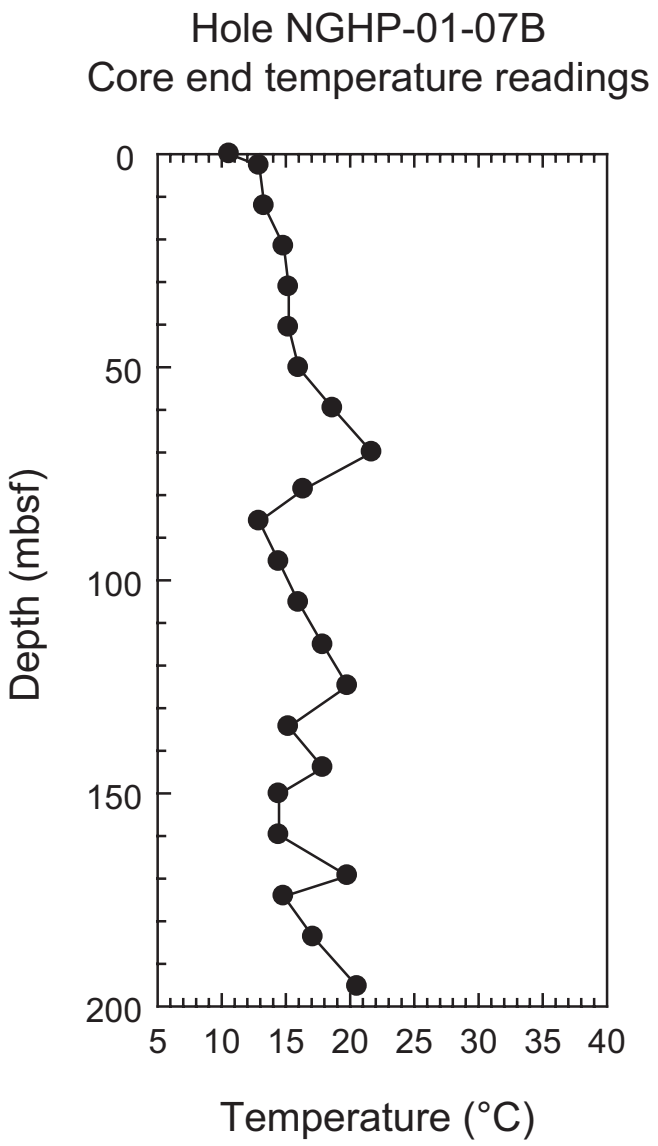

Figure 19. Core-end temperature measurements for Hole NGHP-01-07B.

Downhole Temperature Measurements

A number of different tools are available for determining downhole sediment temperature (see "Physical Properties" section of "Methods" chapter). Although six attempts were made, only three provided good quality *in situ* temperature data for Site NGHP-01-07. Seafloor temperature intercept was determined to be 5.3 ± 0.2 °C and the geothermal gradient was determined to be 52 ± 2 °C per km (table 22; fig. 25). Uncertainties are poorly constrained because of the lack of data. Nonetheless, the predicted depth to the BGHS of 198 mbsf is similar to the observed BSR depth of 188 mbsf (shipboard calculated seafloor temperature 5.2 °C, geothermal gradient 51 °C per km).

Pressure Coring

The main objectives of pressure coring during NGHP Expedition 01 were to quantify natural gas composition and concentration in sediments and to determine the nature and distribution of gas hydrate and free gas within the sediment matrix. Secondary objectives were to obtain measurements of physical properties on gas-hydrate-bearing sediments under *in situ* conditions, which can be used to help interpret regional seismic data, and obtain samples under full pressure for shorebased studies. To achieve these objectives, we conducted depressurization experiments and captured resultant gas to calculate gas hydrate quantity, made nondestructive measurements (X-ray imaging, P-wave velocity, gamma density) at *in situ* pressures and during depressurization to examine gas hydrate habit within sediments, and archived gas-hydrate-bearing sediments at *in situ* pressures for more comprehensive investigations on shore.

The BSR at Site NGHP-01-07, located in the Krishna-Godavari Basin, had an estimated depth of 188 mbsf, and there was a set of bright reflectors between 125–150 mbsf. LWD data from Hole NGHP-01-07A showed two layers of elevated electrical resistivities from 78–94 mbsf and 138–152 mbsf (see "Downhole Logging"). Specific objectives at Site NGHP-01-07 were to confirm and quantify the presence of gas hydrate in the two layers of elevated electrical resistivity as well as to investigate the gas hydrate content of the highly reflective sediment.

Pressure-Core Operations and Measurements

Pressure-coring tools were deployed seven times in Hole NGHP-01-07B (table 23); three PCS cores, three FPC cores, and one HRC core. Figures 26 and 27 show the pressure and temperature history of the cores during deployment, coring, recovery, and chilling (in the ice shuck) of the pressure-coring tools. Figures 28 and 29 show the measurements made on the four successful cores at full pressure and during depressurization. Figure 30 shows the gas and fluid released from the successful cores.

Core NGHP-01-07B-11P (84.2 mbsf), collected within the upper layer of elevated electrical resistivity, retrieved a full core (1.00 m) at pressure (table 23). The autoclave was placed in the MSCL–P for X-ray and gamma density measurements, which showed a somewhat disturbed core in the X-ray of the top half and that sediment existed in the lower half (fig. 29A). The core was depressurized, releasing 1.24 liters of methane, which is less than methane saturation at *in situ* temperature and pressure (table 24). After depressurization, the autoclave was again measured in the MSCL–P (fig. 29A). One chlorinity measurement was made on this core but the baseline chlorinity at this site was extremely hard to determine and so no gas-hydrate estimate could be made from porewater freshening.

Table 15. Moisture and density physical properties for Holes NGHP-01-07B and NGHP-01-07D.

Core, section, interval (cm)	Sample code	Depth (mbsf)	WCt (%)	WCs (%)	Grain density (g/cm³)	Bulk density (g/cm³)	Dry bulk density (g/cm³)	Porosity (%)	Void ratio	Unit weight (kN/m³)
NGHP-01-07B										
1H-2,32-34	MAD	1.82	56.23	128.45	2.51	1.38	0.61	75.87	3.14	13.57
2H-2,26-28	MAD	4.46	53.6	115.5	2.65	1.43	0.67	74.90	2.98	14.06
2H-3,26-28	MAD	5.96	52.57	110.85	2.56	1.43	0.68	73.48	2.77	14.06
2H-4,26-28	MAD	7.46	48.21	93.09	2.66	1.50	0.78	70.71	2.41	14.75
2H-5,26-28	MAD	8.96	47.78	91.49	2.74	1.52	0.80	70.95	2.44	14.94
2H-6,26-28	MAD	10.46	49.56	98.25	2.57	1.47	0.74	71.12	2.46	14.43
3H-1,80-82	MAD	13.00	50.93	103.8	2.68	1.47	0.72	73.04	2.71	14.42
3H-2,59-61	MAD	14.29	50.18	100.73	2.62	1.47	0.73	72.01	2.57	14.43
3H-3,58-60	MAD	15.78	47.9	91.93	2.55	1.49	0.78	69.60	2.29	14.61
3H-4,58-60	MAD	17.28	42.23	73.09	2.72	1.60	0.93	65.99	1.94	15.72
3H-5,59-61	MAD	18.79	37.96	61.19	2.74	1.68	1.04	62.04	1.63	16.44
3H-6,58-60	MAD	20.28	37.56	60.14	2.74	1.68	1.05	61.64	1.61	16.51
3H-7,57-59	MAD	21.77	37.69	60.48	2.71	1.67	1.04	61.52	1.60	16.42
4H-1,100-102	MAD	22.70	32.05	47.18	2.76	1.79	1.22	55.97	1.27	17.56
4H-2,79-81	MAD	23.99	30.89	44.7	2.79	1.82	1.26	54.91	1.22	17.88
4H-3,79-81	MAD	25.49	30.61	44.11	2.73	1.81	1.26	54.03	1.18	17.76
4H-4,9-11	MAD	26.29	31.34	45.65	2.73	1.79	1.23	54.81	1.21	17.59
4H-5,9-11	MAD	27.79	30.34	43.56	2.76	1.83	1.27	54.00	1.17	17.90
4H-6,7-9	MAD	29.27	32.9	49.02	2.75	1.77	1.19	56.80	1.31	17.37
4H-7,9-11	MAD	30.29	33.03	49.31	2.72	1.76	1.18	56.70	1.31	17.27
5H-1,58-60	MAD	31.78	34.24	52.07	2.75	1.74	1.15	58.13	1.39	17.08
5H-2,58-60	MAD	33.28	35.84	55.86	2.73	1.71	1.10	59.75	1.48	16.77
5H-3,58-60	MAD	34.78	37.19	59.2	2.71	1.68	1.06	61.01	1.57	16.50
5H-4,60-62	MAD	36.30	31.87	46.79	2.74	1.79	1.22	55.55	1.25	17.53
5H-5,58-60	MAD	37.78	33.79	51.04	2.71	1.74	1.15	57.41	1.35	17.09
5H-6,58-60	MAD	39.28	33.05	49.36	2.69	1.75	1.17	56.46	1.30	17.18
5H-7,58-60	MAD	40.78	35.63	55.34	2.69	1.71	1.10	59.25	1.45	16.73
6H-1,22-24	MAD	40.92	32.12	47.32	2.74	1.78	1.21	55.81	1.26	17.48
6H-2,32-34	MAD	42.52	33.65	50.73	2.74	1.75	1.16	57.54	1.36	17.20
6H-3,9-11	MAD	43.79	35.88	55.95	2.71	1.70	1.09	59.62	1.48	16.72
6H-4,11-13	MAD	45.31	34.72	53.19	2.70	1.72	1.13	58.37	1.40	16.91
6H-5,17-19	MAD	46.87	32.13	47.33	2.73	1.78	1.21	55.75	1.26	17.45
6H-6,19-21	MAD	48.39	30.41	43.69	2.76	1.82	1.27	54.02	1.17	17.87
6H-7,7-9	MAD	49.04	32.49	48.12	2.74	1.77	1.20	56.21	1.28	17.40
7H-1,106-108	MAD	51.26	35.84	55.86	2.73	1.71	1.10	59.80	1.49	16.78
7H-2,17-19	MAD	51.87	32.45	48.03	2.72	1.77	1.20	56.03	1.27	17.37
7H-3,14-16	MAD	53.26	33.31	49.95	2.72	1.75	1.17	57.00	1.33	17.21
7H-4,9-11	MAD	54.71	33.26	49.84	2.72	1.76	1.17	56.93	1.32	17.21
7H-5,7-9	MAD	56.19	33.91	51.3	2.72	1.74	1.15	57.62	1.36	17.09
7H-6,6-8	MAD	57.68	34.35	52.33	2.69	1.73	1.13	57.89	1.37	16.95
7H-7,7-9	MAD	59.19	31.73	46.47	2.73	1.79	1.22	55.27	1.24	17.52
8H-1,8-10	MAD	59.78	33.73	50.9	2.71	1.75	1.16	57.39	1.35	17.11
8H-2,9-11	MAD	61.16	32.39	47.9	2.75	1.78	1.20	56.20	1.28	17.45
8H-3,6-8	MAD	62.62	32.96	49.17	2.73	1.76	1.18	56.71	1.31	17.31
8H-4,10-12	MAD	64.08	26.09	35.29	2.72	1.90	1.41	48.37	0.94	18.65
8H-5,9-11	MAD	65.57	30.42	43.72	2.75	1.82	1.27	53.97	1.17	17.85
8H-6,14-16	MAD	67.12	31.26	45.47	2.72	1.79	1.23	54.68	1.21	17.60
8H-7,10-12	MAD	68.08	30.13	43.12	2.71	1.81	1.27	53.29	1.14	17.79
9H-2,19-21	MAD	70.20	31.09	45.13	2.71	1.79	1.24	54.36	1.19	17.58
9H-3,11-13	MAD	70.74	30.84	44.59	2.72	1.80	1.25	54.18	1.18	17.67
9H-4,23-25	MAD	72.36	28.76	40.36	2.75	1.85	1.32	51.99	1.08	18.19
9H-5,2-4	MAD	73.65	31.32	45.6	2.76	1.81	1.24	55.14	1.23	17.71
9H-6,27-29	MAD	75.30	31.31	45.58	2.73	1.80	1.23	54.80	1.21	17.61
9H-7,8-10	MAD	76.13	30.14	43.14	2.75	1.82	1.27	53.61	1.16	17.89
9H-8,4-6	MAD	77.56	29.13	41.11	2.73	1.84	1.30	52.26	1.09	18.04
10X-1,25-27	MAD	78.95	30.39	43.65	2.79	1.83	1.27	54.25	1.19	17.96
10X-2,9-11	MAD	80.29	29.15	41.14	2.77	1.85	1.31	52.64	1.11	18.16
10X-3,5-7	MAD	81.75	28.75	40.35	2.75	1.85	1.32	51.99	1.08	18.19
10X-4,12-14	MAD	83.32	31.44	45.85	2.75	1.85	1.27	56.58	1.30	18.10

Table 15. Moisture and density physical properties for Holes NGHP-01-07B and NGHP-01-07D.—Continued

Core, section, interval (cm)	Sample code	Depth (mbsf)	WCt (%)	WCs (%)	Grain density (g/cm³)	Bulk density (g/cm³)	Dry bulk density (g/cm³)	Porosity (%)	Void ratio	Unit weight (kN/m³)
NGHP-01-07B—Continued										
10X-5,8-10	MAD	84.78	31.22	45.38	2.73	1.80	1.24	54.72	1.21	17.63
10X-6,15-17	MAD	86.35	29.02	40.88	2.75	1.85	1.31	52.25	1.09	18.11
11P-1,14-16	MAD	84.34	31.97	46.99	2.73	1.78	1.21	55.56	1.25	17.48
12Y-1,14-16	MAD	85.34	29.67	42.19	2.75	1.84	1.29	53.10	1.13	18.00
13X-1,14-16	MAD	86.34	34.39	52.41	2.74	1.74	1.14	58.36	1.40	17.07
13X-2,14-16	MAD	86.64	35.28	54.51	2.75	1.73	1.12	59.38	1.46	16.93
13X-4,14-16	MAD	88.74	30.52	43.92	2.73	1.81	1.26	53.88	1.17	17.76
14X-1,75-77	MAD	96.45	29.13	41.1	2.77	1.85	1.31	52.59	1.11	18.16
14X-2,77-79	MAD	97.97	28.8	40.45	2.74	1.85	1.32	51.95	1.08	18.14
14X-3,16-18	MAD	98.86	27.96	38.81	2.75	1.87	1.35	50.97	1.04	18.34
14X-4,41-43	MAD	100.11	27.57	38.07	2.73	1.87	1.36	50.33	1.01	18.36
14X-5,12-14	MAD	100.52	26.37	35.81	2.75	1.90	1.40	48.96	0.96	18.68
15X-1,24-26	MAD	105.54	28.64	40.13	2.73	1.85	1.32	51.65	1.07	18.14
15X-2,30-32	MAD	107.06	28.63	40.12	2.75	1.86	1.33	51.84	1.08	18.21
15X-3,5-7	MAD	108.31	27.08	37.14	2.74	1.89	1.38	49.85	0.99	18.51
15X-4,22-24	MAD	109.98	27.64	38.19	2.75	1.87	1.35	50.44	1.02	18.36
15X-5,18-20	MAD	111.44	26.45	35.96	2.74	1.90	1.40	48.96	0.96	18.62
16Y-1,13-15	MAD	114.33	23.2	30.21	2.72	1.97	1.51	44.50	0.80	19.29
17X-2,15-17	MAD	116.85	29.87	42.59	2.75	1.83	1.28	53.36	1.14	17.97
17X-3,25-27	MAD	118.45	31.51	46	2.69	1.78	1.22	54.68	1.21	17.46
17X-4,14-16	MAD	119.80	26.3	35.68	2.72	1.89	1.40	48.59	0.94	18.58
17X-5,14-16	MAD	121.30	28.87	40.58	2.73	1.85	1.31	51.93	1.08	18.10
17X-6,14-16	MAD	122.64	28.7	40.25	2.72	1.84	1.32	51.62	1.07	18.09
18X-1,98-100	MAD	125.78	27.75	38.41	2.76	1.88	1.36	50.80	1.03	18.41
18X-2,14-16	MAD	126.24	26.4	35.87	2.74	1.90	1.40	48.92	0.96	18.64
18X-3,14-16	MAD	127.74	27.54	38.01	2.76	1.88	1.37	50.59	1.02	18.48
18X-4,14-16	MAD	129.24	27.04	37.06	2.76	1.89	1.38	49.95	1.00	18.58
19X-1,4-6	MAD	134.44	28.66	40.17	2.71	1.84	1.31	51.46	1.06	18.06
19X-2,4-6	MAD	135.94	28.43	39.72	2.69	1.84	1.32	51.03	1.04	18.06
19X-3,4-6	MAD	136.75	28.12	39.11	2.67	1.84	1.32	50.45	1.02	18.05
19X-4,4-6	MAD	137.74	28.44	39.73	2.71	1.85	1.32	51.26	1.05	18.13
20X-1,11-13	MAD	144.11	32.43	47.99	2.79	1.79	1.21	56.62	1.31	17.56
20X-2,18-20	MAD	145.19	34.47	52.59	2.76	1.74	1.14	58.56	1.41	17.09
20X-3,5-7	MAD	146.56	33.62	50.64	2.76	1.76	1.17	57.67	1.36	17.26
20X-4,8-10	MAD	148.09	29.48	41.8	2.69	1.82	1.28	52.32	1.10	17.85
20X-5,10-12	MAD	149.61	27.87	38.64	2.76	1.88	1.35	50.99	1.04	18.40
21P-1,62-64	MAD	148.82	28.88	40.61	2.69	1.83	1.30	51.56	1.06	17.95
22E-1,31-33	MAD	149.51	28.31	39.49	2.70	1.85	1.32	50.96	1.04	18.11
23X-1,12-14	MAD	150.32	31.66	46.33	2.66	1.77	1.21	54.58	1.20	17.34
23X-2,16-18	MAD	151.86	29.89	42.62	2.71	1.82	1.27	52.98	1.13	17.83
23X-3,15-17	MAD	153.35	30.33	43.53	2.69	1.80	1.26	53.27	1.14	17.67
23X-4,10-12	MAD	154.80	29.82	42.48	2.71	1.82	1.28	52.84	1.12	17.83
24X-1,14-16	MAD	159.94	30.4	43.68	2.68	1.80	1.25	53.29	1.14	17.63
24X-2,13-15	MAD	161.43	30.31	43.5	2.69	1.80	1.26	53.33	1.14	17.70
25X-1,114-116	MAD	170.54	28.76	40.37	2.68	1.83	1.31	51.37	1.06	17.97
25X-2,32-34	MAD	171.22	29.18	41.21	2.72	1.83	1.30	52.20	1.09	17.99
25X-3,73-75	MAD	172.41	29.3	41.44	2.70	1.83	1.29	52.20	1.09	17.92
25X-4,37-39	MAD	173.55	28.31	39.48	2.69	1.84	1.32	50.91	1.04	18.09
25X-6,35-37	MAD	176.53	31.1	45.14	2.68	1.78	1.23	54.09	1.18	17.49
26X-2,62-64	MAD	176.32	29.45	41.75	2.77	1.84	1.30	52.97	1.13	18.09
26X-3,8-10	MAD	177.28	29.21	41.25	2.69	1.82	1.29	51.94	1.08	17.89
27X-1,8-10	MAD	183.88	30.53	43.94	2.69	1.80	1.25	53.50	1.15	17.63
27X-2,22-24	MAD	185.52	29.83	42.51	2.70	1.81	1.27	52.77	1.12	17.79
27X-3,6-8	MAD	186.86	31.51	46.01	2.66	1.77	1.21	54.44	1.20	17.38
27X-4,6-8	MAD	187.96	27.36	37.67	2.71	1.87	1.36	49.86	0.99	18.33
28P-1,82-84	MAD	194.22	30.02	42.91	2.69	1.81	1.27	52.95	1.13	17.74
29Y-1,33-35	MAD	194.73	12.08	13.73	2.72	2.27	1.99	26.71	0.36	22.25
30X-1,21-23	MAD	195.61	35.98	56.21	2.70	1.70	1.09	59.67	1.48	16.68
30X-2,14-16	MAD	196.07	31.39	45.76	2.71	1.79	1.23	54.76	1.21	17.55

Table 15. Moisture and density physical properties for Holes NGHP-01-07B and NGHP-01-07D.—Continued

Core, section, interval (cm)	Sample code	Depth (mbsf)	WCt (%)	WCs (%)	Grain density (g/cm³)	Bulk density (g/cm³)	Dry bulk density (g/cm³)	Porosity (%)	Void ratio	Unit weight (kN/m³)
NGHP-01-07B—Continued										
30X-3,15-17	MAD	197.58	29.39	41.61	2.66	1.81	1.28	51.92	1.08	17.77
30X-4,15-17	MAD	199.08	28.86	40.57	2.70	1.84	1.31	51.92	1.08	18.09
30X-5,7-9	MAD	200.50	30.99	44.91	2.66	1.78	1.23	53.76	1.16	17.45
30X-6,31-33	MAD	202.24	28.93	40.7	2.74	1.85	1.31	52.06	1.09	18.10
30X-7,8-10	MAD	203.51	26.62	36.27	2.69	1.88	1.38	48.71	0.95	18.41
31X-1,28-30	MAD	202.18	30.74	44.38	2.69	1.80	1.24	53.83	1.17	17.61
31X-2,12-14	MAD	203.52	32.72	48.63	2.69	1.76	1.18	56.05	1.28	17.23
NGHP-01-07D										
1X-1,24-26	MAD	231.44	30.32118952	43.51565319	2.71	1.81	1.26	53.48	1.15	17.74
1X-2,24-26	MAD	232.94	29.1102154	41.06404833	2.72	1.84	1.30	52.16	1.09	18.02
1X-3,24-26	MAD	234.44	27.96750341	38.82623085	2.71	1.86	1.34	50.60	1.02	18.20
1X-4,24-26	MAD	235.94	26.04181923	35.21154652	2.71	1.90	1.40	48.22	0.93	18.62
1X-5,24-26	MAD	237.44	26.35766253	35.79145289	2.69	1.89	1.39	48.46	0.94	18.49
1X-6,34-36	MAD	239.04	27.05237565	37.08465614	2.73	1.88	1.37	49.64	0.99	18.46
2X-1,82-84	MAD	239.82	30.3349201	43.54393928	2.74	1.82	1.27	53.80	1.16	17.84
2X-2,28-30	MAD	240.78	26.67870308	36.3860218	2.72	1.89	1.38	49.13	0.97	18.52
2X-3,18-20	MAD	242.18	26.80132937	36.61450288	2.75	1.89	1.39	49.50	0.98	18.58
2X-4,28-30	MAD	243.78	27.316753	37.58328656	2.73	1.88	1.36	49.96	1.00	18.40
2X-5,23-25	MAD	245.23	26.37461443	35.82271824	2.75	1.90	1.40	48.98	0.96	18.68
2X-6,25-27	MAD	246.75	24.02380805	31.6201792	2.74	1.95	1.49	45.79	0.84	19.17
3X-1,32-34	MAD	246.92	29.99838789	42.85385291	2.71	1.82	1.27	53.10	1.13	17.81
3X-2,32-34	MAD	248.42	28.54171761	39.94179073	2.70	1.84	1.32	51.24	1.05	18.06
3X-3,32-34	MAD	249.92	28.91856962	40.68371931	2.68	1.83	1.30	51.57	1.07	17.94
3X-4,33-35	MAD	251.43	27.63548199	38.18927114	2.70	1.86	1.35	50.13	1.01	18.25
4X-1,33-35	MAD	253.63	25.40395381	34.05536233	2.73	1.92	1.43	47.54	0.91	18.82
4X-2,33-35	MAD	255.13	27.90523909	38.70633419	2.75	1.87	1.35	50.89	1.04	18.34
4X-3,33-35	MAD	256.63	27.9108963	38.7172192	2.72	1.86	1.34	50.67	1.03	18.26
4X-4,34-36	MAD	258.14	27.19753786	37.35799184	2.73	1.88	1.37	49.85	0.99	18.44
4X-5,33-35	MAD	259.63	26.62896514	36.29356624	2.68	1.87	1.38	48.66	0.95	18.38
4X-6,33-35	MAD	261.13	26.42972618	35.92446353	2.71	1.89	1.39	48.67	0.95	18.52

Core NGHP-01-07B-21P (148.2 mbsf), collected within the lower layer of elevated electrical resistivity, retrieved a full core (1.00 m) at pressure (table 23). This core warmed more than most pressure cores because the ice shuck was leaking. The autoclave was placed in the MSCL–P for X-ray and gamma density measurements, which showed a relatively uniform core in the x ray of the top half and that sediment existed in the lower half (fig. 29). The core was depressurized, releasing 3.26 liters of methane, corresponding to 1.0 percent methane hydrate as a percent of pore volume, or 8.2 mL of methane hydrate (table 24). After depressurization, the autoclave was again measured in the MSCL–P (fig. 29), and a final X-ray image was collected when the outer barrel was removed, showing the overall expansion of the core due to gas (fig. 29). One chlorinity measurement was made on this core but the baseline chlorinity at this site was extremely hard to determine and so no gas-hydrate estimate could be made from porewater freshening.

Core NGHP-1-07B-22E (149.2 mbsf), collected within the lower layer of elevated electrical resistivity, retrieved a partial core (0.54 m) at low pressure (table 23). The autoclave sealed at approximately 75 bar, leaked instantaneously, and resealed at 45 bar, only seconds after falling outside gas-hydrate stability. Further pressure loss was due to volume changes in the tool, not loss of material from the core. Core NGHP-01-07B-22E was transferred to the MSCL–P and X-ray images and gamma density measurements were collected (fig. 28). There was no evidence from these records of any gas-hydrate structures. Core NGHP-01-07B-22E was depressurized in the MSCL–P, releasing 1.23 liters of methane, which is less than methane saturation at *in situ* temperature and pressure (table 24). A final MSCL–P scan was collected at atmospheric pressure which showed a highly fractured core (fig. 29C). The line scan image shows the split core surface without any postsplitting treatment (scraping). One chlorinity measurement was made on this core but the baseline chlorinity at this site was extremely hard to determine and so no gas-hydrate estimate could be made from porewater freshening.

Core NGHP-01-07B-28P (193.4 mbsf), collected below the estimated depth of the BSR (188 mbsf), retrieved a full core (1.00 m) at pressure (table 23). No data were recorded during the deployment of this core. The autoclave was placed in the MSCL–P for X-ray and gamma density measurements, which showed dense layers in the x ray of the top half and

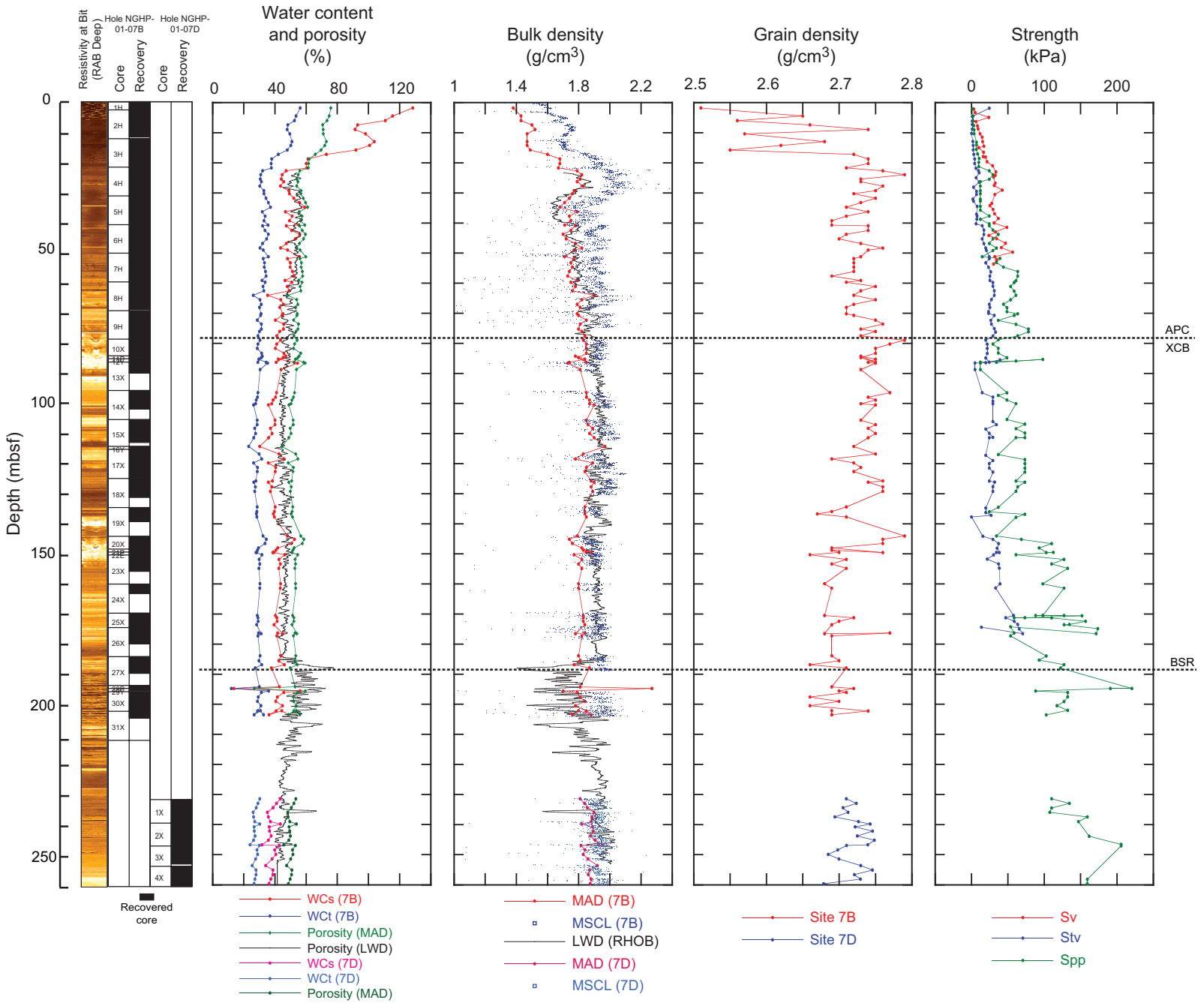

Figure 20. Profiles of LWD resistivity-at-bit, core recovery, index and strength properties for Holes NGHP-01-07B and NGHP-01-07D. [LWD, logging-while-drilling]

Table 16. Vane shear strength results for Hole NGHP-01-07B.

Core, section	Sample	Top (cm)	Depth (mbsf)	Sv (kPa)	Sres (kPa)	Srem (kPa)	St
NGHP-01-07B							
1H-2	VS	14	1.64	2.5	1.6	0.4	6.0
2H-2	VS	27	4.47	4.9	2.5	1.6	3.0
2H-3	VS	35	6.05	5.4	3.3	1.6	2.1
2H-4	VS	60	7.8	6.6	3.3	3.3	2.0

that sediment existed in the lower half (fig. 29). The core was depressurized, releasing 0.93 liters of methane, which is less than methane saturation at *in situ* temperature and pressure (table 24). After depressurization, the autoclave was again measured in the MSCL–P (fig. 29), and a final X-ray image was collected when the outer barrel was removed, showing the overall expansion of the core due to gas along with more dense layers (fig. 29). Dense layers were revealed as carbonate layers (fig. 29). One chlorinity measurement was made on this core but the baseline chlorinity at this site was extremely hard to determine and so no gas-hydrate estimate could be made from porewater freshening.

Gas-Hydrate Concentration, Nature, and Distribution from Pressure Coring

Four of the seven pressure cores at Site NGHP-01-07 were recovered at sufficient pressures to accurately assess the total concentration of methane and hence the predicted amount of gas hydrate. The calculated methane concentration for these cores is shown in figure 31 in relation to the phase boundaries for Structure I methane hydrate. (All pressure cores released nearly pure methane with less than 20 ppm ethane, confirming the suitability of Structure I methane hydrate for stability calculations; see "Organic Geochemistry"). Of three cores placed in the layers of elevated resistivity, only one (Core NGHP-01-07B-21P) returned a core oversaturated in methane. The gas-hydrate concentration estimated for this core was less than 1 percent of pore volume. The single core placed below the BSR, which appeared to be above the base of gas-hydrate stability, was also undersaturated in methane, providing no evidence for free gas or gas hydrate beneath the BSR.

Downhole Logging

Logging While Drilling

Operations

After tagging the seafloor at 1,297 mbrf (driller's depth), Hole NGHP-01-07A was spudded at 1540 hr on May 27, 2006. LWD tools in the BHA included the GeoVISION resistivity, the EcoScope, the SonicVISION, and the TeleScope MWD. For details on each LWD tool and measurements, see the "Downhole Logging" section in the "Methods" chapter.

To avoid washing out the hole near the seafloor, Hole NGHP-01-07A was spudded at a relatively low flow rate. The first 10 m were drilled while circulating 100 gpm with a rotation rate of 20 rpm and a rate of penetration (ROP) of 25 m/h. Below 10 mbsf, the rotation rate was increased to 30 rpm; over the range of 30–35 mbsf, the rotation rate was increased to 60 rpm and the flow rate was increased until the LWD tools turned on (~370 gpm), continuing to drill with a ROP of 25 m/h. The target depth of 260 mbsf (1,557 mbrf) was reached at 0528 hr on May 28, 2006. The tools were brought back to the surface at 0920 hr, and after downloading all the data, the rig down was completed at 1140 hr on May 28. (The depths in mbsf mentioned above are referenced to the seafloor depth tagged by the driller.)

Gas Monitoring with Real Time LWD/MWD Data

The LWD logs were acquired in the first hole drilled at Site NGHP-01-07 to plan coring and pressure coring operations in subsequent holes. As Hole NGHP-01-07A was drilled without coring, the LWD data had to be monitored for safety to detect gas entering the wellbore. As explained in the "Downhole Logging" section of the "Methods" chapter, the primary measurement used for this monitoring was the "annular pressure while drilling" (APWD) measured by the EcoScope tool in the borehole annulus. We looked for sudden decreases of more than 100 psi in the annular pressure, which could be due to low-density gas entering the wellbore. We also monitored pressure increases of the same magnitude, which could be due to fluid acceleration caused by a gas kick (Aldred and others, 1998).

Figure 32 shows the measured borehole fluid pressure profile in Hole NGHP-01-07A after subtraction of the hydrostatic pressure. This residual pressure curve shows only minor fluctuations that are well below the 100 psi level that would have required preventive action. We also monitored the coherence of the sonic waveforms acquired by the SonicVISION tool, focusing on the sound velocity in the borehole fluid. Gas indicators would be loss of coherence in the waveforms and a slower sound velocity for the drilling fluid. We found no significant decrease of sonic velocity or waveform coherence throughout the drilled interval.

LWD Log Quality

Figure 32 also shows the quality control logs for Hole NGHP-01-07A. The two curves for rate of penetration are an instantaneous rate of penetration (ROP_RM) and a rate of penetration averaged over the last 5 feet (ROP5_RM). The occasional large peaks in the instantaneous rate of penetration are artifacts due to depth fluctuations during pipe connections. The ROP is generally below 25 m/h, which is sufficient to record high-resolution GeoVISION resistivity images (for details, see "Downhole Logging" in the "Methods" chapter).

The density (DCAV) and ultrasonic caliper logs (UCAV) show an enlarged hole near the seafloor (30–77 mbsf). The bit size (dashed line in fig. 32) is 9 7/8 in, and the ultrasonic caliper shows that most of the borehole below 77 mbsf is about 10.5 in. The density caliper, however, shows a borehole that is

Table 17. Torvane strength results for Hole NGHP-01-07B.

Core, section, interval (cm)	Sample	Depth (mbsf)	Stv (kPa)	Core, section, interval (cm)	Sample	Depth (mbsf)	Stv (kPa)
NGHP-01-07B							
1H-2,36-38	TV	1.86	4.9	30X-1,24-26	TV	195.64	98.1
2H-2,48-50	TV	4.68	4.9	30X-2,13-15	TV	196.06	110.3
2H-3,48-50	TV	6.18	4.9	30X-3,15-17	TV	197.58	122.6
2H-4,12-14	TV	7.32	4.9	30X-4,19-21	TV	199.12	103.0
2H-5,12-14	TV	8.82	4.9	30X-5,68-70	TV	201.11	105.4
2H-6,12-14	TV	10.32	1.5	30X-6,29-31	TV	202.22	120.1
3H-1,77-79	TV	12.97	9.8	30X-7,63-65	TV	204.06	134.8
3H-2,54-56	TV	14.24	12.3	9H-2,6-8	TV	70.07	58.8
3H-3,54-56	TV	15.74	12.3	9H-3,14-16	TV	70.77	78.5
3H-4,54-56	TV	17.24	16.7	9H-4,26-28	TV	72.39	66.2
3H-5,54-56	TV	18.74	22.1	9H-5,5-7	TV	73.68	68.6
3H-6,53-55	TV	20.23	22.1	9H-6,16-18	TV	75.19	78.5
3H-7,70-72	TV	21.90	31.4	9H-7,27-29	TV	76.32	83.4
4H-1,96-98	TV	22.66	49.0	9H-8,13-15	TV	77.65	73.5
4H-2,14-16	TV	23.34	53.9	10X-1,23-25	TV	78.93	49.0
4H-3,31-33	TV	25.01	32.4	10X-2,13-15	TV	80.33	53.9
4H-4,24-26	TV	26.44	53.9	10X-3,2-4	TV	81.72	53.9
4H-5,46-48	TV	28.16	14.7	10X-4,17-19	TV	83.37	53.9
4H-6,35-37	TV	29.55	34.3	10X-5,20-22	TV	84.90	49.0
4H-7,35-37	TV	30.55	34.3	10X-6,12-14	TV	86.32	61.3
5H-1,96-98	TV	32.16	9.8	12Y-1,40-42	TV	85.60	98.1
5H-2,9-11	TV	32.79	14.7	13X-1,33-35	TV	86.53	49.0
5H-3,32-34	TV	34.52	39.2	14X-1,76-78	TV	96.46	36.8
5H-4,142-144	TV	37.12	34.3	14X-2,74-76	TV	97.94	73.5
5H-5,54-56	TV	37.74	39.2	14X-3,59-61	TV	99.29	73.5
5H-6,9-11	TV	38.79	36.8	14X-4,42-44	TV	100.12	73.5
5H-7,9-11	TV	40.29	31.9	15X-1,75-44	TV	106.05	73.5
6H-1,25-27	TV	40.95	36.8	15X-2,34-77	TV	107.10	85.8
6H-2,19-21	TV	42.39	42.9	15X-3,26-36	TV	108.52	49.0
6H-3,14-16	TV	43.84	42.9	15X-4,17-28	TV	109.93	61.3
6H-4,15-17	TV	45.35	36.8	15X-5,6-19	TV	111.32	73.5
6H-5,20-22	TV	46.90	42.9	15X-5,18-	TV	111.44	61.3
6H-6,15-17	TV	48.35	49.0	17X-2,60-20	TV	117.30	49.0
6H-7,20-22	TV	49.17	51.5	17X-3,79-62	TV	118.99	73.5
7H-1,111-113	TV	51.31	61.3	17X-4,36-81	TV	120.02	61.3
7H-2,19-21	TV	51.89	61.3	17X-5,36-38	TV	121.52	61.3
7H-3,16-18	TV	53.28	49.0	17X-6,38-40	TV	122.88	73.5
7H-4,17-19	TV	54.79	58.8	18X-1,102-104	TV	125.82	61.3
7H-5,17-19	TV	56.29	66.2	18X-2,7-9	TV	126.17	79.7
7H-6,6-8	TV	57.68	63.7	18X-3,7-9	TV	127.67	73.5
7H-7,3-5	TV	59.15	63.7	18X-4,14-16	TV	129.24	73.5
8H-1,15-17	TV	59.85	73.5	19X-1,34-36	TV	134.74	49.0
8H-2,4-6	TV	61.11	73.5	19X-2,40-42	TV	136.30	49.0
8H-3,3-5	TV	62.59	78.5	19X-3,50-52	TV	137.21	67.4
8H-4,7-9	TV	64.05	78.5	20X-1,17-19	TV	144.17	39.2
8H-5,4-6	TV	65.52	68.6	20X-2,22-24	TV	145.23	73.5
8H-6,13-15	TV	67.11	61.3	20X-3,9-11	TV	146.60	93.2
8H-7,13-15	TV	68.11	63.7	20X-4,14-16	TV	148.15	88.3
9H-1,35-37	TV	69.55	58.8	20X-5,7-9	TV	149.58	95.6
25X-2,34-36	TV	171.24	117.7	22E-1,32-34	TV	149.52	85.8
25X-3,74-76	TV	172.42	147.1	23X-1,19-21	TV	150.39	76.0
25X-4,35-37	TV	173.53	159.4	23X-2,8-10	TV	151.78	53.9
25X-5,25-27	TV	174.93	164.3	23X-3,20-22	TV	153.40	93.2
25X-6,34-36	TV	176.52	176.5	23X-4,6-8	TV	154.76	95.6
27X-1,16-18	TV	183.96	122.6	24X-1,18-20	TV	159.98	98.1
27X-2,20-22	TV	185.50	132.4	24X-2,7-9	TV	161.37	83.4
27X-3,14-16	TV	186.94	127.5	25X-1,114-116	TV	170.54	144.6
27X-4,7-9	TV	187.97	137.3				

Table 18. Pocket Penetrometer strength results for Site NGHP-01-07.

Core, section	Sample	Top (cm)	Depth (mbsf)	Spp (kPa)	Core, section	Sample	Top (cm)	Depth (mbsf)	Spp (kPa)
NGHP-01-07B									
1H-2	PP	60	2.10	1.5	25X-5	PP	22	174.90	174.0
2H-2	PP	26	4.46	2.1	25X-6	PP	37	176.55	171.5
2H-3	PP	43	6.13	2.3	27X-1	PP	13	183.93	102.9
2H-4	PP	43	7.63	3.1	27X-2	PP	6	185.36	93.1
2H-5	PP	43	9.13	3.8	27X-3	PP	8	186.88	127.4
2H-6	PP	17	10.37	3.8	27X-4	PP	10	188.00	122.5
3H-1	PP	104	13.24	6.9	29Y-1	PP	34	194.74	220.5
3H-2	PP	45	14.15	6.9	29Y-1	PP	37	194.77	191.1
3H-3	PP	42	15.62	6.7	30X-1	PP	23	195.63	88.2
3H-4	PP	42	17.12	8.4	30X-2	PP	12	196.05	132.3
3H-5	PP	34	18.54	10.7	30X-3	PP	13	197.56	132.3
3H-6	PP	18	19.88	10.0	30X-4	PP	17	199.10	127.4
3H-7	PP	6	21.26	10.0	30X-5	PP	8	200.51	117.6
4H-1	PP	100	22.70	24.5	30X-6	PP	13	202.06	132.3
4H-2	PP	80	24.00	29.4	30X-7	PP	10	203.53	102.9
4H-3	PP	80	25.50	24.5	9H-2	PP	20	70.21	63.7
4H-4	PP	10	26.30	12.3	9H-3	PP	12	70.75	58.8
4H-5	PP	10	27.80	12.3	9H-4	PP	29	72.42	36.8
4H-6	PP	8	29.28	12.3	9H-5	PP	7	73.70	61.3
4H-7	PP	10	30.30	12.3	9H-6	PP	26	75.29	78.4
5H-1	PP	96	32.16	12.3	9H-7	PP	18	76.23	78.4
5H-2	PP	10	32.80	12.3	9H-8	PP	5	77.57	63.7
5H-3	PP	33	34.53	12.3	10X-1	PP	20	78.90	36.8
5H-4	PP	10	35.80	12.3	10X-2	PP	8	80.28	29.4
5H-5	PP	53	37.73	24.5	10X-3	PP	6	81.76	36.8
5H-6	PP	15	38.85	12.3	10X-4	PP	8	83.28	36.8
5H-7	PP	15	40.35	24.5	10X-5	PP	14	84.84	49.0
6H-1	PP	28	40.98	24.5	10X-6	PP	15	86.35	34.3
6H-2	PP	22	42.42	29.4	12Y-1	PP	15	85.35	98.0
6H-3	PP	13	43.83	36.8	12Y-1	PP	70	85.90	61.3
6H-4	PP	14	45.34	29.4	13X-1	PP	13	86.33	12.3
6H-5	PP	11	46.81	24.5	13X-2	PP	13	86.63	12.3
6H-6	PP	17	48.37	34.3	13X-4	PP	13	88.73	12.3
6H-7	PP	23	49.20	29.4	14X-1	PP	80	96.50	49.0
7H-1	PP	110	51.30	14.7	14X-2	PP	15	97.35	36.8
7H-2	PP	11	51.81	39.2	14X-3	PP	15	98.85	49.0
7H-3	PP	11	53.23	34.3	14X-4	PP	39	100.09	61.3
7H-4	PP	11	54.73	44.1	15X-1	PP	10	105.40	49.0
7H-5	PP	9	56.21	63.7	15X-2	PP	15	106.91	73.5
7H-6	PP	10	57.72	63.7	15X-3	PP	17	108.43	61.3
7H-7	PP	10	59.22	61.3	15X-4	PP	14	109.90	73.5
8H-1	PP	9	59.79	58.8	15X-5	PP	15	111.41	73.5
8H-2	PP	10	61.17	53.9	15X-5	PP	15	111.41	61.3
8H-3	PP	15	62.71	58.8	17X-2	PP	30	117.00	36.8
8H-4	PP	10	64.08	61.3	17X-3	PP	49	118.69	73.5
8H-5	PP	11	65.59	53.9	17X-4	PP	35	120.01	73.5
8H-6	PP	8	67.06	44.1	17X-5	PP	34	121.50	73.5
8H-7	PP	17	68.15	49.0	17X-6	PP	33	122.83	73.5
9H-1	PP	35	69.55	49.0	18X-1	PP	100	125.80	61.3
23X-4	PP	10	154.80	132.3	18X-2	PP	12	126.22	73.5
24X-1	PP	16	159.96	98.0	18X-3	PP	12	127.72	63.7
24X-2	PP	13	161.43	127.4	18X-4	PP	12	129.22	61.3
25X-1	PP	108	170.48	98.0	19X-1	PP	15	134.55	36.8
25X-1	PP	110	170.50	127.4	19X-2	PP	15	136.05	24.5
25X-1	PP	113	170.53	88.2	19X-3	PP	20	136.91	73.5
25X-1	PP	120	170.60	151.9	19X-4	PP	20	137.90	61.3
25X-2	PP	32	171.22	73.5	20X-1	PP	12	144.12	34.3
25X-2	PP	35	171.25	58.8	20X-2	PP	20	145.21	68.6
25X-2	PP	40	171.30	110.3	20X-3	PP	8	146.59	110.3
25X-3	PP	73	172.41	156.8	20X-4	PP	8	148.09	93.1
25X-4	PP	34	173.52	134.8	20X-5	PP	12	149.63	102.9
25X-4	PP	39	173.57	127.4	22E-1	PP	32	149.52	112.7

Table 18. Pocket Penetrometer strength results for Site NGHP-01-07.—Continued

Core, section	Sample	Top (cm)	Depth (mbsf)	Spp (kPa)
NGHP-01-07B—Continued				
23X-1	PP	13	150.33	61.3
23X-2	PP	16	151.86	127.4
23X-3	PP	16	153.36	110.3
NGHP-01-07D				
1X-1	PP	25	231.45	110.25
1X-2	PP	25	232.95	134.75
1X-3	PP	25	234.45	110.25
1X-4	PP	25	235.95	107.8
1X-5	PP	25	237.45	159.25
1X-6	PP	35	239.05	147
2X-6	PP	8	243.85	161.7
2X-6	PP	75	246.58	205.8
2X-6	PP	55	247.05	205.8
4X-4	PP	35	258.15	159.25
4X-5	PP	35	259.65	159.25
4X-6	PP	35	261.15	159.25

smaller than the bit size for most of the interval below 77 mbsf; the ultrasonic caliper is a direct measurement of borehole size and is probably more reliable. Both the density and ultrasonic caliper show a rough borehole with small-scale variations in diameter between 185 and 218 mbsf.

The density correction, calculated from the difference between the short-and long-spaced density measurements, is everywhere less than 0.2 g/cm^3 (fig. 32), suggesting that the density measurements should be of good quality (see below, however).

Figure 33 is a summary of the LWD gamma ray, density, neutron porosity, and resistivity logs measured in Hole NGHP-01-07A. The gamma ray and resistivity logs measured by the GeoVISION and EcoScope tools generally agree. The GeoVISION and EcoScope gamma ray curves have the same shape, but are offset by about 20–30 gAPI; this difference is most likely due to tool calibration.

Figure 34 shows a comparison of the ring resistivity measured by GeoVISION with the attenuation and phase resistivity curves obtained by the EcoScope tool at different frequencies and transmitter-receiver spacings. For a given transmitter-receiver spacing, the phase-shift EcoScope resistivities have higher vertical resolution than the attenuation resistivities and thus show more detail.

Figure 33 also shows two bulk density curves: RHOB is the average density obtained by the EcoScope tool while rotating, while IDRO (image-derived density) is the density value measured when the sensors were in closest contact with the formation. The two density curves are generally very close, except between 30 and 40 mbsf, where the EcoScope density shows a slight decrease. The comparison with density measurements made on core samples from Holes NGHP-01-07B and NGHP-01-07D shows that the two log curves give generally slightly higher values, in particular between 140 and 185 mbsf. This is partially due to the effect of core expansion during the recovery of the samples.

The bottom of the gas-hydrate stability zone (BGHSZ) was expected to be at a depth of 188 mbsf in this hole. This depth is near the top of an interval where the densities, the neutron porosity, and all the high vertical resolution resistivities show an interval of prominent small-scale fluctuations between 185 and 218 mbsf. This is also the interval where the caliper logs show small-scale hole rugosity (fig. 32). A possible explanation for the coincidence of the BGHSZ with the top of this irregular interval is that free gas in the pore space weakens the sediment and makes it more likely to be washed out by the circulating drilling fluid. The small-scale variations in hole diameter may be due to a formation composed of thin layers whose strength is affected differently by free gas (for example, unconsolidated sands and clay-rich layers). If free gas was present below the BSR, it had to be in small enough amounts not to cause a decrease of the annulus pressure while drilling (see the gas monitoring results above). An alternative explanation for the hole rugosity in this interval is that there was no free gas but only thin unconsolidated sands that were washed out during drilling. The match of the top of this interval to the estimated depth of the BGHSZ would then be a coincidence.

The depths relative to seafloor were fixed for all of the LWD logs by identifying the step change in the GeoVISION gamma ray log at the seafloor. For Hole NGHP-01-07A, the gamma ray log identified the seafloor at 1,296.5 mbrf, 0.5 m above the initial depth estimated by the drillers (1,297 mbrf). The rig floor logging datum was located 10.5 m above sea level.

LWD Porosities

Sediment porosities can be determined from analyses of recovered cores and from downhole measurements (see “Physical Properties” and “Downhole Logging” in the “Methods” chapter). Sediment porosities were calculated from the LWD density and neutron logs in Hole NGHP-01-07A. Core-derived physical property data, including porosities (see “Physical Properties”), were used to calibrate and evaluate the log-derived sediment porosities.

The LWD EcoScope density measurements (r_b) from Hole NGHP-01-07A were used to calculate sediment porosities (φ) with the standard density-porosity relation: $\varphi = (r_g - r_b) / (r_g - r_w)$. We used a constant water density (r_w) of 1.03 g/cm^3 and a grain/matrix density (r_g) of 2.75 g/cm^3. The density log-derived porosities from Hole NGHP-01-07A range from just below 60 percent at 30 mbsf to about 45 percent at 250 mbsf (fig. 33). After coring Holes NGHP-01-07B and -07D, we were able to improve this porosity estimation by using the grain densities measured on core samples. In the same track in figure 33 we show the ”corrected” results derived by using at each depth the grain density measurement made from the closest sample. The difference from the original estimate is mostly negligible, except between 140 and 185 mbsf where the difference between log- and core-densities was the largest.

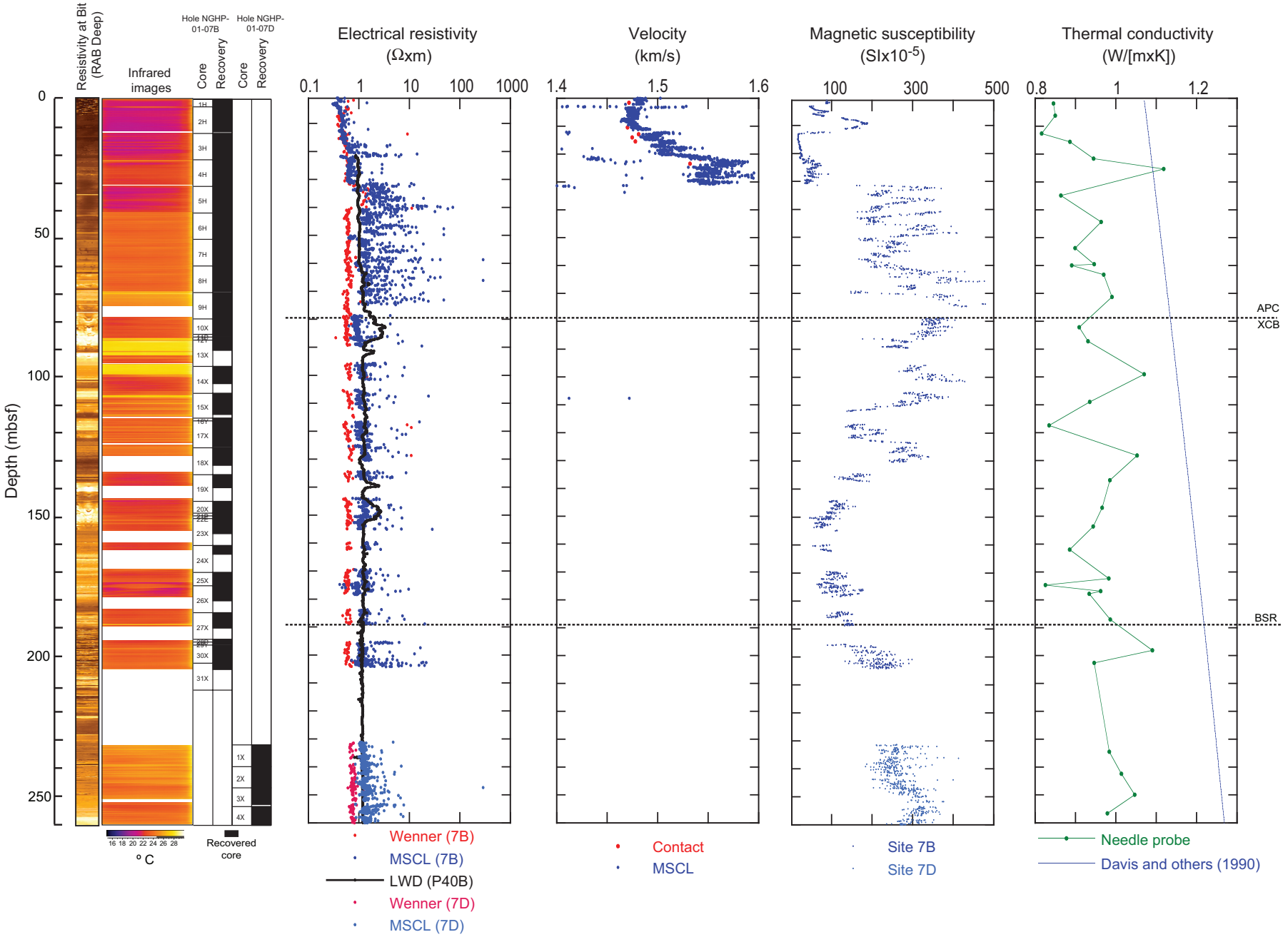

Figure 21. Shear strengths normalized by the effective vertical stress versus sub-bottom depth for Holes NGHP-01-07B and NGHP-01-07D.

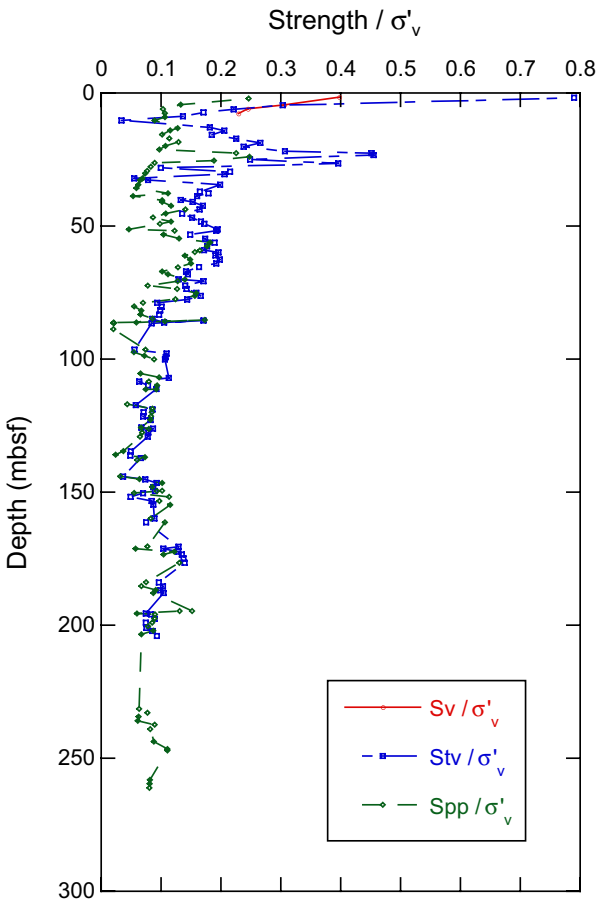

Figure 22. Peak and remolded vane shear strengths and sensitivity for Hole NGHP-01-07B.

The LWD neutron porosity log from Hole NGHP-01-07A (fig. 33) yielded sediment porosities ranging from an average value of about 60 percent at 30 mbsf to about 50 percent at 250 mbsf. Porosities measured by the neutron log are expected to be higher than those computed from the density log in clay-rich sediments, because the neutron log essentially quantifies hydrogen abundance, and counts hydrogen in clay minerals as porosity. The neutron porosity measured by the EcoScope tool shown in figure 3 is the "best thermal neutron porosity" (BPHI); it has been corrected for density so that the effect of clay is reduced (Adolph and others, 2005), and it is only marginally higher than the density porosity. Surprisingly, it shows in general a better agreement with the core measurements than the density-porosity.

LWD Borehole Images

The GeoVISION and EcoScope tools generate high-resolution images of borehole log data. The EcoScope tool produces images of density and hole radius (computed on the basis of the density correction, which depends on the borehole standoff). The GeoVISION produces a gamma ray image and resistivity images with shallow, medium and deep depth of investigation.

Table 19. Wenner array electrical resistivity and formation factor results for Holes NGHP-01-07B and NGHP 01-07D. (To view complete table, please refer to the ASCII files.)

Core, section	Sample	Top (cm)	Depth (mbsf)	Electrical resistivity (W×m)	Apparent formation factor
NGHP-01-7B					
1H-2	ER	20	1.70	0.785	3.926
1H-2	ER	40	1.90	0.449	2.243
1H-2	ER	60	2.10	0.612	3.062
2H-2	ER	15	4.35	0.558	2.789
2H-2	ER	35	4.55	0.618	3.088
2H-2	ER	55	4.75	0.612	3.062
2H-2	ER	75	4.95	0.618	3.088
2H-2	ER	95	5.15	0.413	2.067
2H-2	ER	115	5.35	0.562	2.808
2H-3	ER	15	5.85	0.529	2.646
2H-3	ER	35	6.05	0.523	2.613
2H-3	ER	55	6.25	0.710	3.549
2H-3	ER	75	6.45	0.403	2.015
2H-3	ER	95	6.65	0.484	2.418
2H-4	ER	15	7.35	0.404	2.022
2H-4	ER	35	7.55	0.374	1.872
2H-4	ER	55	7.75	0.406	2.028
2H-4	ER	75	7.95	0.419	2.093
2H-4	ER	95	8.15	0.400	2.002
2H-4	ER	115	8.35	0.403	2.015
2H-5	ER	15	8.85	0.415	2.074
2H-5	ER	35	9.05	0.428	2.139
2H-5	ER	55	9.25	0.468	2.340
2H-5	ER	75	9.45	0.530	2.652
2H-6	ER	15	10.35	0.386	1.931
2H-6	ER	35	10.55	0.382	1.911
2H-6	ER	80	11.00	0.402	2.009
3H-1	ER	75	12.95	0.503	2.516
3H-1	ER	105	13.25	0.528	2.639
3H-1	ER	125	13.45	0.510	2.548
3H-2	ER	15	13.85	0.625	3.127
3H-2	ER	15	13.85	0.633	3.166
3H-2	ER	35	14.05	0.501	2.503
3H-2	ER	55	14.25	0.560	2.802
3H-2	ER	75	14.45	0.556	2.782
3H-2	ER	95	14.65	0.502	2.509
3H-2	ER	115	14.85	0.445	2.223
3H-3	ER	20	15.40	0.402	2.009
3H-3	ER	35	15.55	0.462	2.308
3H-3	ER	55	15.75	0.488	2.438
3H-3	ER	75	15.95	0.480	2.399
3H-3	ER	90	16.10	0.576	2.880
3H-4	ER	15	16.85	0.491	2.457
3H-4	ER	35	17.05	0.511	2.555
3H-4	ER	55	17.25	0.517	2.587
3H-4	ER	75	17.45	0.555	2.776
3H-4	ER	95	17.65	0.559	2.795
3H-4	ER	115	17.85	0.529	2.646
3H-5	ER	25	18.45	0.554	2.769
3H-5	ER	75	18.95	0.562	2.808
3H-6	ER	30	20.00	0.521	2.607
3H-6	ER	55	20.25	0.503	2.516
3H-6	ER	108	20.78	0.582	2.912
3H-7	ER	18	21.38	0.576	2.880
3H-7	ER	71	21.91	0.549	2.743
4H-1	ER	50	22.20	0.568	2.841
4H-1	ER	100	22.70	0.601	3.003
4H-2	ER	15	23.35	0.585	2.925

Table 19. Wenner array electrical resistivity and formation factor results for Holes NGHP-01-07B and NGHP 01-07D. (To view complete table, please refer to the ASCII files.)—Continued

Core, section	Sample	Top (cm)	Depth (mbsf)	Electrical resistivity (W×m)	Apparent formation factor	Core, section	Sample	Top (cm)	Depth (mbsf)	Electrical resistivity (W×m)	Apparent formation factor
NGHP-01-7B—Continued											
4H-2	ER	83	24.03	0.611	3.055	6H-7	ER	35	49.32	0.598	2.990
4H-3	ER	32	25.02	0.579	2.893	6H-7	ER	55	49.52	0.593	2.964
4H-3	ER	80	25.50	0.621	3.107	6H-7	ER	75	49.72	0.615	3.075
4H-5	ER	30	28.00	0.546	2.730	7H-1	ER	107	51.27	0.654	3.270
4H-6	ER	35	29.55	0.553	2.763	7H-1	ER	125	51.45	0.651	3.257
4H-6	ER	67	29.87	0.577	2.886	7H-1	ER	145	51.65	0.651	3.257
4H-7	ER	35	30.55	0.525	2.626	7H-2	ER	15	51.85	0.671	3.354
5H-1	ER	43	31.63	0.642	3.211	7H-2	ER	35	52.05	0.637	3.185
5H-1	ER	60	31.80	0.670	3.348	7H-2	ER	55	52.25	0.649	3.244
5H-1	ER	93	32.13	0.845	4.225	7H-2	ER	75	52.45	0.580	2.899
5H-1	ER	117	32.37	0.785	3.926	7H-2	ER	95	52.65	0.638	3.192
5H-2	ER	74	33.44	1.500	7.501	7H-2	ER	115	52.85	0.592	2.958
5H-2	ER	122	33.92	1.589	7.943	7H-3	ER	14	53.26	0.611	3.055
5H-3	ER	33	34.53	1.214	6.071	7H-3	ER	38	53.50	0.632	3.159
5H-3	ER	101	35.21	1.381	6.903	7H-3	ER	55	53.67	0.608	3.042
5H-4	ER	19	35.89	1.365	6.825	7H-3	ER	75	53.87	0.611	3.055
5H-4	ER	123	36.93	1.559	7.794	7H-3	ER	98	54.10	0.619	3.094
5H-5	ER	25	37.45	1.342	6.708	7H-4	ER	17	54.79	0.607	3.036
5H-5	ER	53	37.73	1.245	6.227	7H-4	ER	40	55.02	0.593	2.964
5H-5	ER	86	38.06	1.242	6.208	7H-4	ER	55	55.17	0.597	2.984
5H-6	ER	15	38.85	1.200	6.000	7H-4	ER	89	55.51	0.559	2.795
5H-6	ER	36	39.06	1.132	5.662	7H-4	ER	105	55.67	0.545	2.724
5H-6	ER	116	39.86	1.411	7.053	7H-4	ER	125	55.87	0.629	3.146
5H-7	ER	15	40.35	0.711	3.556	7H-4	ER	143	56.05	0.658	3.289
5H-7	ER	68	40.88	0.632	3.159	7H-5	ER	15	56.27	0.621	3.107
6H-1	ER	15	40.85	0.646	3.231	7H-5	ER	35	56.47	0.571	2.854
6H-1	ER	37	41.07	0.568	2.841	7H-5	ER	55	56.67	0.558	2.789
6H-1	ER	55	41.25	0.588	2.938	7H-5	ER	75	56.87	0.594	2.971
6H-1	ER	77	41.47	0.640	3.198	7H-5	ER	95	57.07	0.590	2.951
6H-1	ER	93	41.63	0.623	3.114	7H-6	ER	12	57.74	0.573	2.867
6H-1	ER	118	41.88	0.642	3.211	7H-6	ER	32	57.94	0.867	4.336
6H-1	ER	135	42.05	0.611	3.055	7H-6	ER	32	57.94	0.870	4.349
6H-2	ER	15	42.35	0.615	3.075	7H-6	ER	32	57.94	0.867	4.336
6H-2	ER	35	42.55	0.597	2.984	7H-6	ER	55	58.17	0.662	3.309
6H-2	ER	55	42.75	0.564	2.821	7H-6	ER	75	58.37	0.584	2.919
6H-2	ER	75	42.95	0.582	2.912	7H-6	ER	98	58.60	0.573	2.867
6H-2	ER	95	43.15	0.577	2.886	7H-6	ER	101	58.63	0.672	3.361
6H-2	ER	115	43.35	0.541	2.704	7H-6	ER	129	58.91	0.532	2.659
6H-2	ER	132	43.52	0.575	2.873	7H-7	ER	8	59.20	0.703	3.517
6H-3	ER	15	43.85	0.527	2.633	7H-7	ER	40	59.52	0.541	2.704
6H-3	ER	35	44.05	0.514	2.568	8H-1	ER	15	59.85	0.628	3.140
6H-3	ER	58	44.28	0.614	3.068	8H-1	ER	35	60.05	0.598	2.990
6H-3	ER	75	44.45	0.585	2.925	8H-1	ER	55	60.25	0.576	2.880
6H-3	ER	95	44.65	0.586	2.932	8H-1	ER	75	60.45	0.619	3.094
6H-4	ER	15	45.35	0.633	3.166	8H-1	ER	95	60.65	0.597	2.984
6H-4	ER	35	45.55	0.638	3.192	8H-1	ER	115	60.85	0.606	3.029
6H-4	ER	55	45.75	0.629	3.146	8H-1	ER	132	61.02	0.632	3.159
6H-4	ER	73	45.93	0.632	3.159	8H-2	ER	15	61.22	0.875	4.375
6H-4	ER	95	46.15	0.651	3.257	8H-2	ER	35	61.42	0.680	3.400
6H-4	ER	125	46.45	0.624	3.120	8H-2	ER	55	61.62	0.589	2.945
6H-5	ER	18	46.88	0.629	3.146	8H-2	ER	75	61.82	0.625	3.127
6H-5	ER	35	47.05	0.572	2.860	8H-2	ER	109	62.16	0.582	2.912
6H-5	ER	60	47.30	0.650	3.250	8H-2	ER	125	62.32	0.659	3.296
6H-5	ER	75	47.45	0.601	3.003	8H-2	ER	145	62.52	0.558	2.789
6H-5	ER	86	47.56	0.590	2.951	8H-3	ER	8	62.64	0.568	2.841
6H-6	ER	16	48.36	0.632	3.159	8H-3	ER	35	62.91	0.615	3.075
6H-6	ER	35	48.55	0.641	3.205	8H-3	ER	54	63.10	0.705	3.523
6H-6	ER	55	48.75	0.593	2.964	8H-3	ER	77	63.33	0.633	3.166
6H-6	ER	73	48.93	0.615	3.075	8H-4	ER	15	64.13	0.625	3.127
6H-7	ER	21	49.18	0.580	2.899	8H-4	ER	35	64.33	0.689	3.445

Table 19. Wenner array electrical resistivity and formation factor results for Holes NGHP-01-07B and NGHP 01-07D. (To view complete table, please refer to the ASCII files.)—Continued

Core, section	Sample	Top (cm)	Depth (mbsf)	Electrical resistivity (W×m)	Apparent formation factor	Core, section	Sample	Top (cm)	Depth (mbsf)	Electrical resistivity (W×m)	Apparent formation factor
NGHP-01-7B—Continued											
8H-4	ER	55	64.53	0.758	3.790	10X-2	ER	15	80.35	0.569	2.847
8H-4	ER	122	65.20	0.632	3.159	10X-2	ER	34	80.54	0.554	2.769
8H-5	ER	11	65.59	0.620	3.101	10X-2	ER	55	80.75	0.585	2.925
8H-5	ER	41	65.89	0.575	2.873	10X-2	ER	77	80.97	0.588	2.938
8H-5	ER	69	66.17	0.715	3.575	10X-2	ER	95	81.15	0.541	2.704
8H-5	ER	84	66.32	0.689	3.445	10X-2	ER	115	81.35	0.567	2.834
8H-6	ER	15	67.13	0.685	3.426	10X-3	ER	7	81.77	0.709	3.543
8H-6	ER	35	67.33	0.703	3.517	10X-3	ER	35	82.05	0.602	3.010
8H-6	ER	70	67.68	0.634	3.172	10X-3	ER	55	82.25	0.529	2.646
8H-6	ER	97	67.95	0.706	3.530	10X-3	ER	75	82.45	0.556	2.782
8H-7	ER	15	68.13	0.676	3.380	10X-3	ER	95	82.65	0.538	2.691
8H-7	ER	35	68.33	0.673	3.367	10X-4	ER	15	83.35	0.575	2.873
8H-7	ER	60	68.58	0.703	3.517	10X-4	ER	35	83.55	0.616	3.081
9H-1	ER	54	69.74	0.581	2.906	10X-4	ER	55	83.75	0.558	2.789
9H-2	ER	6	70.07	0.510	2.548	10X-4	ER	75	83.95	0.602	3.010
9H-2	ER	24	70.25	0.525	2.626	10X-4	ER	95	84.15	0.560	2.802
9H-2	ER	45	70.46	0.597	2.984	10X-4	ER	115	84.35	0.597	2.984
9H-3	ER	15	70.78	0.615	3.075	10X-4	ER	135	84.55	0.585	2.925
9H-3	ER	36	70.99	0.482	2.412	10X-5	ER	15	84.85	0.567	2.834
9H-3	ER	62	71.25	0.586	2.932	10X-5	ER	35	85.05	0.545	2.724
9H-4	ER	26	72.39	0.563	2.815	10X-5	ER	55	85.25	0.573	2.867
9H-4	ER	62	72.75	0.610	3.049	10X-5	ER	75	85.45	0.563	2.815
9H-4	ER	106	73.19	0.612	3.062	10X-6	ER	15	86.35	0.581	2.906
9H-5	ER	4	73.67	0.577	2.886	10X-6	ER	32	86.52	0.516	2.581
9H-5	ER	15	73.78	1.082	5.408	12Y-1	ER	15	85.35	0.593	2.964
9H-5	ER	44	74.07	0.556	2.782	12Y-1	ER	40	85.60	0.645	3.224
9H-5	ER	79	74.42	0.598	2.990	12Y-1	ER	70	85.90	0.685	3.426
9H-5	ER	108	74.71	0.610	3.049	13X-1	ER	19	86.39	0.555	2.776
9H-6	ER	10	75.13	0.523	2.613	13X-2	ER	15	86.65	0.350	1.749
9H-6	ER	35	75.38	0.588	2.938	13X-2	ER	60	87.10	0.598	2.990
9H-6	ER	53	75.56	0.595	2.977	13X-2	ER	80	87.30	0.547	2.737
9H-6	ER	69	75.72	0.560	2.802	13X-2	ER	105	87.55	0.620	3.101
9H-7	ER	9	76.14	0.517	2.587	13X-2	ER	124	87.74	0.593	2.964
9H-7	ER	34	76.39	0.625	3.127	13X-4	ER	15	88.75	0.582	2.912
9H-7	ER	61	76.66	0.584	2.919	13X-4	ER	35	88.95	0.580	2.899
9H-7	ER	86	76.91	0.575	2.873	13X-4	ER	55	89.15	0.663	3.315
9H-7	ER	111	77.16	0.588	2.938	13X-4	ER	75	89.35	0.603	3.016
9H-7	ER	127	77.32	0.627	3.133	14X-1	ER	22	95.92	0.702	3.510
9H-7	ER	138	77.43	0.634	3.172	14X-1	ER	45	96.15	0.589	2.945
9H-8	ER	18	77.70	0.628	3.140	14X-1	ER	60	96.30	0.660	3.302
9H-8	ER	61	78.13	0.696	3.478	14X-1	ER	80	96.50	0.585	2.925
9H-8	ER	74	78.26	0.702	3.510	14X-1	ER	100	96.70	0.541	2.704
9H-8	ER	91	78.43	0.659	3.296	14X-2	ER	15	97.35	0.659	3.296
9H-8	ER	110	78.62	0.659	3.296	14X-2	ER	35	97.55	0.671	3.354
10X-1	ER	20	78.90	0.572	2.860	14X-2	ER	55	97.75	0.566	2.828
10X-1	ER	37	79.07	0.499	2.496	14X-2	ER	75	97.95	0.640	3.198
10X-1	ER	52	79.22	0.543	2.717	14X-3	ER	15	98.85	0.673	3.367
10X-1	ER	70	79.40	0.493	2.464	14X-3	ER	35	99.05	0.612	3.062
10X-1	ER	90	79.60	0.620	3.101	14X-3	ER	60	99.30	0.606	3.029
10X-1	ER	110	79.80	0.536	2.678	14X-4	ER	19	99.89	0.632	3.159
10X-1	ER	130	80.00	0.529	2.646	14X-4	ER	40	100.10	0.705	3.523

Table 19. Wenner array electrical resistivity and formation factor results for Holes NGHP-01-07B and NGHP 01-07D. (To view complete table, please refer to the ASCII files.)—Continued

Core, section	Sample	Top (cm)	Depth (mbsf)	Electrical resistivity (W×m)	Apparent formation factor	Core, section	Sample	Top (cm)	Depth (mbsf)	Electrical resistivity (W×m)	Apparent formation factor
NGHP-01-7B—Continued											
14X-5	ER	15	100.55	0.680	3.400	17X-6	ER	105	123.55	0.624	3.120
14X-5	ER	44	100.84	0.659	3.296	18X-1	ER	60	125.40	0.768	3.842
14X-5	ER	65	101.05	0.629	3.146	18X-1	ER	110	125.90	0.640	3.198
14X-5	ER	77	101.17	0.649	3.244	18X-2	ER	15	126.25	0.797	3.985
14X-5	ER	105	101.45	0.662	3.309	18X-2	ER	35	126.45	0.672	3.361
15X-1	ER	20	105.50	0.488	2.438	18X-2	ER	52	126.62	0.757	3.783
15X-1	ER	50	105.80	0.511	2.555	18X-2	ER	87	126.97	0.689	3.445
15X-1	ER	70	106.00	0.588	2.938	18X-3	ER	15	127.75	0.712	3.562
15X-1	ER	100	106.30	0.581	2.906	18X-3	ER	33	127.93	0.725	3.627
15X-1	ER	130	106.60	0.598	2.990	18X-3	ER	89	128.49	0.689	3.445
15X-2	ER	15	106.91	0.705	3.523	18X-4	ER	21	129.31	0.646	3.231
15X-2	ER	35	107.11	0.627	3.133	18X-4	ER	62	129.72	0.649	3.244
15X-2	ER	70	107.46	0.606	3.029	18X-4	ER	125	130.35	0.719	3.595
15X-2	ER	92	107.68	0.631	3.153	19X-1	ER	15	134.55	0.607	3.036
15X-3	ER	17	108.43	0.651	3.257	19X-1	ER	35	134.75	0.681	3.406
15X-3	ER	57	108.83	0.621	3.107	19X-1	ER	65	135.05	0.694	3.471
15X-3	ER	90	109.16	0.611	3.055	19X-1	ER	90	135.30	0.528	2.639
15X-3	ER	110	109.36	0.688	3.439	19X-1	ER	115	135.55	0.641	3.205
15X-3	ER	136	109.62	0.724	3.621	19X-2	ER	15	136.05	0.551	2.756
15X-4	ER	15	109.91	0.751	3.757	19X-2	ER	40	136.30	0.647	3.237
15X-4	ER	35	110.11	0.651	3.257	19X-2	ER	70	136.60	0.585	2.925
15X-4	ER	52	110.28	0.671	3.354	19X-3	ER	20	136.91	0.761	3.803
15X-4	ER	78	110.54	0.659	3.296	19X-3	ER	50	137.21	0.624	3.120
15X-5	ER	15	111.41	0.644	3.218	19X-4	ER	20	137.90	0.620	3.101
15X-5	ER	40	111.66	0.637	3.185	20X-1	ER	15	144.15	0.543	2.717
15X-5	ER	80	112.06	0.746	3.731	20X-1	ER	35	144.35	0.495	2.477
16Y-1	ER	15	114.35	0.768	3.842	20X-1	ER	55	144.55	0.541	2.704
16Y-1	ER	35	114.55	0.753	3.764	20X-1	ER	71	144.71	0.564	2.821
16Y-1	ER	80	115.00	0.793	3.965	20X-2	ER	15	145.16	0.584	2.919
17X-2	ER	15	116.85	0.547	2.737	20X-2	ER	35	145.36	0.641	3.205
17X-2	ER	35	117.05	0.549	2.743	20X-2	ER	55	145.56	0.619	3.094
17X-2	ER	60	117.30	0.575	2.873	20X-2	ER	75	145.76	0.653	3.263
17X-2	ER	80	117.50	0.536	2.678	20X-2	ER	95	145.96	0.584	2.919
17X-2	ER	108	117.78	0.499	2.496	20X-2	ER	115	146.16	0.707	3.536
17X-2	ER	130	118.00	0.524	2.620	20X-2	ER	135	146.36	0.633	3.166
17X-3	ER	25	118.45	0.506	2.529	20X-3	ER	15	146.66	0.572	2.860
17X-3	ER	50	118.70	0.542	2.711	20X-3	ER	35	146.86	0.546	2.730
17X-3	ER	80	119.00	0.559	2.795	20X-3	ER	55	147.06	0.603	3.016
17X-4	ER	15	119.81	0.607	3.036	20X-3	ER	75	147.26	0.575	2.873
17X-4	ER	35	120.01	0.589	2.945	20X-4	ER	15	148.16	0.592	2.958
17X-4	ER	55	120.21	0.684	3.419	20X-4	ER	35	148.36	0.608	3.042
17X-4	ER	75	120.41	0.612	3.062	20X-4	ER	55	148.56	0.667	3.335
17X-4	ER	95	120.61	0.631	3.153	20X-4	ER	75	148.76	0.611	3.055
17X-4	ER	120	120.86	0.537	2.685	20X-5	ER	15	149.66	0.612	3.062
17X-5	ER	15	121.31	0.601	3.003	20X-5	ER	35	149.86	0.605	3.023
17X-5	ER	35	121.51	0.614	3.068	20X-5	ER	55	150.06	0.638	3.192
17X-5	ER	60	121.76	0.588	2.938	20X-5	ER	75	150.26	0.644	3.218
17X-6	ER	15	122.65	0.633	3.166	20X-5	ER	95	150.46	0.606	3.029
17X-6	ER	35	122.85	0.572	2.860	20X-5	ER	115	150.66	0.649	3.244
17X-6	ER	60	123.10	0.663	3.315	20X-5	ER	135	150.86	0.701	3.504
17X-6	ER	82	123.32	0.683	3.413						

Table 19. Wenner array electrical resistivity and formation factor results for Holes NGHP-01-07B and NGHP 01-07D. (To view complete table, please refer to the ASCII files.)—Continued

Core, section	Sample	Top (cm)	Depth (mbsf)	Electrical resistivity (W×m)	Apparent formation factor	Core, section	Sample	Top (cm)	Depth (mbsf)	Electrical resistivity (W×m)	Apparent formation factor
NGHP-01-7B—Continued											
23X-1	ER	13	150.33	0.686	3.432	26X-1	ER	86	175.06	0.619	3.094
23X-1	ER	35	150.55	0.664	3.322	26X-1	ER	135	175.55	0.556	2.782
23X-1	ER	55	150.75	0.619	3.094	26X-2	ER	68	176.38	0.628	3.140
23X-1	ER	75	150.95	0.673	3.367	26X-3	ER	36	177.56	0.558	2.789
23X-1	ER	95	151.15	0.668	3.341	26X-3	ER	75	177.95	0.520	2.600
23X-2	ER	15	151.85	0.746	3.731	27X-1	ER	15	183.95	0.662	3.309
23X-2	ER	35	152.05	0.584	2.919	27X-1	ER	32	184.12	0.593	2.964
23X-2	ER	55	152.25	0.624	3.120	27X-1	ER	57	184.37	0.593	2.964
23X-2	ER	75	152.45	0.636	3.179	27X-1	ER	75	184.55	0.616	3.081
23X-2	ER	93	152.63	0.607	3.036	27X-1	ER	95	184.75	0.589	2.945
23X-2	ER	115	152.85	0.684	3.419	27X-1	ER	115	184.95	0.582	2.912
23X-2	ER	135	153.05	0.572	2.860	27X-1	ER	135	185.15	0.571	2.854
23X-3	ER	15	153.35	0.629	3.146	27X-2	ER	15	185.45	0.619	3.094
23X-3	ER	35	153.55	0.616	3.081	27X-2	ER	35	185.65	0.580	2.899
23X-3	ER	54	153.74	0.590	2.951	27X-2	ER	55	185.85	0.672	3.361
23X-4	ER	16	154.86	0.586	2.932	27X-2	ER	65	185.95	0.481	2.405
23X-4	ER	25	154.95	0.585	2.925	27X-3	ER	15	186.95	0.675	3.374
24X-1	ER	15	159.95	0.662	3.309	27X-3	ER	35	187.15	0.554	2.769
24X-1	ER	33	160.13	0.614	3.068	27X-4	ER	15	188.05	0.710	3.549
24X-1	ER	59	160.39	0.579	2.893	27X-4	ER	35	188.25	0.564	2.821
24X-2	ER	15	161.45	0.631	3.153	27X-4	ER	55	188.45	0.642	3.211
24X-2	ER	35	161.65	0.585	2.925	27X-4	ER	75	188.65	0.624	3.120
24X-2	ER	55	161.85	0.705	3.523	27X-4	ER	93	188.83	0.666	3.328
24X-2	ER	75	162.05	0.657	3.283	30X-1	ER	15	195.55	0.651	3.257
24X-2	ER	95	162.25	0.585	2.925	30X-1	ER	34	195.74	0.581	2.906
25X-1	ER	10	169.50	0.788	3.939	30X-2	ER	13	196.06	0.666	3.328
25X-1	ER	35	169.75	0.602	3.010	30X-2	ER	38	196.31	0.572	2.860
25X-1	ER	55	169.95	0.671	3.354	30X-2	ER	55	196.48	0.582	2.912
25X-1	ER	75	170.15	0.599	2.997	30X-2	ER	77	196.70	0.640	3.198
25X-1	ER	94	170.34	0.624	3.120	30X-3	ER	15	197.58	0.629	3.146
25X-1	ER	114	170.54	0.620	3.101	30X-3	ER	35	197.78	0.623	3.114
25X-1	ER	135	170.75	0.553	2.763	30X-3	ER	60	198.03	0.592	2.958
25X-2	ER	15	171.05	0.579	2.893	30X-3	ER	75	198.18	0.533	2.665
25X-2	ER	35	171.25	0.572	2.860	30X-3	ER	98	198.41	0.543	2.717
25X-2	ER	60	171.50	0.549	2.743	30X-3	ER	122	198.65	0.588	2.938
25X-3	ER	16	171.84	0.616	3.081	30X-4	ER	15	199.08	0.627	3.133
25X-3	ER	35	172.03	0.550	2.750	30X-4	ER	30	199.23	0.520	2.600
25X-3	ER	55	172.23	0.533	2.665	30X-4	ER	60	199.53	0.582	2.912
25X-3	ER	75	172.43	0.598	2.990	30X-5	ER	10	200.53	0.608	3.042
25X-4	ER	15	173.33	0.640	3.198	30X-5	ER	29	200.72	0.632	3.159
25X-4	ER	35	173.53	0.524	2.620	30X-5	ER	56	200.99	0.627	3.133
25X-4	ER	55	173.73	0.586	2.932	30X-5	ER	74	201.17	0.579	2.893
25X-4	ER	75	173.93	0.603	3.016	30X-5	ER	95	201.38	0.588	2.938
25X-4	ER	95	174.13	0.646	3.231	30X-5	ER	118	201.61	0.601	3.003
25X-4	ER	115	174.33	0.582	2.912	30X-5	ER	137	201.80	0.576	2.880
25X-4	ER	135	174.53	0.619	3.094	30X-6	ER	12	202.05	0.703	3.517
25X-5	ER	13	174.81	0.610	3.049	30X-6	ER	34	202.27	0.554	2.769
25X-5	ER	40	175.08	0.629	3.146	30X-6	ER	57	202.50	0.569	2.847
25X-5	ER	58	175.26	0.624	3.120	30X-6	ER	72	202.65	0.766	3.829
25X-6	ER	18	176.36	0.612	3.062	30X-6	ER	108	203.01	1.034	5.168
25X-6	ER	38	176.56	0.571	2.854	30X-6	ER	132	203.25	0.553	2.763
25X-6	ER	59	176.77	0.592	2.958	30X-7	ER	10	203.53	0.660	3.302
25X-6	ER	80	176.98	0.551	2.756	30X-7	ER	10	203.53	0.655	3.276
25X-6	ER	93	177.11	0.593	2.964	30X-7	ER	52	203.95	0.683	3.413
26X-1	ER	38	174.58	0.549	2.743	30X-7	ER	66	204.09	0.712	3.562

Table 19. Wenner array electrical resistivity and formation factor results for Holes NGHP-01-07B and NGHP 01-07D. (To view complete table, please refer to the ASCII files.)—Continued

Core, section	Sample	Top (cm)	Depth (mbsf)	Electrical resistivity (W×m)	Apparent formation factor	Core, section	Sample	Top (cm)	Depth (mbsf)	Electrical resistivity (W×m)	Apparent formation factor
NGHP-01-7D											
1X-1	ER	25	231.45	0.789	3.945	3X-1	ER	62	247.22	0.740	3.700
1X-1	ER	46	231.66	0.758	3.790	3X-1	ER	96	247.56	0.608	3.040
1X-1	ER	80	232.00	0.674	3.370	3X-1	ER	115	247.75	0.747	3.735
1X-1	ER	110	232.30	0.711	3.555	3X-1	ER	134	247.94	0.857	4.285
1X-1	ER	130	232.50	0.677	3.385	3X-2	ER	17	248.27	0.786	3.930
1X-2	ER	30	233.00	0.657	3.285	3X-2	ER	33	248.43	0.710	3.550
1X-2	ER	65	233.35	0.663	3.315	3X-2	ER	56	248.66	0.738	3.690
1X-2	ER	105	233.75	0.700	3.500	3X-2	ER	86	248.96	1.286	6.430
1X-2	ER	135	234.05	0.878	4.390	3X-2	ER	86	248.96	1.275	6.375
1X-3	ER	15	234.35	0.749	3.745	3X-2	ER	102	249.12	0.774	3.870
1X-3	ER	49	234.69	0.664	3.320	3X-2	ER	115	249.25	0.739	3.695
1X-4	ER	20	235.90	0.766	3.830	3X-2	ER	133	249.43	0.879	4.395
1X-4	ER	85	236.55	0.721	3.605	3X-3	ER	18	249.78	0.749	3.745
1X-4	ER	120	236.90	0.691	3.455	3X-3	ER	33	249.93	0.737	3.685
2X-1	ER	20	239.20	0.782	3.910	3X-3	ER	52	250.12	0.777	3.885
2X-1	ER	35	239.35	0.780	3.900	3X-4	ER	15	251.25	0.817	4.085
2X-1	ER	54	239.54	0.675	3.375	3X-4	ER	34	251.44	0.881	4.405
2X-1	ER	75	239.75	0.660	3.300	3X-4	ER	55	251.65	0.771	3.855
2X-1	ER	92	239.92	0.698	3.490	3X-4	ER	73	251.83	0.755	3.775
2X-1	ER	114	240.14	0.721	3.605	3X-4	ER	95	252.05	0.861	4.305
2X-1	ER	137	240.37	0.820	4.100	4X-1	ER	20	253.50	0.772	3.860
2X-2	ER	21	240.71	0.704	3.520	4X-1	ER	36	253.66	0.903	4.515
2X-2	ER	36	240.86	0.746	3.730	4X-1	ER	56	253.86	0.712	3.560
2X-2	ER	54	241.04	0.768	3.840	4X-1	ER	78	254.08	0.763	3.815
2X-2	ER	79	241.29	0.721	3.605	4X-1	ER	95	254.25	0.645	3.225
2X-2	ER	93	241.43	0.821	4.105	4X-1	ER	113	254.43	0.658	3.290
2X-2	ER	113	241.63	0.794	3.970	4X-1	ER	134	254.64	0.702	3.510
2X-2	ER	141	241.91	0.714	3.570	4X-2	ER	16	254.96	0.796	3.980
2X-3	ER	21	242.21	0.692	3.460	4X-2	ER	36	255.16	0.749	3.745
2X-3	ER	35	242.35	0.825	4.125	4X-2	ER	56	255.36	0.700	3.500
2X-3	ER	59	242.59	0.859	4.295	4X-2	ER	76	255.56	0.698	3.490
2X-4	ER	25	243.75	0.840	4.200	4X-2	ER	97	255.77	0.773	3.865
2X-4	ER	35	243.85	0.817	4.085	4X-2	ER	115	255.95	0.756	3.780
2X-4	ER	63	244.13	0.729	3.645	4X-2	ER	138	256.18	0.669	3.345
2X-4	ER	79	244.29	0.857	4.285	4X-3	ER	13	256.43	0.756	3.780
2X-4	ER	92	244.42	0.749	3.745	4X-3	ER	37	256.67	0.758	3.790
2X-4	ER	111	244.61	0.747	3.735	4X-3	ER	54	256.84	0.792	3.960
2X-4	ER	140	244.90	0.836	4.180	4X-4	ER	18	257.98	0.743	3.715
2X-5	ER	18	245.18	0.740	3.700	4X-4	ER	35	258.15	0.698	3.490
2X-5	ER	35	245.35	0.742	3.710	4X-4	ER	55	258.35	0.867	4.335
2X-5	ER	52	245.52	0.909	4.545	4X-4	ER	73	258.53	0.786	3.930
2X-5	ER	75	245.75	0.710	3.550	4X-4	ER	98	258.78	0.733	3.665
2X-5	ER	95	245.95	0.815	4.075	4X-4	ER	115	258.95	0.856	4.280
2X-5	ER	115	246.15	0.771	3.855	4X-4	ER	134	259.14	0.781	3.905
2X-5	ER	135	246.35	0.750	3.750	4X-5	ER	16	259.46	0.793	3.965
2X-6	ER	13	246.63	0.749	3.745	4X-5	ER	34	259.64	0.787	3.935
2X-6	ER	38	246.88	0.948	4.740	4X-5	ER	53	259.83	0.742	3.710
2X-6	ER	55	247.05	0.838	4.190	4X-5	ER	75	260.05	0.813	4.065
2X-6	ER	75	247.25	0.786	3.930	4X-5	ER	97	260.27	0.829	4.145
2X-6	ER	86	247.36	0.855	4.275	4X-6	ER	17	260.97	0.782	3.910
3X-1	ER	13	246.73	0.701	3.505	4X-6	ER	35	261.15	0.698	3.490
3X-1	ER	33	246.93	0.777	3.885	4X-6	ER	55	261.35	0.697	3.485
3X-1	ER	57	247.17	0.674	3.370	4X-6	ER	75	261.55	0.839	4.195
						4X-6	ER	96	261.76	0.771	3.855

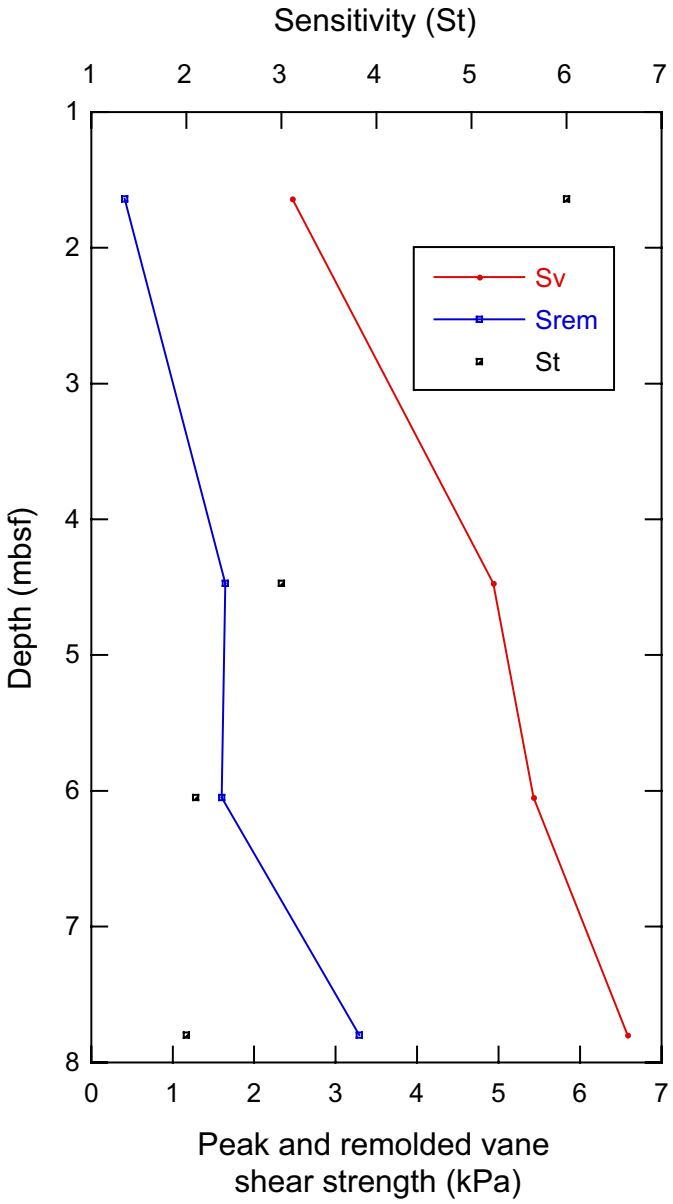

Figure 23. Profiles of LWD resistivity-at-bit, infrared images, core recovery, electrical resistivity, acoustic *P*-wave velocity, magnetic susceptibility, and thermal conductivity for Holes NGHP-01-07B and NGHP-01-07D. [LWD, logging-while-drilling]

Figure 35 shows some of the LWD images collected by the EcoScope and GeoVISION tools. It should be noted that the display in this figure is highly compressed in the vertical direction. The unwrapped images are about 80 cm wide (for a 10 in diameter borehole) and the vertical scale is compressed relative to the horizontal by a factor of about 55:1. These high-resolution images can be used for detailed sedimentological and structural interpretations and to image gas hydrate distribution in sediments (for example, in layers, nodules, fractures). Gas-hydrate-bearing sediments exhibit high resistivities within intervals of uniform or low bulk density. Layers with high resistivities and high densities are likely to be low porosity, compacted, or carbonate-rich sediments. The two resistivity images in figure 35 correspond to two depths of investigation (for details, see "Downhole Logging" in the "Methods" chapter).

The most interesting features in the borehole images are the "bright" high-resistivity layers in two intervals, 75–93 mbsf and 138–152 mbsf. These high resistivities do not correspond to high densities in the density image and thus are likely to be gas-hydrate accumulations. Figures 36A and 36B display in detail these two high resistivity intervals; in each figure, the image on the right ("Dynamic Deep Image") has been equalized in a moving 2-m-thick window to emphasize small-scale features. Figures 36A and 36B show that several fractures intersect the borehole in these high resistivity intervals. In the unwrapped resistivity images, these fractures appear as dark sinusoidal curves (for example, Bonner and others, 1996). The vertical distance between the top and the bottom of the sinusoids is 4–5 m; as the borehole diameter is

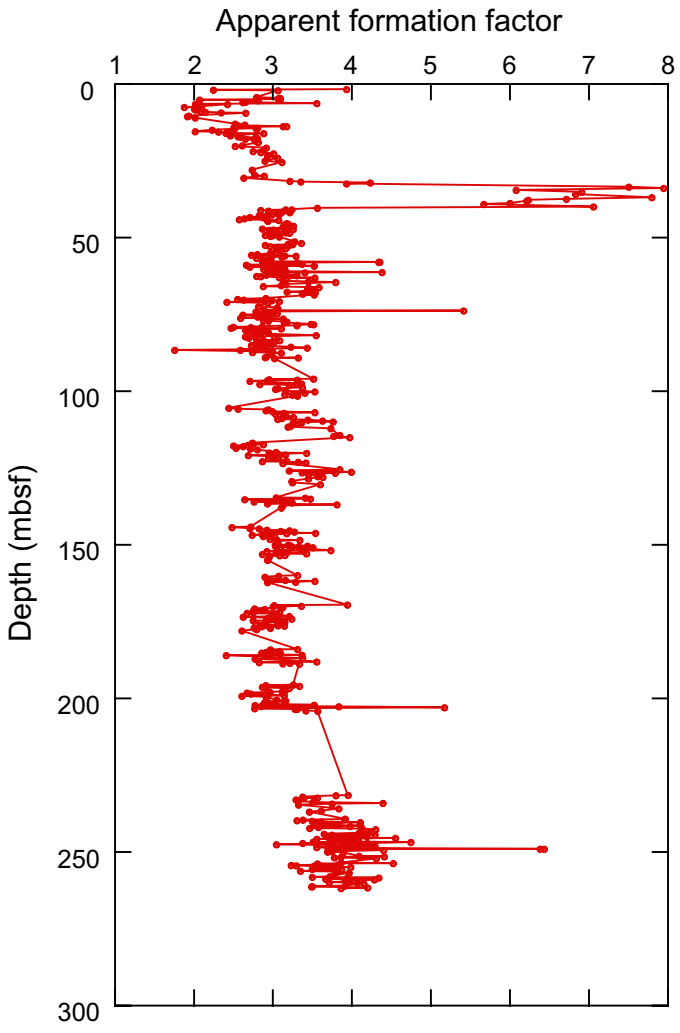

Figure 24. Apparent formation factor versus sub-bottom depth for Hole NGHP-01-07B.

around 11 in (28 cm), this means that these fractures are nearly vertical. This suggests that the gas hydrate in these intervals was formed by gas migrating upward along these fractures into the hydrate stability field.

Wire-Line Logging

Operations

.8Because of the requirement to fire the seismic source only during daylight, the next logging run was the vertical seismic profile. The VSI tool, configured with its longer arm, was complete at 1033 hr, RIH at 1048 hr and at bottom of the hole (1,555 mbrf) at 1235 hr, without experiencing any problem either at the bit or at any of the potential hole restriction identified earlier. The watch for marine mammal activity and the rigup and ramp-up of the GI-gun had started at 0830 hr, while the triple combo run was still proceeding, so that it was possible to start acquisition of the VSP immediately. The first shot for the first station at 1,554 mbrf (258 mbsf) was fired at 1240 hr. The plan was to space the deepest stations by 10 m, to reduce the spacing to 5 m between 220 and 160 mbsf across the BSR at ~190 mbsf, and to resume a 10-m spacing in the upper part of the hole. Twenty-five stations were attempted, but it was possible to record and stack reliable shots in only 18 stations, none shallower than 1,425 mbrf (~124 mbsf). The VSP was complete after firing the last shot at 1755 hr; the tool was brought back without problem to the surface at 1845 hr, and rigged down by 1900. A total of 430 shots were fired during the survey.

Assembly of the last tool string, the FMS/Sonic, started at 1915 hr, and the tool was RIH at 1950 hr. It reached the bottom of the hole (1,560 mbrf) at 2030 hr, when the first pass started at a logging speed of 900 ft/hr with the DSI configured for the following acquisition modes: low frequency monopole, low frequency upper dipole, standard frequency lower dipole, and stoneley. At 2115 hr the FMS calipers were closed and the WHC deactivated as we prepared to enter the pipe to record sonic data as close to the bit as possible. The top of the tool could not enter the pipe at the first attempt and we decided not to try any further to limit possible efforts on the wire line to the end of the second pass. The tool was sent back to the bottom of the hole and the final pass started from 1558 mbrf at 2135 hr, with the DSI configured for the low frequency monopole and cross-dipole modes. At 2210 hr, after closing the calipers and turning the WHC off, we failed to enter the pipe on our first attempt. It was necessary to circulate heavily and to rotate the pipe 180° to be able to bring the tool string fully inside at 2300 hr. The tool was back at the surface at 2350 hr with some minor damage to the rope socket above the cable head. The tool string was rigged down by 0025 hr July 10, 2006, and the rig floor was ready to resume operations at 0110 hr.

Table 20. Contact *P*-wave velocity results determined on split core sections from Hole NGHP-01-07B.

Core, section	Top (cm)	Depth (mbsf)	VP (km/s)
NGHP-01-7B			
1H-2	14	1.64	1.472
2H-2	27	4.47	1.477
2H-4	60	7.80	1.472
2H-5	30	9.00	1.477
2H-6	30	10.50	1.470
3H-1	75	12.95	1.481
3H-2	35	14.05	1.475
3H-3	35	15.55	1.478
3H-4	35	17.05	1.497
3H-5	25	18.45	1.364
3H-6	35	20.05	1.514
4H-1	15	21.85	1.542
4H-2	32	23.52	1.532

Table 21. Thermal conductivity results for Holes NGHP-01-07B and NGHP-01-07D.

Core, section	Sample	Top (cm)	Depth (mbsf)	Thermal conductivity (W/[m•K])
NGHP-01-07B				
1H-2	TC	38	1.88	0.846
2H-3	TC	58	6.28	0.850
3H-1	TC	47	12.67	0.817
3H-3	TC	47	15.67	0.887
3H-7	TC	47	21.67	0.945
4H-3	TC	70	25.40	1.119
5H-3	TC	70	34.90	0.864
6H-3	TC	70	44.40	0.964
7H-3	TC	70	53.82	0.899
7H-7	TC	42	59.54	0.947
8H-1	TC	30	60.00	0.891
8H-3	TC	79	63.35	0.970
9H-3	TC	71	71.34	0.991
10X-3	TC	50	82.20	0.910
13X-2	TC	75	87.25	0.932
14X-3	TC	40	99.10	1.070
15X-3	TC	76	109.02	0.936
17X-2	TC	75	117.45	0.835
18X-3	TC	61	128.21	1.053
19X-3	TC	35	137.06	0.986
20X-3	TC	45	146.96	0.967
23X-3	TC	50	153.70	0.944
24X-2	TC	70	162.00	0.886
25X-3	TC	70	172.38	0.983
25X-6	TC	70	176.88	0.963
26X-1	TC	50	174.70	0.826
26X-3	TC	70	177.90	0.934
27X-3	TC	25	187.05	0.987
30X-3	TC	70	198.13	1.091
31X-1	TC	75	202.65	0.947
NGHP-01-07D				
1X-3	TC	36	234.56	0.984
2X-3	TC	40	242.40	1.014
3X-3	TC	35	249.95	1.047
4X-3	TC	35	256.65	0.979

Table 22. *In situ* temperature estimates for Site NGHP-01-07.

Depth (mbsf)	Core	Assumed thermal conductivity (W/m×K)	Tool	Ad-hoc calibration correction	Temperature (°C)	Corrected temperature (°C)	Data quality
21.7	B03H	0.95	APCT-3	0	NA		poor
40.7	B05h	0.95	APCT-3	0	NA		failed
59.7	B07H	0.95	APCT16	0.45	7.96	8.41	good
116.6	B16Y	0.95	DVTP	0.50	10.89	11.39	good
175.6	B25X	0.95	DVTP	0.50	13.89	14.39	good
261.4	D04x	0.95	DVTP	0.50	NA		poor

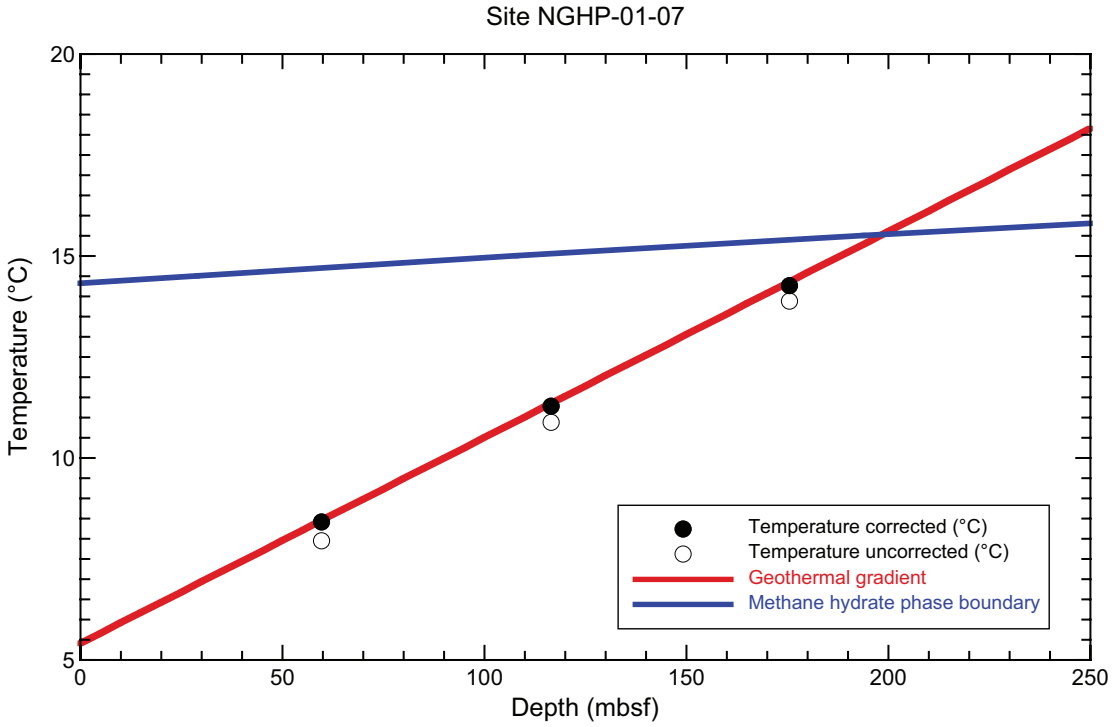

Figure 25. Geothermal gradient and estimated depth to the BSR from *in situ* temperature measurements for Site NGHP-01-07. [BSR, bottom seismic reflector]

Table 23. Summary of pressure-coring operations at Site NGHP-01-07.

Core ID	Top of core (mbsf)	Length recovered (cm)*	Length curated (cm)*	Pressure at core depth (bar)	Pressure recovered (bar)			Comments
					logged**		gauge***	
NGHP-01-07B								
11P	84.2	100	89	139	89	@6 °C	91	normal operation
12Y	85.2	--	90	139	0		--	premature lifting of inner sleeve
16Y	114.2	--	80	142	0		--	premature lifting of inner sleeve
21P	148.2	100	120	145	95	@21 °C	100	normal operation
22E	149.2	54	79	145	27	@18 °C	30	leaked pressure during recovery
28P	193.4	100	92	149	--		75	data logger did not record
29Y	194.4	--	70	150	0		--	premature lifting of inner sleeve; imploded liner

Notes:

Water depth at Site NGHP-01-07 is 1296 m. P=PCS, Y=FPC, E=HRC.

*Length measured from X-ray and gamma density analysis, which may not match curated core length.

**Last pressure recorded before data logger disconnected from corer autoclave. Temperature 2–4 °C unless otherwise noted.

***Pressure measured when autoclave pressure transducer connected to external gauge. Pressure measured at 7 °C unless otherwise noted.

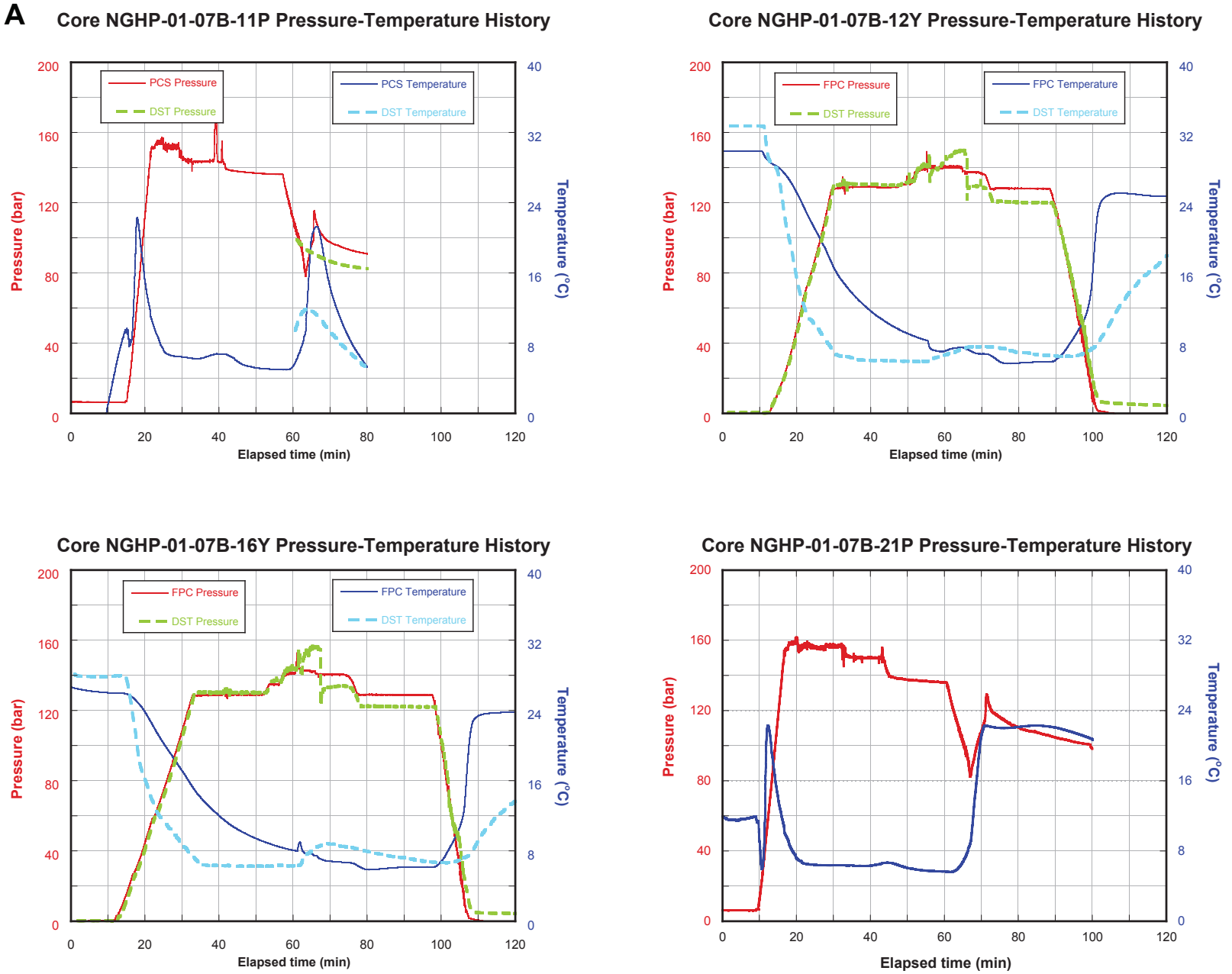

Figure 26. Temperature and pressure versus elapsed time for each pressure corer deployment as recorded by the corer's internal data logger. There are no data for Core NGHP-01-07B-28P.

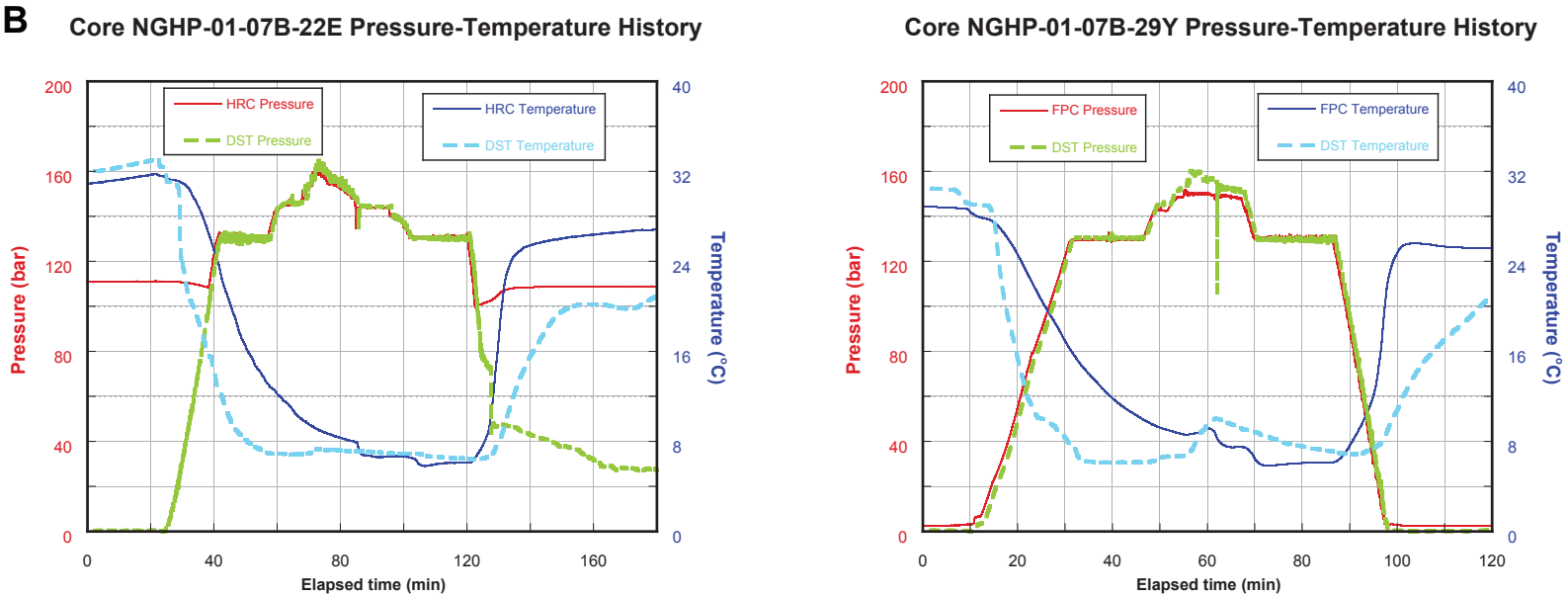

Figure 26. Temperature and pressure versus elapsed time for each pressure corer deployment as recorded by the corer's internal data logger. There are no data for Core NGHP-01-07B-28P.—Continued

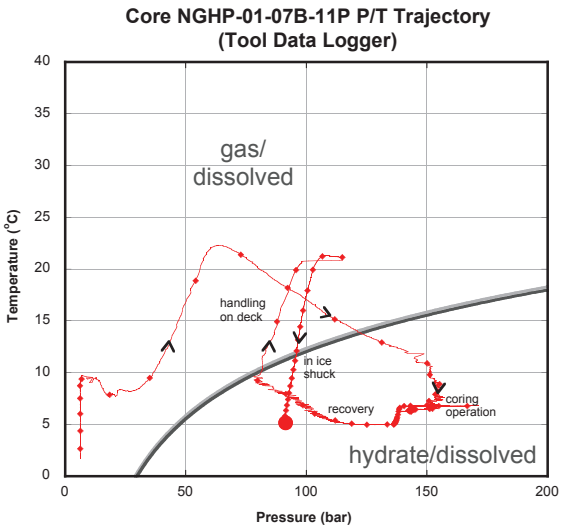

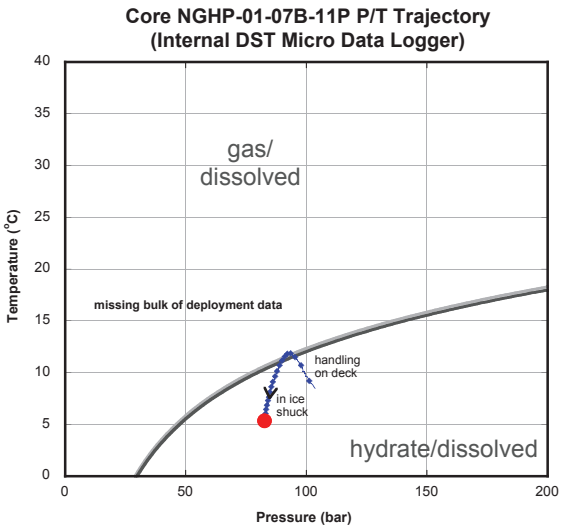

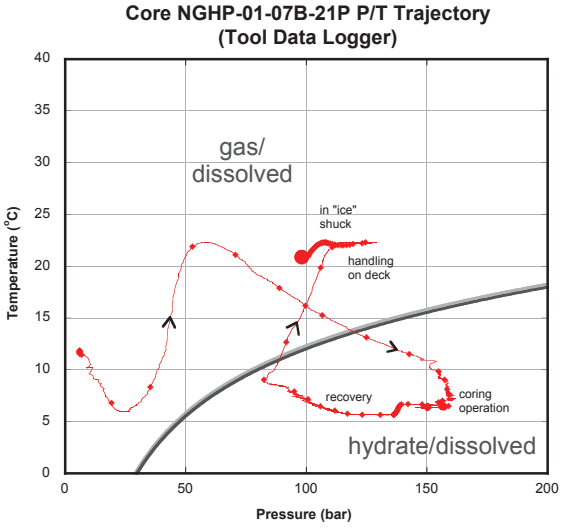

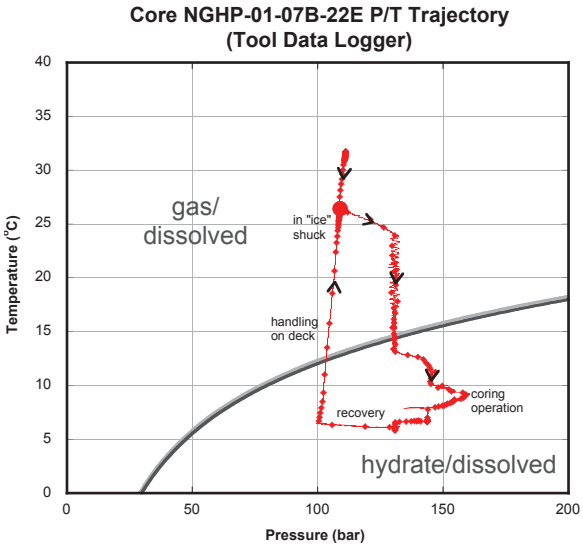

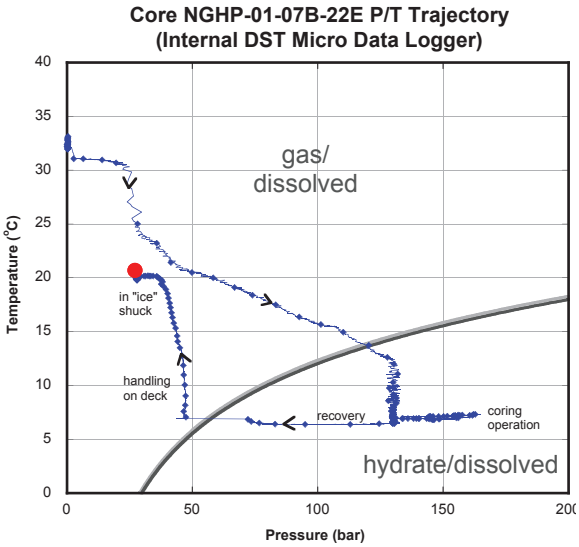

Figure 27. Temperature versus pressure for each successful pressure corer deployment, showing trajectories relative to gas-hydrate stability at 30 ppt and 35 ppt salinity, calculated from Xu (2002, 2004). Small dots are approximately every minute. Large dot is final temperature and pressure of autoclave prior to data logger removal. There are no data for Core NGHP-01-07B-28P.

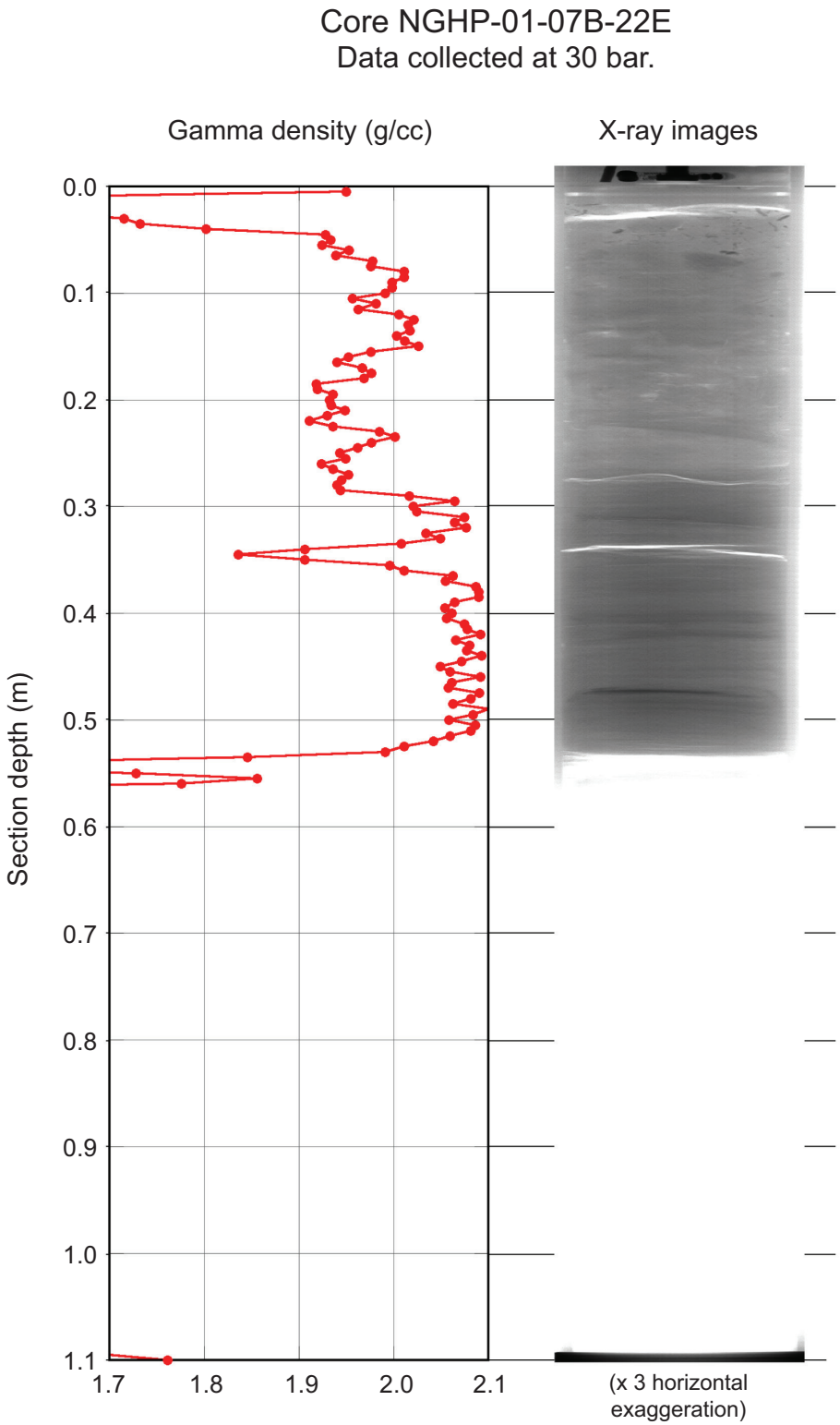

Figure 28. X-ray images and gamma density measurements collected at near *in situ* pressure and 7 °C for Core NGHP-01-07B-22E. X-ray images have been stretched 300 percent in the cross-core direction to show detail.

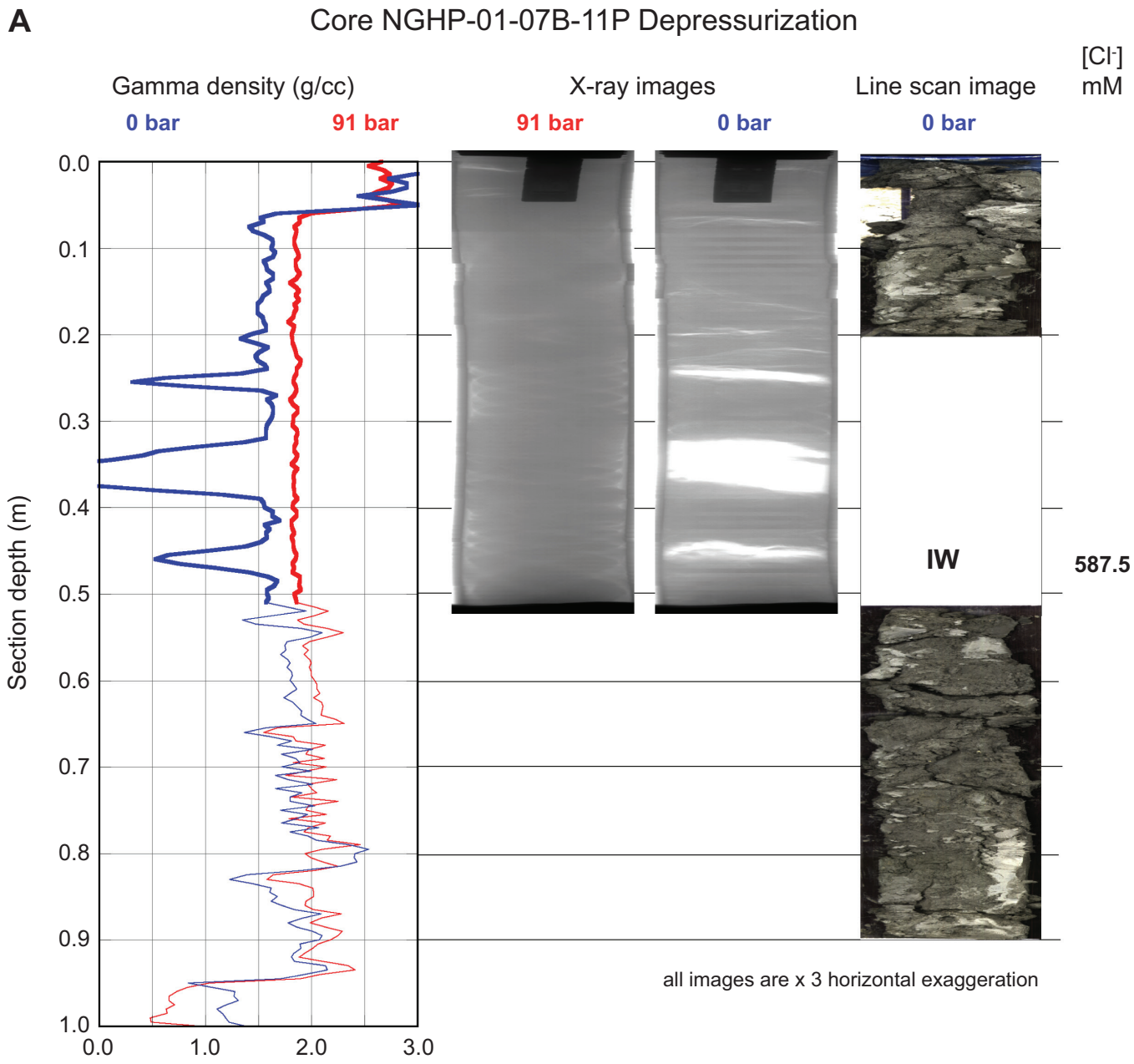

Figure 29. Summary of data taken from successful pressure cores before, during, and after depressurization, including gamma-density profiles collected before and after depressurization, X-ray images collected before and after depressurization, and line scan images collected after depressurization.

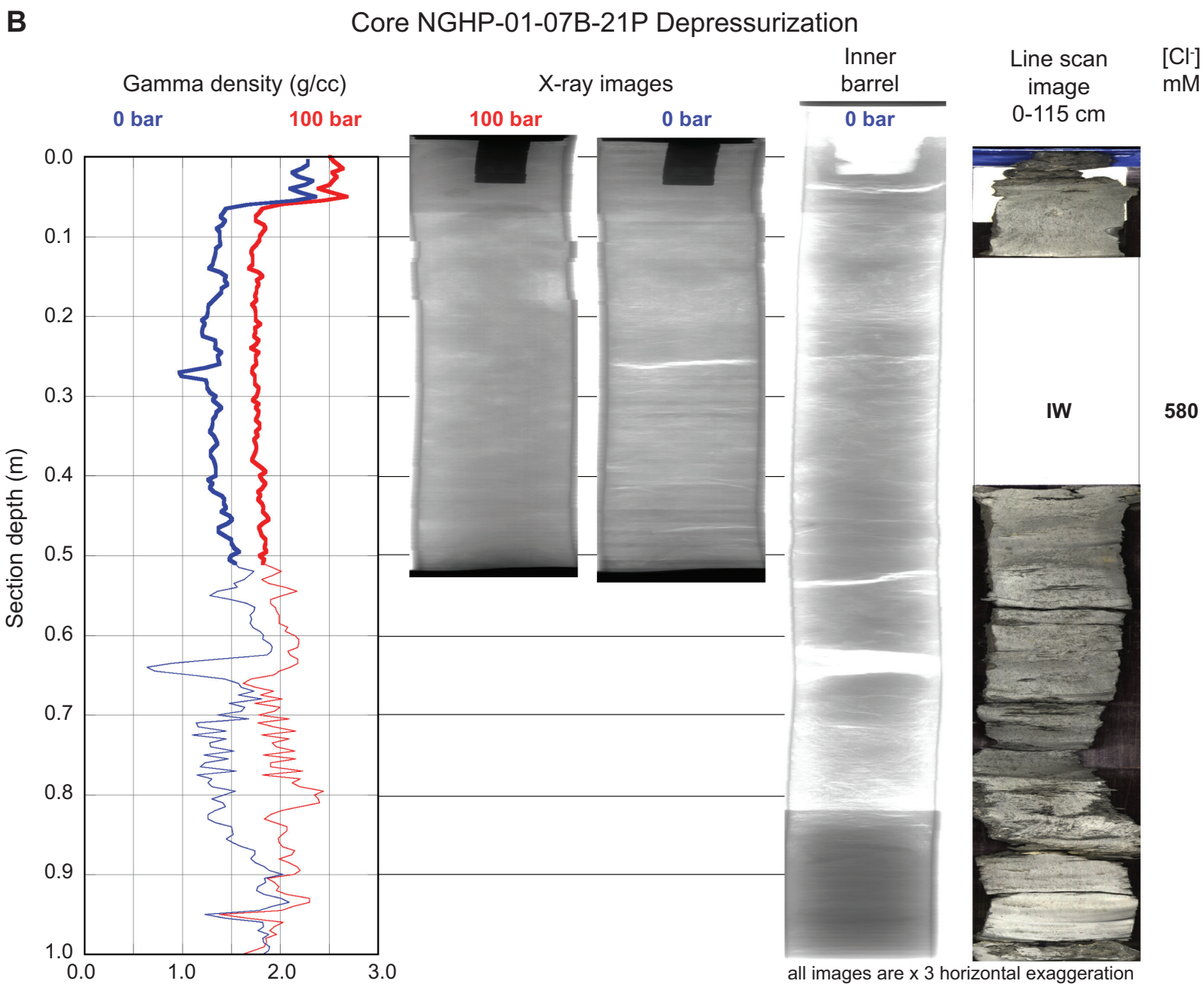

Figure 29. Summary of data taken from successful pressure cores before, during, and after depressurization, including gamma-density profiles collected before and after depressurization, X-ray images collected before and after depressurization, and line scan images collected after depressurization.—Continued

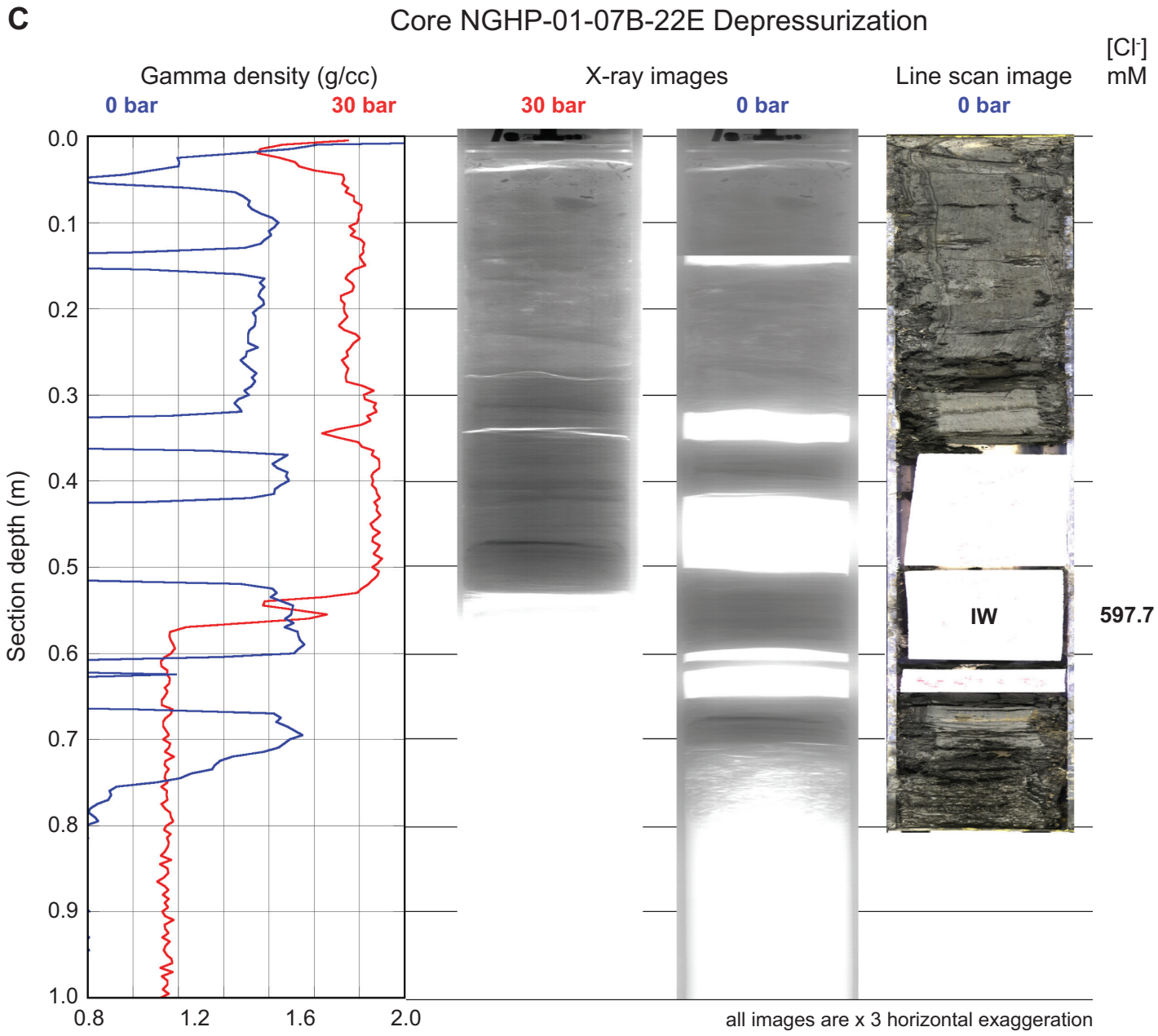

Figure 29. Summary of data taken from successful pressure cores before, during, and after depressurization, including gamma-density profiles collected before and after depressurization, X-ray images collected before and after depressurization, and line scan images collected after depressurization.—Continued

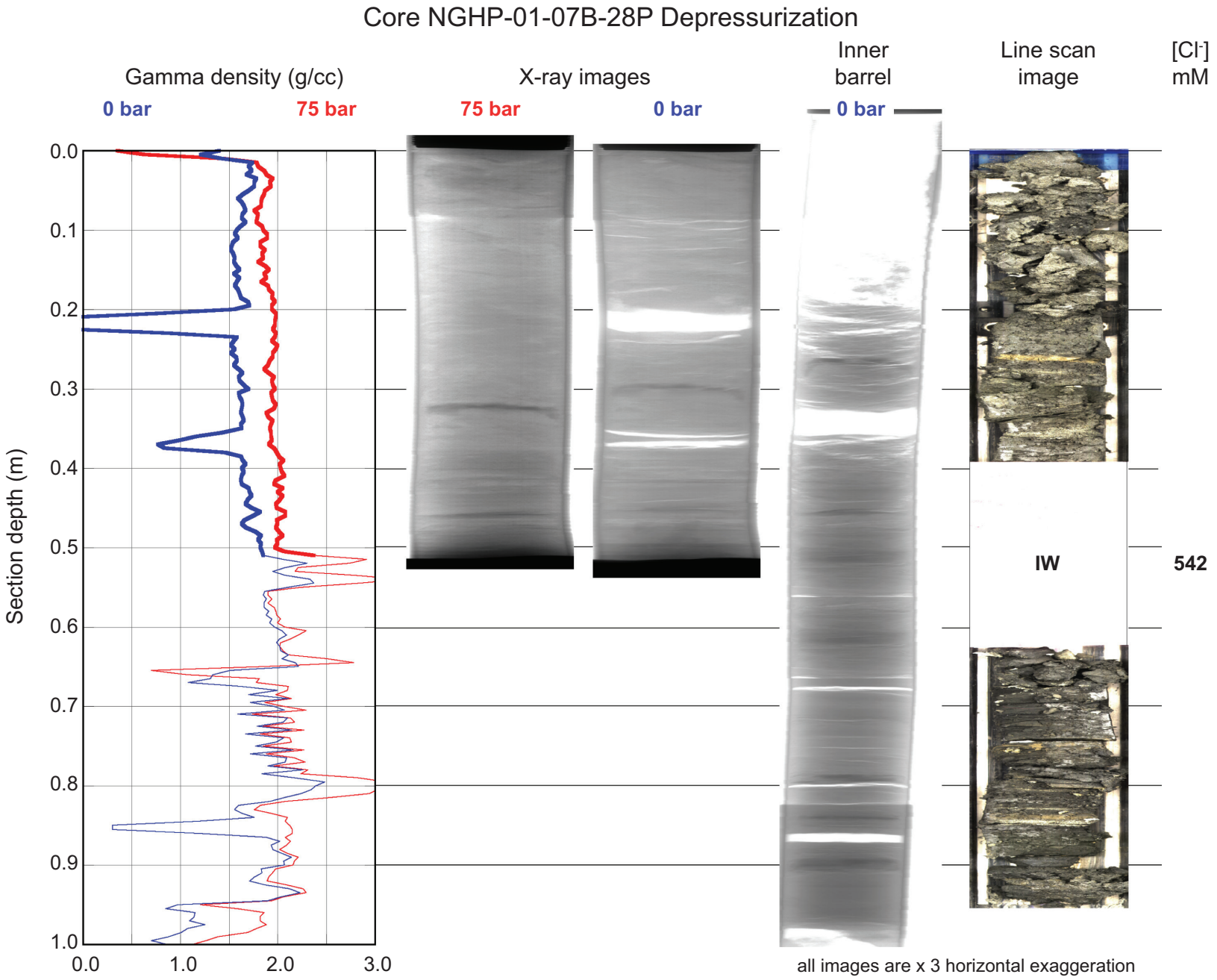

Figure 29. Summary of data taken from successful pressure cores before, during, and after depressurization, including gamma-density profiles collected before and after depressurization, X-ray images collected before and after depressurization, and line scan images collected after depressurization.—Continued

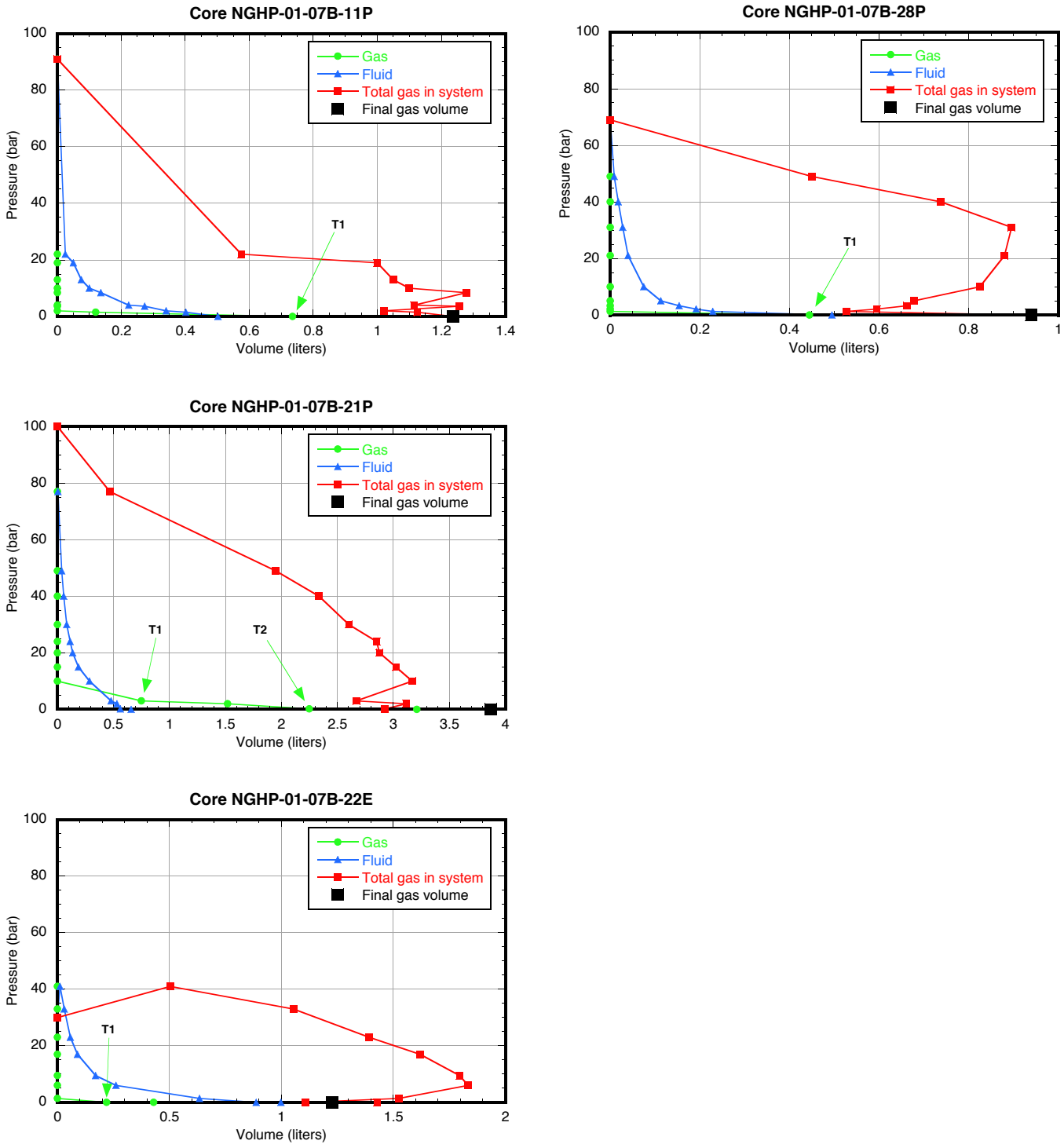

Figure 30. Pressure versus volume for successful pressure cores, also showing placement of gas samples (see "Organic Geochemistry"). [Green circles, collected gas; blue triangles, collected fluid; red squares, total gas in system (calculated as described in the "Methods" chapter); large black square, final calculated gas from cores; T(number), gas samples]

Table 24. Methane hydrate volume and concentration in pore space for successful pressure cores at Site NGHP-01-07. Values required for calculation of methane hydrate concentration are also included.

Parameter	Units	NGHP-01-07B-11P	NGHP-01-07B-21P	NGHP-01-07B-22E	NGHP-01-07B-28P
Core diameter	mm	43.2	43.2	51	43.2
Sediment length	cm	100	100	54	100
Sediment porosity	%	54	54	46	48
Pore volume	*liters*	*0.787*	*0.787*	*0.507*	*0.700*
Volume methane collected	liters	1.24	3.26	1.23	0.93
Methane concentration in pore fluids	mM	0.6	0.8	0*	2.5
Total methane in core	*mmol*	*53.8*	*141.8*	*53.4*	*40.3*
In situ salinity	ppt	34.0	34.0	34.0	34.0
Methane saturation**	mM	74	98	98.6	126.2
Methane in pore fluids, assuming saturation	*mmol*	*58.3*	*77.1*	*50.0*	*88.3*
Excess methane	*mmol*	*–4.0*	*65.3*	*3.4*	*–46.3*
Volume of methane hydrate	ml	0.0	8.9	0.5	0.0
*Methane hydrate, % of pore volume***	*%*	*0.0*	*1.1*	*0.1*	*0.0*

Notes:

Rows in italics are calculated parameters.

*Methane concentration (via headspace) was not measured on these cores. Zero concentration generates a conservative (minimum) estimate of gas hydrate volume.

**Methane saturation calculated from Xu (2002, 2004) using a water depth of 1,296 mbsl, a thermal gradient of 51 °C/km, a seafloor temperature of 5.21 °C, and the above salinities.

***Assuming all gas hydrate evenly distributed throughout the pore space.

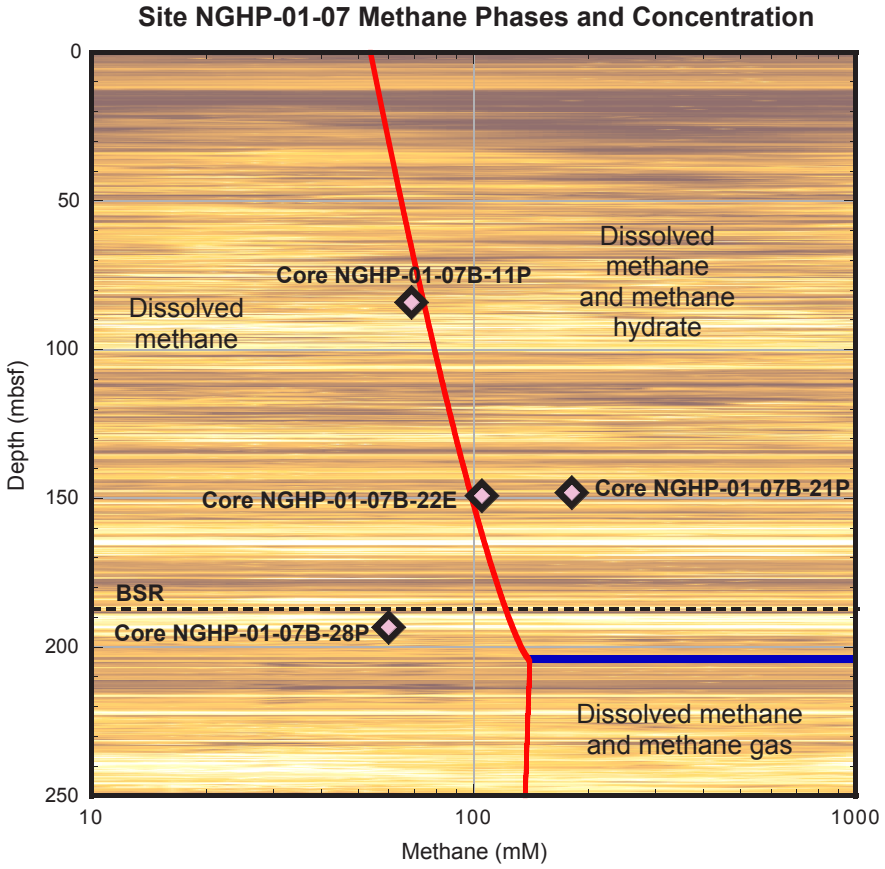

Figure 31. Methane phase diagram for Site NGHP-01-07, with total methane concentration measured from the four successful pressure cores at Site NGHP-01-07. The shipboard-calculated seafloor temperature (5.21 °C) and thermal gradient (51 °C/km) were taken from "Downhole Temperature Measurements" in "Physical Properties"; the salinity was the baseline salinity around the depths of the pressure cores (35 ppt; from table 6); and methane saturation was calculated according to Xu (2002, 2004). Background is LWD deep borehole resistivity (RAB) image. [LWD, logging while drilling]

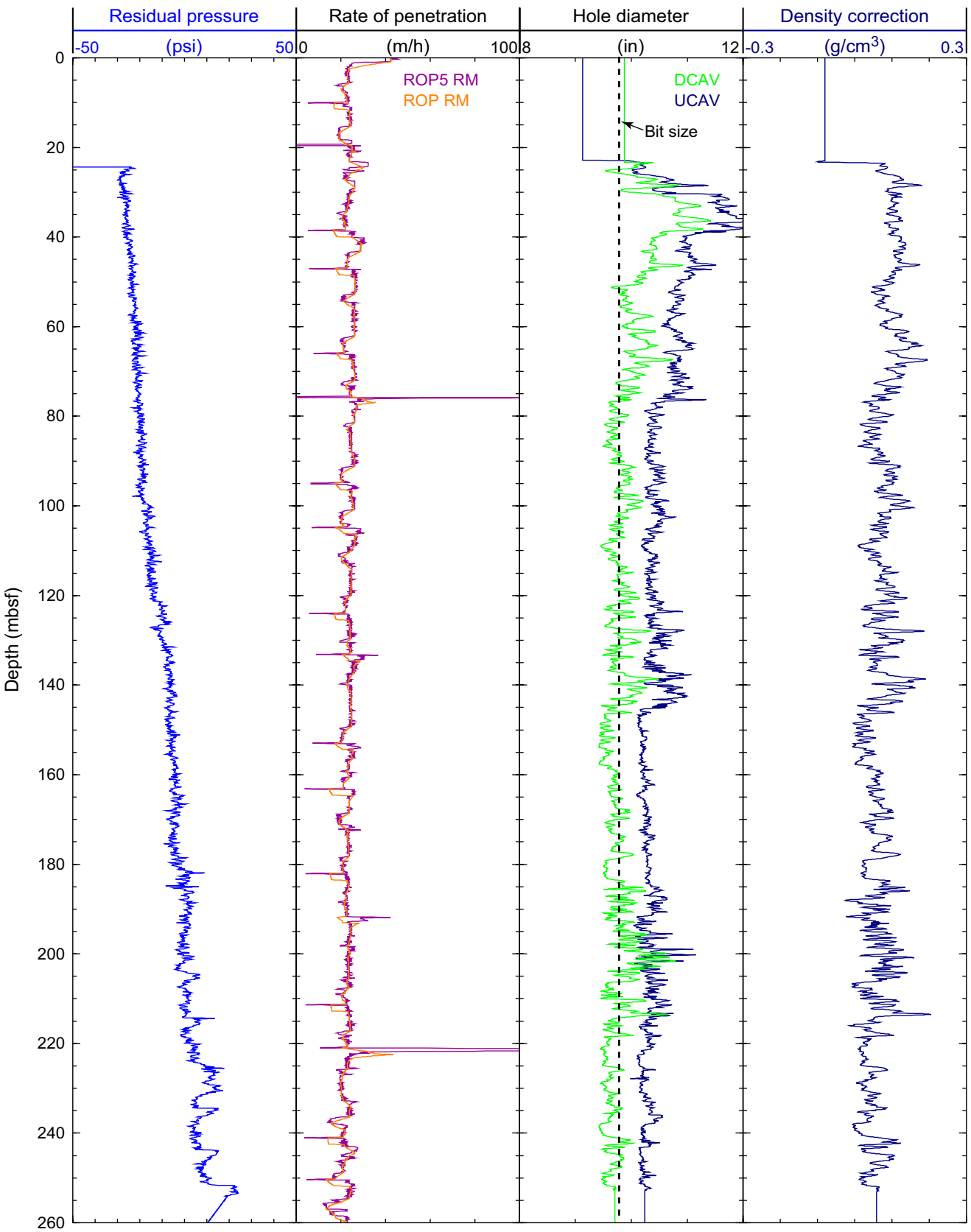

Figure 32. Monitoring and quality-control LWD/MWD logs from Hole NGHP-01-07A. [LWD/MWD, logging while drilling/measurement while drilling; ROP, Rate of penetration; ROP_RM, Instantaneous rate of penetration; ROP5_RM, Rate of penetration averaged over a 5-ft interval; UCAV, Ultrasonic caliper; DCAV, Density caliper]

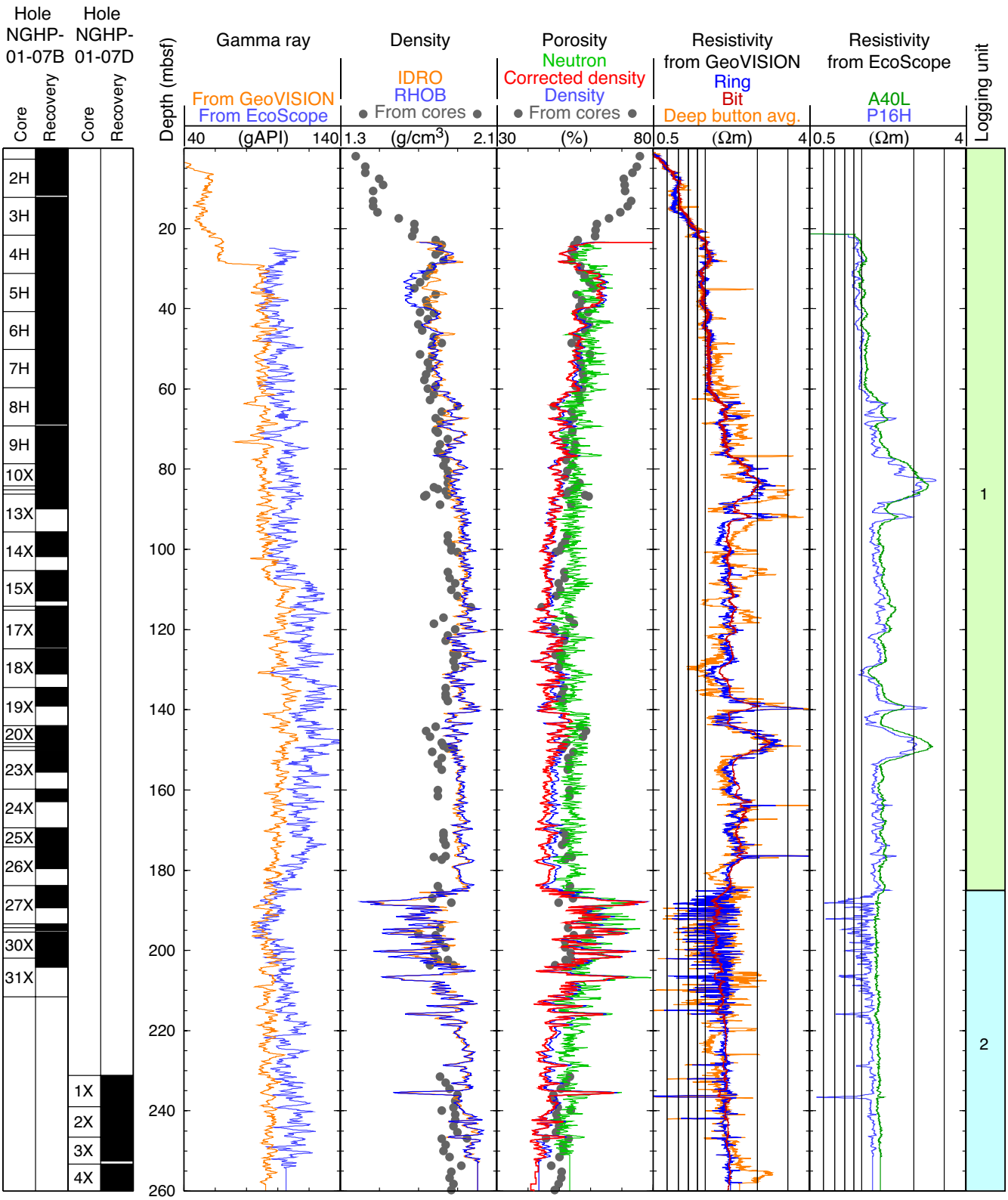

Figure 33. Summary of LWD log data from Hole NGHP-01-07A. [LWD, logging while drilling; gAPI, American Petroleum Institute gamma ray units; IDRO, Image-derived density (EcoScope); RHOB, Bulk density (EcoScope); neutron, Thermal neutron porosity (EcoScope); corrected density, density porosity with core derived grain densities (EcoScope); density, density porosity; RING, Ring resistivity (GeoVISION); BIT, Bit resistivity (GeoVISION); Deep Button avg., Button deep resistivity (GeoVISION); A40L, Attenuation resistivity measured at 400 kHz and a transmitter-receiver spacing of 40 in (EcoScope); and P16H, Phase-shift resistivity at 2 MHZ and a transmitter-receiver spacing of 16 in (EcoScope)]

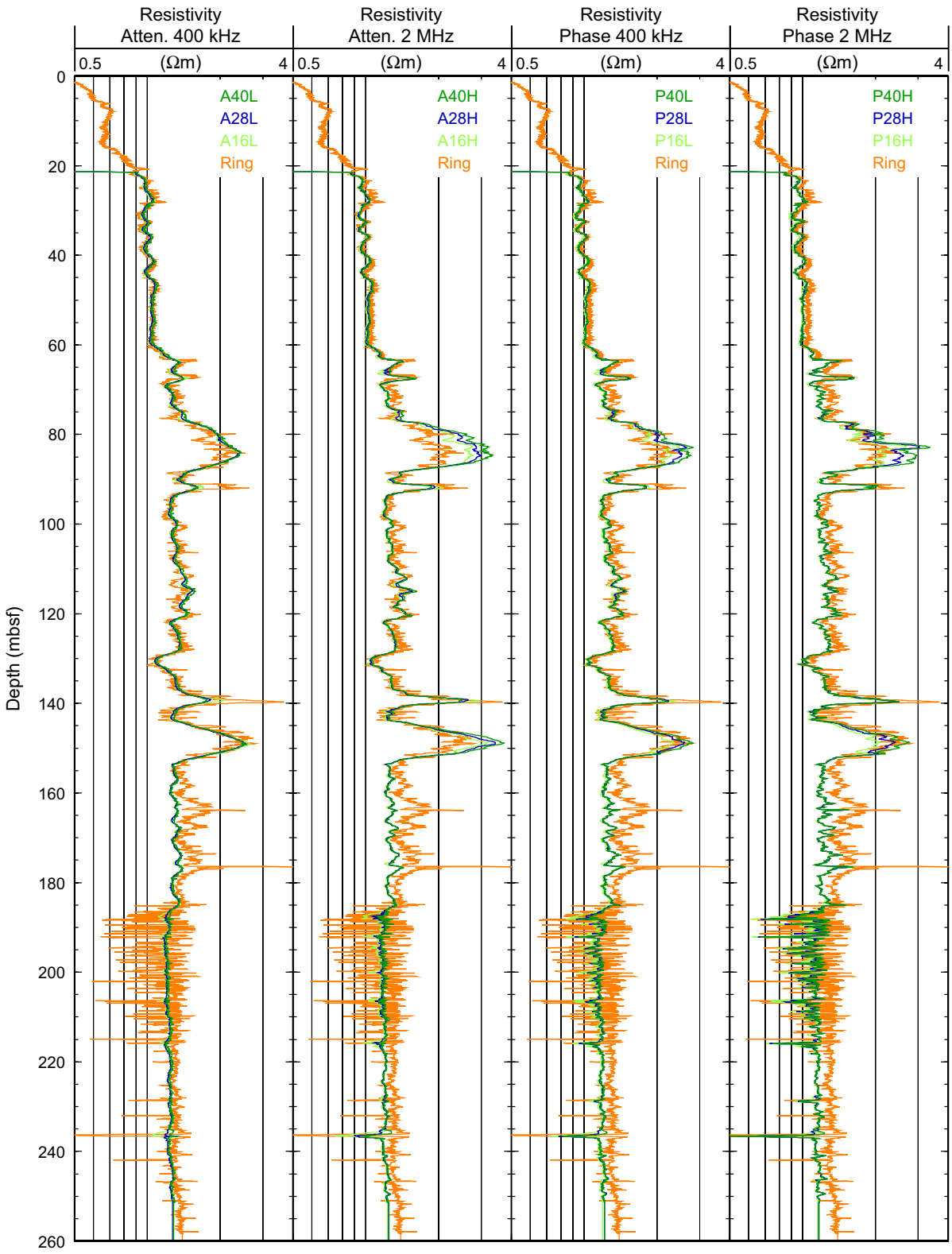

Figure 34. Comparison of LWD resistivity curves from Hole NGHP-01-07A. [LWD, logging while drilling; RING , Ring resistivity (GeoVISION); AXXL, Attenuation resistivity measured at a frequency of 400 kHz, where XX is the transmitter-receiver spacing in inches (EcoScope); AXXH, Attenuation resistivity measured at a frequency of 2 MHz, where XX is the transmitter-receiver spacing in inches (EcoScope); PXXL, Phase-shift resistivity measured at a frequency of 400 kHz, where XX is the transmitter-receiver spacing in inches (EcoScope); PXXH, Phase-shift resistivity measured at a frequency of 2 MHz, where XX is the transmitter-receiver spacing in inches (EcoScope)]

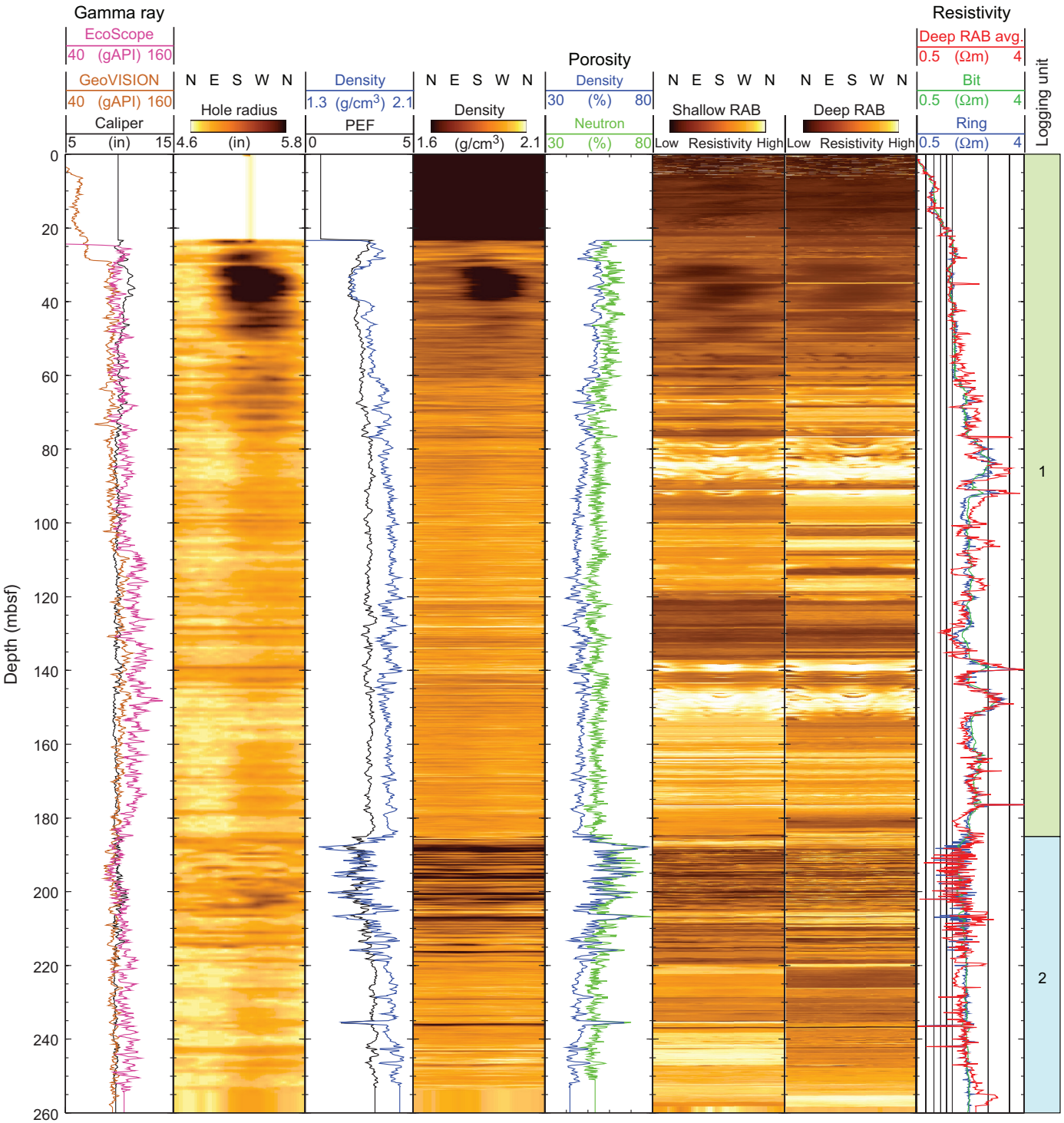

Figure 35. LWD image data from Hole NGHP-01-07A. [LWD, logging while drilling; gAPI, American Petroleum Institute gamma ray units; RAB, resistivity-at-bit image obtained by the GeoVISIO tool]

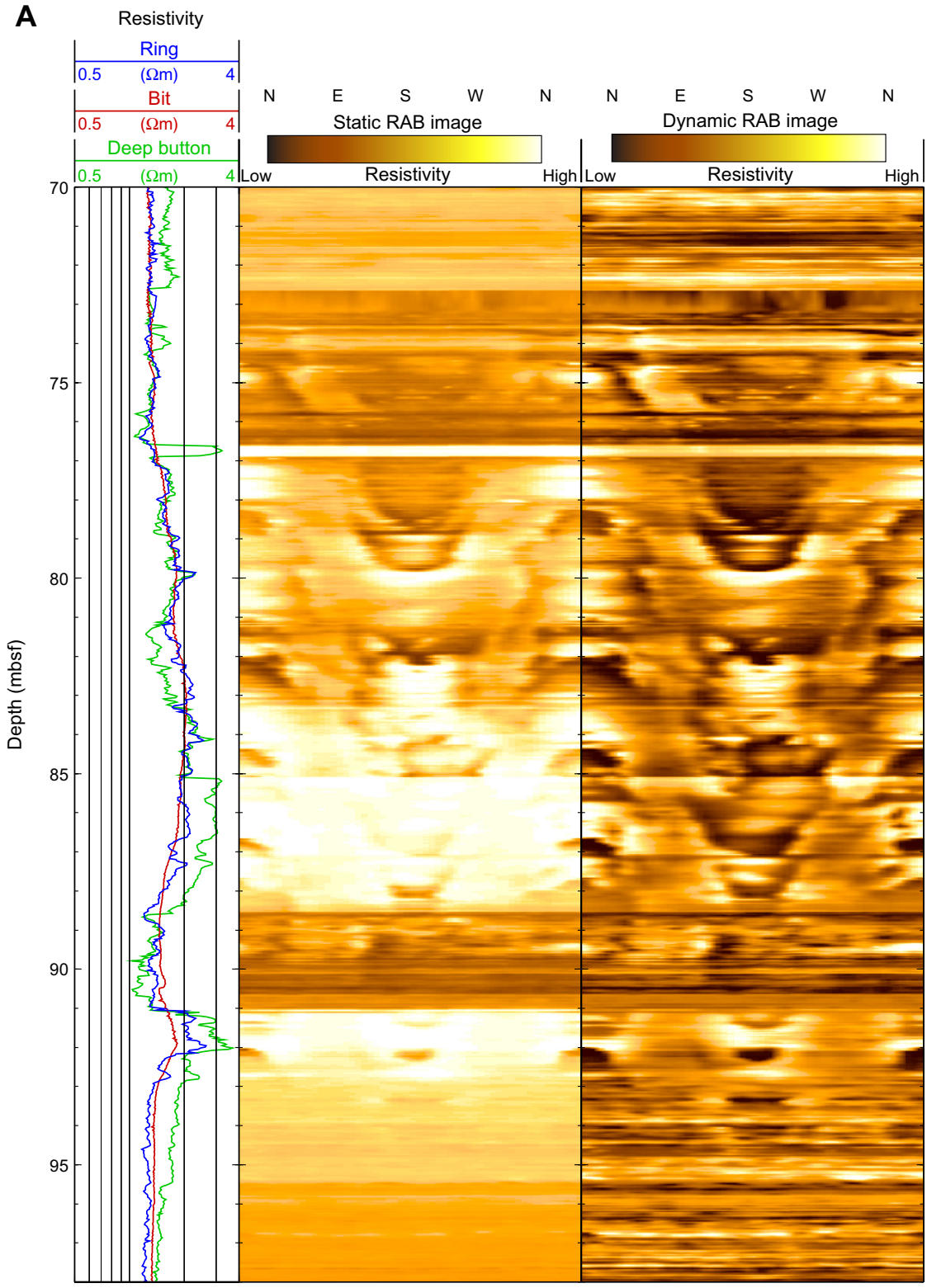

Figure 36. LWD resistivity image (GeoVISION deep button) from Hole NGHP-01-07A. The image on the left ("Static Image") has been equalized throughout the entire logged interval to enhance the contrast between low and high resistivity regions. The image on the right ("Dynamic Image") has been equalized in a 2 m-thick moving window to enhance small-scale features, and it clearly shows a number of sinusoidal features interpreted as steeply dipping fractures that intersect the borehole. Gas-hydrate-rich intervals are found near these fractures and show up as bright, high-resistivity intervals in the image on the left at 75–93 mbsf (A) and 138–152 mbsf (B). [LWD, logging while drilling; mbsf, meters below sea floor]

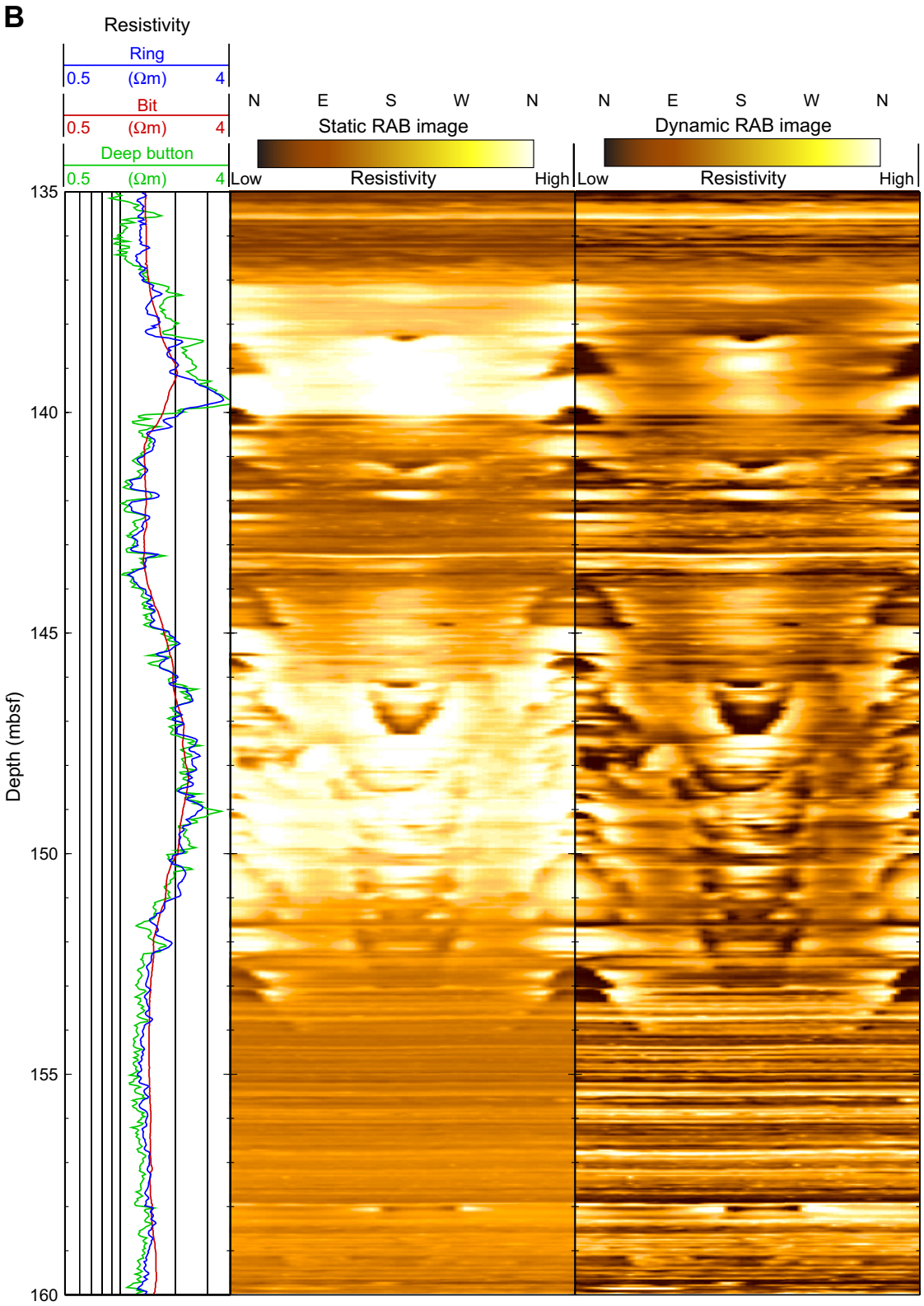

Figure 36. LWD resistivity image (GeoVISION deep button) from Hole NGHP-01-07A. The image on the left ("Static Image") has been equalized throughout the entire logged interval to enhance the contrast between low and high resistivity regions. The image on the right ("Dynamic Image") has been equalized in a 2 m-thick moving window to enhance small-scale features, and it clearly shows a number of sinusoidal features interpreted as steeply dipping fractures that intersect the borehole. Gas-hydrate-rich intervals are found near these fractures and show up as bright, high-resistivity intervals in the image on the left at 75–93 mbsf (A) and 138–152 mbsf (B). [LWD, logging while drilling; mbsf, meters below sea floor]—Continued

Wire-Line Log Quality

Figure 37 shows the main logs recorded by the triple combo run in Hole NGHP-01-07D. The caliper log shows that the hole was of good quality over most of the interval logged, except for a ledge at ~120 mbsf and some small enlargements between 195 and 215 mbsf. These enlargements correspond to similar features observed during LWD operations in Hole NGHP-01-07A and seem to correlate with low gamma ray readings, indicating possibly a succession of fine sandy layers. The poor recovery over this interval prevents confirmation of this theory, but could by itself be an indication of such alternation. Except for these intervals, the hole size is only slightly larger than the bit size and the data should be of good quality.

Below 80 mbsf, the density and the density porosity derived from the density log show a good agreement with the data measured on core samples from Holes NGHP-01-07B and NGHP-01-07D. The density porosity was derived by assuming a grain density of 2.72 g/cm^3, which is the average of the values measured on the core samples. The density log values are generally slightly higher than the core measurements, which translates into slightly lower porosity values, but both data sets follow the same trend and such difference is commonly due to core expansion. Above 80 mbsf, the density log indicates anomalously low values because the caliper was closed and the tool could not make proper contact with the formation. As a result these values, as well as the corresponding density porosity data, are not reliable. Despite the good hole conditions, the neutron porosity is strongly affected by the high clay content of the formation and is consequently higher than the porosity derived from the core or from the density log.

The strong amplitude and the good coherence shown by the monopole waveforms in figure 38 confirms the good hole conditions and indicate that the compressional velocity log is of very high quality. Dipole waveform amplitudes and coherence are also strong and indicative of reliable data below ~110 mbsf, but the waveforms show that above this depth the shear velocity was too low in these unconsolidated sediments for the flexural waves to be properly captured by the recording time window.

The low cohesiveness of these sediments is also the main reason why we could not record reliable VSP stations in the upper part of the hole. Figure 39 shows that some of the travel times measured deeper in the hole display an anomalous variability that indicates the low signal to noise ratio in the waveforms and the need for further reprocessing to pick the correct arrivals. However, the trend of the data allows confirmation of the location of the BSR at ~190 mbsf, which is on good agreement with a decrease in the V_P log at ~185 mbsf (fig. 38).

Logging While Drilling and Wire-Line Logging Comparison

Figure 40 shows a comparison of the LWD and wire-line logging data recorded at Site NGHP-01-07. One of the most significant differences is between the shape of the holes measured by the LWD tool string and the two wire-line runs. This difference is ultimately responsible for some of the discrepancies observed between the other data sets. While the LWD measurements are made very briefly after the bit enters the formation, the coring process provides much more time and disturbances for the hole to deteriorate before the wire-line logs are acquired. Despite this, most of the LWD and wire-line logs display very similar trends, in particular the density and the resistivity data. The most consistent difference is between the neutron porosity logs, which is due to the correction for clay content that is applied to the LWD data but not the wire-line neutron log. In this clay-rich formation, such correction is necessary to derive a reliable porosity estimate. This is confirmed by the good agreement between the LWD neutron porosity log and the core-derived porosity measurements. The difference between the two wire-line gamma ray logs and the LWD log is mostly due to differences in the calibration of the tools.

The various resistivity curves measured by LWD and wire-line tools generally agree and follow the same trend over the entire hole. All the curves agree in particular on the location of most of the intervals with higher resistivity where gas hydrate might be present, although the LWD curves show in general slightly higher values in these intervals. This might possibly reflect the better LWD hole condition and the partial dissociation of gas hydrate in Hole NGHP-01-07D during the coring and hole conditioning operations before the wire-line logs, but it could also indicate some heterogeneity in the gas hydrate distribution at this site. In particular, the extreme variability in the LWD resistivity curves between 185 and 220 mbsf is not observed in the wire-line logs, possibly because of the dissociation of the gas hydrate in these unstable fine layers.

Logging Units

The combined analysis of the gamma-ray, density, porosity, resistivity and velocity logs recorded by the wire-line and LWD tools can help delineate three logging units (see figs. 33, 35, 37**,** and 38):

Logging unit 1 (0–185 mbsf) is characterized by a steady increase with depth in density and sonic velocity, and a related decrease in porosity. Over this same unit, the resistivity logs follow a baseline trend also increasing steadily with depth, but interrupted in several intervals by high resistivity values that

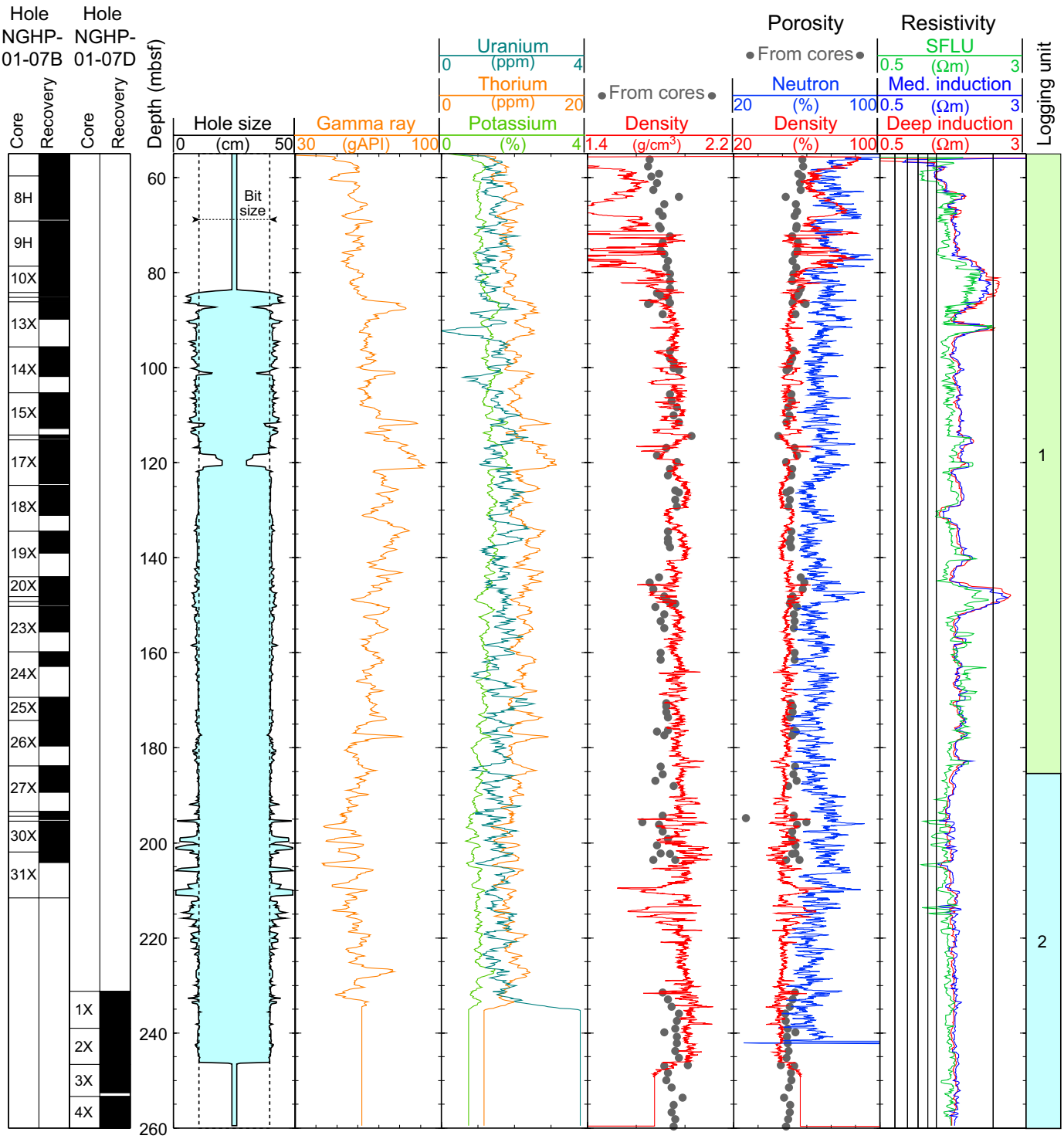

Figure 37. Summary of the wire-line logs recorded by the triple combo in Hole NGHP-01-07D. Porosity and density measurements made on core samples are shown for comparison.

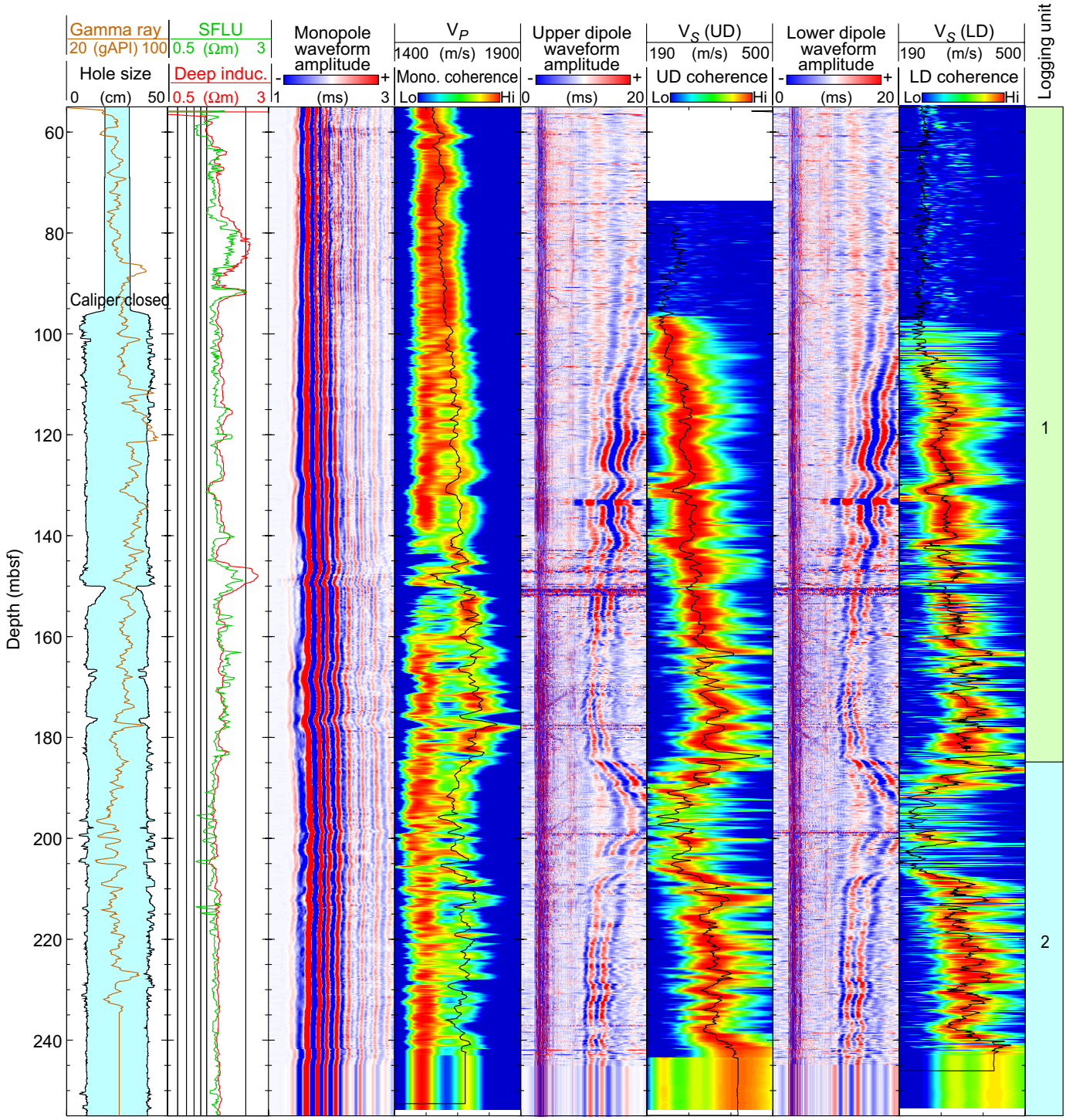

Figure 38. Sonic waveform data, *P*-wave and *S*-wave velocities measured by the DSI wire-line log in Hole NGHP-1-07D. [DSI, dipole sonic log; V_P, *P*-wave velocity; V_S, *S*-wave velocity; LD, Lower dipole; UD, Upper dipole]

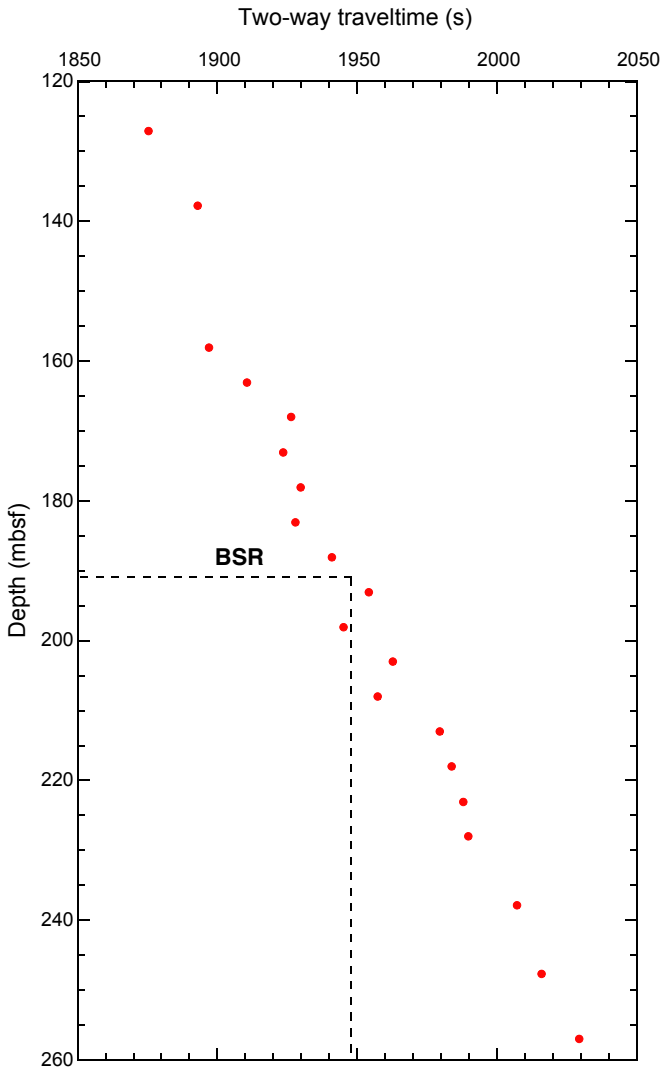

Figure 39. Time-depth plot of the preliminary first break times in the Hole NGHP-01-07D VSP. [VSP, vertical seismic profile]

are likely associated with the occurrence of gas hydrate. Two of these intervals, between ~75 and 93 mbsf and between ~135 and 152 mbsf, are particularly prominent and display similar resistivity curve shape in both the wire-line and LWD logs. It shows that the fractures that are feeding these intervals with gas and are seen in the RAB image from Hole NGHP-01-07A (fig. 36) are also intersecting Hole NGHP-01-07D.

The top of Logging unit 2 (185-260 mbsf) is defined by a sharp decrease in density, resistivity and sonic velocity. It coincides with the depth of the BSR that was predicted from the seismic data and was confirmed by preliminary results of the VSP (fig. 39). Below this depth, the LWD density, porosity and resistivity logs, and to a lesser extent the wire-line logs, display a high variability indicative of a sequence of finer layers of alternating nature. The lower density values in this sequence, more noticeable in the LWD data, and more significantly the low V_P values between ~190 and 210 mbsf are the indication of significant amounts of free gas. The lower V_S values in the same interval illustrate the mechanical disequilibrium that occurred when the drill bit intersected these intervals that were likely fluid-supported and lost their cohesion as some of the gas escaped.

Gas-Hydrate and Free Gas Occurrence

As previously discussed (see "Downhole Logging" in the "Methods" chapter), the presence of gas hydrate is generally characterized by increases in electrical resistivity and acoustic velocity that are not accompanied by a corresponding porosity decrease. A decrease in porosity alone in water-saturated sediments can result in an increase in resistivity and acoustic velocity. Resistivities logged in Hole NGHP-01-07A show a general negative correlation with porosity (fig. 33), except for a few intervals such as the two discussed earlier at 75–93 mbsf and 138–152 mbsf where high resistivities suggest that gas hydrate is present.

To make a quantitative estimate of the amount of gas hydrate at Hole NGHP-01-07A, we followed the procedure described in "Downhole Logging" in the "Methods" chapter, to apply the Archie relationship to the resistivity and porosity logs recorded in Hole NGHP-01-07A. The procedure and the results are shown in figure 41. The pore fluid resistivity (R_w) was estimated from Fofonoff (1985) using a linear temperature profile derived from the *in situ* temperature measurements at Site NGHP-01-07 (5.21 °C at the seafloor; gradient of 51 °C/km, see "Physical Properties") and a constant water salinity of 34 ppt, which is an average of the values measured in Site NGHP-01-07. The estimated m curve is derived from R_w, the porosity (φ) and resistivity (R_t) logs ($m_{est} = -\log F/\log\varphi$, where $F = R_t / R_w$). The chosen value of $m = 2.0$ is given by the baseline of this curve in the low-resistivity water-saturated formation. Using the porosity log and Archie's equation ($R_0 = (a\, R_w) / \varphi^m$), we derive the predicted resistivity of the water-saturated formation R_o. A qualitative influence of gas hydrate on the resistivity log is indicated by the difference between the R_0 and the measured resistivity R_t. The estimated water saturation, assumed to be the numerical complement of the hydrate saturation, is $S_w = (R_0/R_t)^{1/n}$, where n=2 (Pearson and others, 1983). We used the density porosity computed from the image-derived density (IDRO) and the resistivity from the 16 in, phase-shift, high-frequency propagation resistivity (P16H) measured by the EcoScope tool. We use the P16H curve because it is the resistivity with the highest vertical resolution measured by the EcoScope.

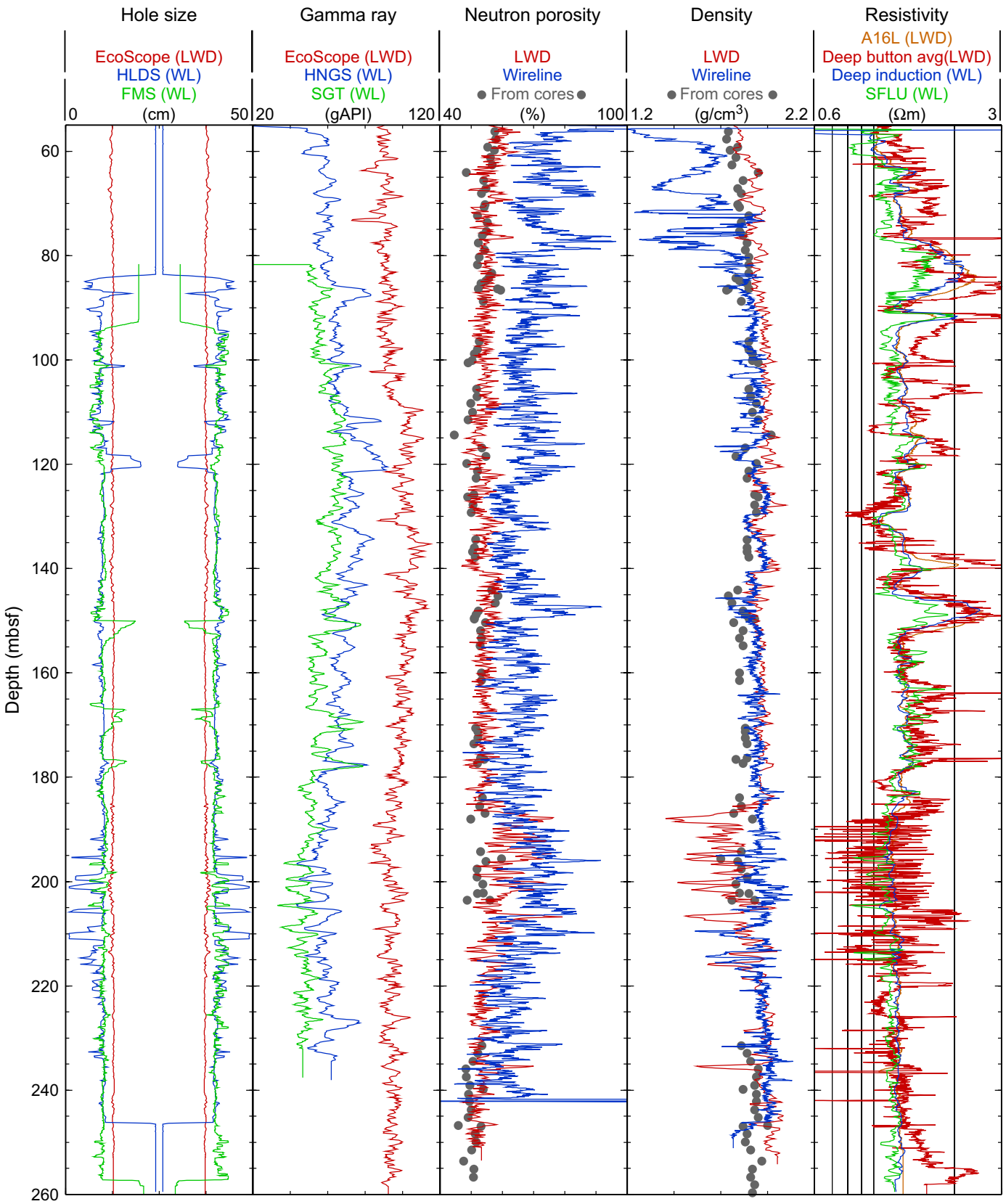

Figure 40. Comparison of LWD (Hole NGHP-01-07A) and wire-line log data (Holes NGHP-01-07D). [LWD, logging while drilling; WL, Wire-line; HLDS, Hostile environment lithodensity sonde; HNGS, Hostile environment natural gamma ray spectroscopy, SFLU; Spherically focused unaveraged resistivity]

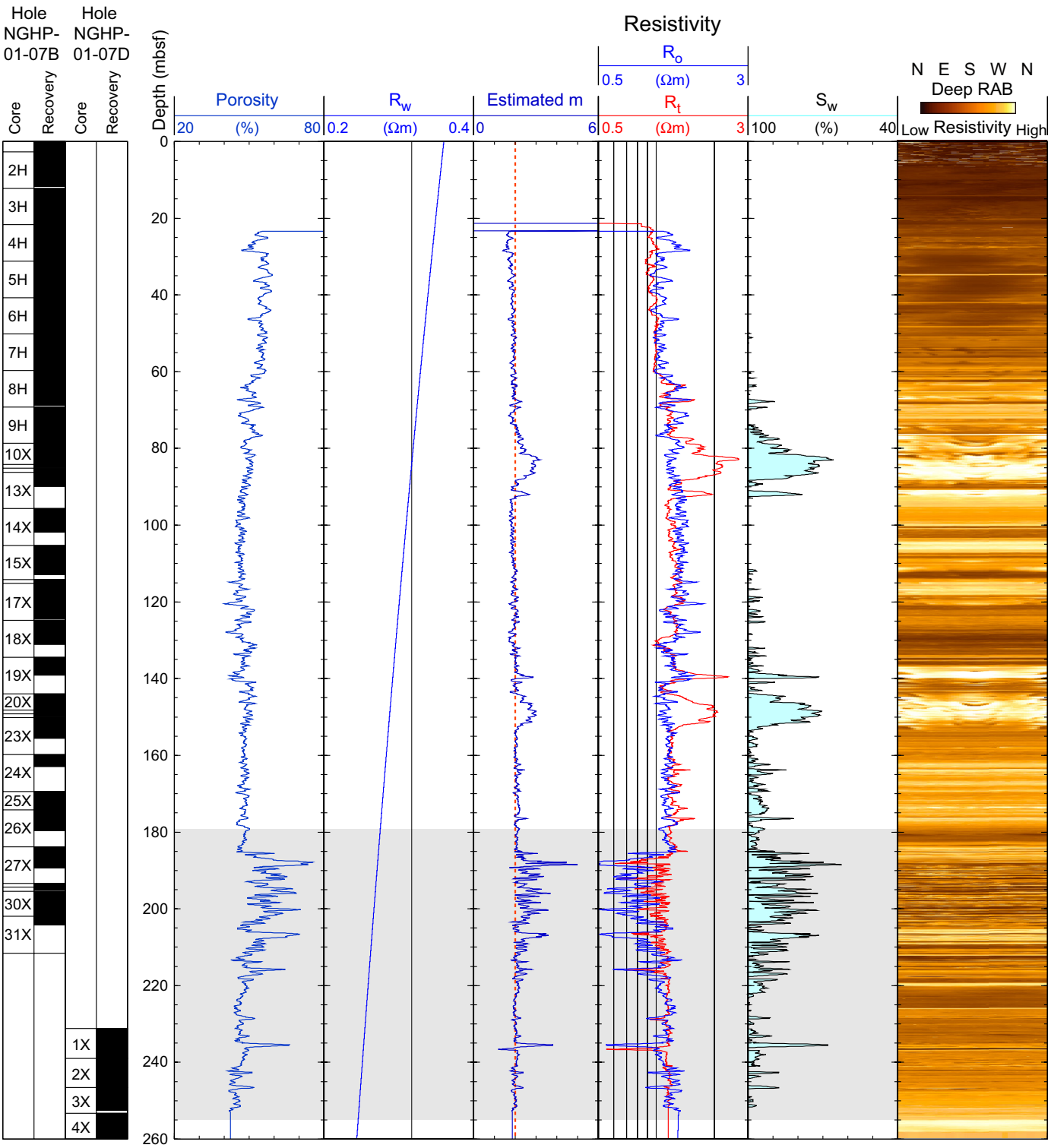

Figure 41. Water saturations from Archie's relationship and LWD porosity and resistivity logs in Hole NGHP-01-07A. The gray area indicates degraded data quality. [LWD, logging while drilling; R_w, Formation water resistivity; R_0, Computed formation resistivity for 100 percent water saturation, R_t, Measured resistivity; S_w, water saturation]

The strongest evidence for gas hydrate is in the intervals at 75–93 mbsf and 138–152 mbsf, where the computed gas-hydrate saturations reach a maximum of about 30 percent (fig. 41). These two intervals are also where the resistivity images show prominent high-resistivity layers (fig. 35) located near steeply dipping fractures (fig. 36).

References Cited

Adolph, B., Archer, M., Codazzi, D., el-Halawani, T., Perciot, P., Weller, G., Evans, M., Grant, J., Griffiths, R., Hartman, D., Sirkin, G., Ichikawa, M., Scott, G., Tribe, I., and White, D., 2005, No more waiting—Formation evaluation while drilling: Oilfield Review, Autumn 2005, p. 4–21.

Aldred, W., Cook, J., Bern, P., Carpenter, B., Hutchinson, M., Lovell, J., Rezmer-Cooper, I., and Leder, P.C., 1998, Using downhole annular pressure measurements to improve drilling performance: Oilfield Review, Winter 1998, p. 40–55.

Bjerrum, L., 1972, Embankments on soft ground: Proceedings of the ASCE Specialty Conference on Performance of Earth and Earth-Supported Structures, Purdue University, v. II, p. 1–54.

Bonner, S., Fredette, M., Lovell, J., Montaron, B., Rosthal, R., Tabanou, J., Wu, P., Clark, B., Mills, R., and Williams, R., 1996, Resistivity while drilling—Images from the string: Oilfield Review, Spring 1996, p. 4–19.

Davis, E.E., Hyndman, R.D., and Villinger, H., 1990, Rates of fluid expulsion across the northern Cascadia accretionary prism—Constraints from new heat flow and multichannel seismic reflection data: Journal of Geophysical Research, v. 95, p. 8869–8889.

Duan, Z., Møller, N., Greenberg, J., and Weare, J.H., 1992, The prediction of methane solubility in natural waters to high ionic strengths from 0° to 250 °C and from 0 to 1600 bar: Geochimica et Cosmochimica Acta, v. 56, p. 1451–1460.

Fofonoff, N.P., 1985, Physical properties of seawater: Journal of Geophysical Research, v. 90, no. C2, p. 3332–3342.

Holtz, R.D., and Kovacs, W.D., 1981, An introduction to geotechnical engineering: Englewood Cliffs, N.J., Prentice-Hall, Inc., 733 p.

Hunt, R.E., 1984, Geotechnical engineering investigation manual: New York, McGraw-Hill Book Company, 983 p.

Kvenvolden, K.A., and Lorenson, T.D., 2000, Methane and other hydrocarbon gases in sediment from the southeastern North American continental margin, *in* Paull, C.K., Matsumoto, R., Wallace, P.J., Black, N.R., Borowski,W.S.,Collett, T.S., Damuth, J.E., Dickens, G.R., Egeberg, P.K., Goodman,K., Hesse, R.F., Hiroki, Y., Holbrook, W.S., Hoskins, H., Ladd, J. ,Lodolo, E., Lorenson, T.D.,Musgrave, R.J., Naehr, T.H., Okada, H., Pierre, C., Ruppel, C.D., Satoh, M., Thiery, R., Watanabe, Y., Wehner, H., Winters, W.J.,and Wood, W.T., Gas hydrate sampling on the Blake ridge and Carolina rise; covering leg 164 of the cruises of the drilling vessel *JOIDES Resolution*, Halifax, Nova Scotia, to Miami, Florida, sites 991–997, 31 October–19 December 1995: Proceedings of the Ocean Drilling Program, Scientific Results, v. 164, p. 29–36.

Ladd, C.C., Foote, R., Ishihara, K., Schlosser, F., and Poulos, H.G., 1977, Stress-deformation and strength characteristics—State-of-the-art report: Proceedings of the Ninth International Conference on Soil Mechanics and Foundation Engineering, Tokyo, v. 2, p. 421–494.

Lambe, T. W. and Whitman, R.V., 1969, Soil mechanics: New York, John Wiley and Sons, 553 p.

Novosel, I., Winters, W.J., Boldina, O.M., Labails, C., and Geli, L., 2007, Thermal conductivity of sediment recovered from the IMAGES VIII/PAGE 127 Gas Hydrate and Paleoclimate Cruise on the *R/V Marion Dufresne* in the Gulf of Mexico, 2–18 July 2002, *in* Winters, W.J., Lorenson, T.D., and Paull, C.K., eds., Initial report of the IMAGES VIII/PAGE 127 gas hydrate and paleoclimate cruise on the RV Marion Dufresne in the Gulf of Mexico, 2–18 July 2002: U.S. Geological Survey Open-File Report 2004–1358.

Pearson, C.F., Halleck, P.M., McGuire, P.L., Hermes, R., and Mathews, M., 1983, Natural gas hydrate deposits—A review of *in situ* properties: Journal of Physical Chemistry, v. 87, p. 4180–4185.

Sloan, E.D., 1998, Clathrate Hydrates of Natural Gases (2d ed.): New York (Marcel Dekker), 705 p.

Xu, W., 2002, Phase balance and dynamic equilibrium during formation and dissociation of methane gas hydrate, *in* International Conference on Gas Hydrates, 4th, Yokohama, Japan, May 2002, Proceedings: Yokohama, Japan, International Conference on Gas Hydrates, p. 195–200.

Xu, W., 2004, Modeling dynamic marine gas hydrate systems: American Mineralogist, v. 89, p. 1271–1279.